

LOW THERMAL INERTIA INJECTION MOLDING

by

BYUNG HOON KIM

B.S., University of California, Berkeley (1978)
M.S., Massachusetts Institute of Technology (1980)

Submitted in partial
fulfillment of the requirements
for the degree of

DOCTOR OF PHILOSOPHY

at the

MASSACHUSETTS INSTITUTE OF TECHNOLOGY

July 1983

© Massachusetts Institute of Technology 1983

Signature of Author Byung H. Kim
Department of Mechanical Engineering
July 28, 1983

Certified by Nam P. Suh
Nam P. Suh
Thesis Supervisor

Accepted by W. N. Rosen
Chairman,
Department Committee on Graduate Students

MASSACHUSETTS INSTITUTE
OF TECHNOLOGY

OCT 21 1983

Archives

LIBRARIES

LOW THERMAL INERTIA INJECTION MOLDING

by

BYUNG HOON KIM

Submitted to the Department of Mechanical Engineering
on July 28, 1983 in partial fulfillment
of the requirements for the Degree of
Doctor of Philosophy in Mechanical Engineering.

ABSTRACT

A low thermal inertia injection molding concept has been investigated to minimize residual stress in the molded part without increasing the total cycle time. The new molding method uncouples the filling and cooling processes, which improves consistency of the part quality and eliminates the freezing surface layer during the filling process. The improved consistency results directly from controllability of the process variables due to the uncoupling. The new process also reduces the temperature and the pressure required for the molding. Furthermore, the uncoupling allows independent control of the mold surface temperature, which can be used to minimize residual stress developed due to flow-induced molecular orientation. Details of the new molding process and development of the new mold are discussed. The mold had a temperature response time of 5.3 seconds from 100°F to 300°F with 48.3 watts/in² power density. Also, the mold endured greater than 20,000 thermal cycles without any deterioration. The nonisothermal and isothermal stress relaxation study indicated that the flow-induced molecular orientation relaxes on the order of a second. Experimental results of the low thermal inertia molding showed that residual stress in the molded part can indeed be minimized.

Thesis Supervisor: Nam P. Suh
Title: Professor of
Mechanical Engineering

Dedicated
to my mother,
Soon Duk Kim

ACKNOWLEDGEMENTS

I would like to thank Professor Nam P. Suh, my thesis advisor, for my professional development. I have gained immeasurably through association with him. I would also like to thank the other members of my thesis committee, Professors Robert Armstrong and Lewis Erwin, for their suggestions.

This research was sponsored by the MIT-Industry Polymer Processing Program. The sponsors of this program are AMP Inc., Boeing Commercial Airplane Company, E.I. duPont de Nemours and Company, Eastman Kodak Company, General Motors Corporation, Instrumentation Laboratories, Inc., Intelitec Corporation, ITT Corporation, Rogers Corporation, and Xerox Corporation. I would like to thank all of the members of this program for their technical support, criticism, and encouragement throughout this project. In particular I would like to thank: Mr. John Diener from AMP Inc., Mr. Dick Reynolds from Xerox Corporation, and Mr. Gordon Brown, Mr. Dave Fisher, Mr. Scott Hardenbrook, Mr. Doug Van Putte, Mr. Jehuda Greener, Mr. Ed Brill, Mr. James Wenskus, and Mr. Bruce Cady from Eastman Kodak Company for their judicious application of experience and for their efforts to help this project. Mr. Fred Buja and Mr. Don Saulsbury also from Eastman Kodak Company gave their sincere effort to help the project, and I appreciate their help very much.

My colleagues around the Laboratory deserve thanks for their time in discussing many technical and non-technical

ideas. They include Dr. Richard Okine, Dr. Kim Stelson, Dr. Jim Rinderle, Dr. Hyo-Chul Sin, Dr. Saka Nannaji, Mr. Bill Westphal, Avi Benatar, Frank Waldman, Steve Burgess, Ken Wright, Jong Chu, Sang Kim, and Jae Youn. My thanks also go to Professor Suh's secretaries--Alice Markunas, Margie MacDonald, and Nancy James--for their assistance in administrative matters. Whenever I needed something built or modified, Fred C. (Andy) Anderson, Ralph Whittemore, Fred Cote, John Ford, Bob Kane, and Mike Demaree were always available to provide their technical expertise.

I would like to give very special thanks to Paul Gabuzda and Gaetane Francis, MIT students in the Undergraduate Research Opportunities Program. They contributed significantly to this project by their inquisitiveness and diligently performed experiments. I would also like to thank Paul for typing and editing this thesis.

Another very special thanks goes to Sae Young Koe whom I met outside of MIT. We have shared so many hours together discussing our ideas, playing tennis, skiing, and traveling. I have enjoyed being with him.

Finally, I would like to thank my parents, my brother, and my three sisters. I am grateful to my family for having encouraged and comforted me throughout the thesis work.

TABLE OF CONTENTS

<u>Chapter</u>		<u>Page</u>
	Title Page	1
	Abstract	2
	Dedication	3
	Acknowledgements	4
	Table of Contents	6
	List of Figures	9
	List of Tables	15
	Nomenclature	16
I	FUNDAMENTALS OF INJECTION MOLDING	19
	I.1 Introduction	19
	I.2 The Injection Molding Process	19
	I.3 Evaluation of Controls in Injection Molding	22
	I.4 Project Goal	25
	References for Chapter I	26
II	PROBLEMS IN INJECTION MOLDING	27
	II.1 Introduction	27
	II.2 The Effect of the Molding Condition on Mold Part Properties	29
	II.3 Summary	34
	References for Chapter II	36
III	METHODS FOR IMPROVING THE MOLDED PART QUALITY	38
	III.1 Introduction	38
	III.2 Isothermal Filling Process	39
	III.3 Differential Cooling Process	46
	References for Chapter III	54

TABLE OF CONTENTS (Cont.)

<u>Chapter</u>		<u>Page</u>
IV	ANALYSIS OF STRESS RELAXATION	55
	IV.1 Introduction	55
	IV.2 The Wagner Model	56
	(a) Background	56
	(b) Steady Shear Flow	58
	(c) Evaluation of Model Parameters	61
	IV.3 Stress-Optical Law	65
	IV.4 Isothermal Stress Relaxation	67
	IV.5 Nonisothermal Stress Relaxation	71
	References for Chapter IV	87
V	DEVELOPMENT OF A LOW THERMAL INERTIA MOLD	88
	V.1 Introduction	88
	V.2 Design of a Low Thermal Inertia Mold	89
	V.3 Experimental Results of the Low Thermal Inertia Block	93
	(a) Temperature Response Experiment	93
	(b) Endurance Experiment	95
	References for Chapter V	97
VI	EXPERIMENTAL RESULTS OF LOW THERMAL INERTIA MOLDING	98
	VI.1 Introduction	98
	VI.2 Conventional Molding	98
	(a) Experimental Procedure	98
	(b) Results	99
	VI.3 Low Thermal Inertia Molding	102
	(a) Preliminary Experiments and Results	102
	(b) Low Thermal Inertia Molding and Discussion	105
	(c) Suggestions for Future Work	109

TABLE OF CONTENTS (Cont.)

<u>Chapter</u>		<u>Page</u>
VII	CONCLUSIONS	111
	APPENDICES	
	A. Evaluation of a Modern Process Control	114
	B. Derivation of Equation (16) in Chapter IV	123
	C. User-Supplied Subroutine for the Powell Nonlinear Regression Program	126
	D. Computer Program Listings for Noniso- thermal Stress Relaxation	128
	E. Simulation Results for Nonisothermal Stress Relaxations	138
	F. Data for the Conventional Molding	166
	Biographical Information	172

LIST OF FIGURES

<u>Figure</u>		<u>Page</u>
I.1	Schematic drawing of the injection end of a reciprocating screw machine. (Courtesy Van Nostrand Reinhold Company)	21
I.2	A typical cavity pressure curve for an injection cycle.	23
III.1	A plot of temperature curve of the mold surface for an isothermal filling process.	40
III.2	Schematic comparison between (a) conventional and (b) isothermal filling process in molding an optical part	42
III.3	A difficult part to mold because of the change in part thickness.	47
III.4	(a) Two dimensional drawing of the part. (b) Differential cooling for the part.	49
III.5	Vitrification rates for thin and thick sections with the passive differential cooling method. ($\alpha_P = .01 \text{ in}^2/\text{s}$, $\alpha_I = .1 \text{ in}^2/\text{s}$, $t_I = .09 \text{ in.}$)	51
III.6	The insulation thickness required to minimize the vitrification rate difference along the linearly varying thickness of the part. ($\alpha_P = .01 \text{ in}^2/\text{s}$, $\alpha_I = .1 \text{ in}^2/\text{s}$)	53
IV.1	The storage modulus (G'), the loss modulus (G'') and the complex viscosity (η^*) data.	62
IV.2	Schematic representation of isothermal filling.	69
IV.3	Flow chart to determine the shear rate as a function of the pressure gradient.	72
IV.4	Shear rates for the two pressure gradients as a function of the gap distance.	73
IV.5	Isothermal relaxation of the shear stress for (a) $dP/dx \cdot a = 62.5 \text{ psi}$ and (b) $dP/dx \cdot a = 31.25 \text{ psi}$.	74

LIST OF FIGURES (Cont.)

<u>Figure</u>		<u>Page</u>
IV.6	Isothermal relaxation of the primary normal stress difference for (a) $dp/dx \cdot a = 62.5$ psi and (b) $dP/dx \cdot a = 31.25$ psi.	75
IV.7	Isothermal relaxation of the birefringence for (a) $dP/dx \cdot a = 62.5$ psi and (b) $dP/dx \cdot a = 31.25$ psi.	76
IV.8	Shear stress relaxation as a function of shear rate for the condition A in Table IV.2	80
IV.9	Flow chart for nonisothermal stress relaxation.	83
IV.10	Nonisothermal relaxation of the shear stress for $dP/dx = 8336$ psi. (Condition A in Table IV.2)	84
IV.11	Nonisothermal relaxation of the primary normal stress difference for $dP/dx = 8336$ psi. (Condition A in Table IV.2)	85
IV.12	Nonisothermal relaxation of the birefringence for $dP/dx = 8336$ psi. (Condition A in Table IV.2)	86
V.1	Configuration of layers to be pressed to form mold.	92
V.2	Assembly of mold showing electrodes and mold release layer.	92
V.3	Experimental set-up for temperature response and thermal cycle endurance tests.	94
V.4	Two cycles of temperature response.	96
VI.1	Cross sectional view of the incomplete filling under the cross polarized plates; part thickness = 0.03", melt temperature = 470°F, mold temperature = 70°F, ram rate = 3 in/sec.	100
VI.2	Cross sectional view of the conventionally molded parts under the cross polarized plates.	101

LIST OF FIGURES (Cont.)

<u>Figure</u>		<u>Page</u>
VI.3	Configuration of LTIM: (a) stainless steel as a heating surface, (b) electrical insulation of the mold	103
VI.4	Cross sections of the molded parts using the low thermal inertia mold with (a) heat off and (b) heat-on under the cross polarized plates.	104
VI.5	Temperature and current response of the thin part of the mold.	106
VI.6	Temperature and current response of the thick part of the mold.	107
A1	Hydraulic pressure for the three molecular weight materials. This is based on constant velocity with a fixed gate pressure.	115
A2	Gate pressure for the three molecular weight materials. This is based on constant velocity with a fixed gate pressure.	116
A3	Mid. pt. pressure for the three molecular weight materials. This is based on constant velocity with a fixed gate pressure.	117
A4	End pressure for the three molecular weight materials. This is based on constant velocity with a fixed gate pressure.	118
A5	Fill time for the three molecular weight materials. This is based on constant velocity with a fixed gate pressure.	119
A6	Boost time for the three molecular weight materials. This is based on constant velocity with a fixed gate pressure.	120
A7	Screw return time for the three molecular weight materials. This is based on constant velocity with a fixed gate pressure.	121
A8	Cycle time for the three molecular weight materials. This is based on constant velocity with a fixed gate pressure.	122

LIST OF FIGURES (Cont.)

<u>Figure</u>		<u>Page</u>
E1	Nonisothermal relaxation of the shear stress for $dP/dx = 4168$ psi. (Condition B in Table IV.2)	139
E2	Nonisothermal relaxation of the primary normal stress difference for $dP/dx = 4168$ psi. (Condition B in Table IV.2)	140
E3	Nonisothermal relaxation of the birefringence for $dP/dx = 4168$ psi. (Condition B in Table IV.2)	141
E4	Nonisothermal relaxation of the shear stress for $dP/dx = 4168$ psi. (Condition C in Table IV.2)	142
E5	Nonisothermal relaxation of the primary normal stress difference for $dP/dx = 4168$ psi. (Condition C in Table IV.2)	143
E6	Nonisothermal relaxation of the birefringence for $dP/dx = 4168$ psi. (Condition C in Table IV.2)	144
E7	Nonisothermal relaxation of the shear stress for $dP/dx = 2084$ psi. (Condition D in Table IV.2)	145
E8	Nonisothermal relaxation of the primary normal stress difference for $dP/dx = 2084$ psi. (Condition D in Table IV.2)	146
E9	Nonisothermal relaxation of the birefringence for $dP/dx = 2084$ psi. (Condition D in Table IV.2)	147
E10	Nonisothermal relaxation of the shear stress for $dP/dx = 2084$ psi. (Condition E in Table IV.2)	148
E11	Nonisothermal relaxation of the primary normal stress difference for $dP/dx = 2084$ psi. (Condition E in Table IV.2)	149
E12	Nonisothermal relaxation of the birefringence for $dP/dx = 2084$ psi. (Condition E in Table IV.2)	150

LIST OF FIGURES (Cont.)

<u>Figure</u>		<u>Page</u>
E13	Nonisothermal relaxation of the shear stress for $dP/dx = 1042$ psi. (Condition F in Table IV.2)	151
E14	Nonisothermal relaxation of the primary normal stress difference for $dP/dx = 1042$ psi. (Condition F in Table IV.2)	152
E15	Nonisothermal relaxation of the birefringence for $dP/dx = 1042$ psi. (Condition F in Table IV.2)	153
E16	Nonisothermal relaxation of the shear stress for $dP/dx = 1042$ psi. (Condition G in Table IV.2)	154
E17	Nonisothermal relaxation of the primary normal stress difference for $dP/dx = 1042$ psi. (Condition G in Table IV.2)	155
E18	Nonisothermal relaxation of the birefringence for $dP/dx = 1042$ psi. (Condition G in Table IV.2)	156
E19	Nonisothermal relaxation of the shear stress for $dP/dx = 521$ psi. (Condition H in Table IV.2)	157
E20	Nonisothermal relaxation of the primary normal stress difference for $dP/dx = 521$ psi. (Condition H in Table IV.2)	158
E21	Nonisothermal relaxation of the birefringence for $dP/dx = 521$ psi. (Condition H in Table IV.2)	159
E22	Nonisothermal relaxation of the shear stress for $dP/dx = 500$ psi. (Condition I in Table IV.2)	160
E23	Nonisothermal relaxation of the primary normal stress difference for $dP/dx = 500$ psi. (Condition I in Table IV.2)	161
E24	Nonisothermal relaxation of the birefringence for $dP/dx = 500$ psi. (Condition I in Table IV.2)	162

LIST OF FIGURES (Cont.)

<u>Figure</u>		<u>Page</u>
E25	Nonisothermal relaxation of the shear stress for $dP/dx = 250$ psi. (Condition J in Table IV.2)	163
E26	Nonisothermal relaxation of the primary normal stress difference for $dP/dx = 250$ psi. (Condition J in Table IV.2)	164
E27	Nonisothermal relaxation of the birefringence for $dP/dx = 250$ psi. (Condition J in Table IV.2)	165

LIST OF TABLES

<u>Table</u>		<u>Page</u>
IV.1	Set of constants which describes the linear memory function of polystyrene (Dow 685D) at 170°C.	64
IV.2	Conditions of the simulated low thermal inertia injection molding with polystyrene (Dow 685D).	82
V.1	Properties of magnamite graphite fibers.	90
VI.1	Conditions of molding 0.045" x 2.5" x 5.2" part with polystyrene (Dow 685D) by LTIM.	108

NOMENCLATURE

a_i	- weighting factor for i-th mode
a_T	- time-temperature shift factor
c	- relative stress-optic coefficient
c_1, c_2	- stress-optic coefficients
\underline{C}^{-1}	- finger relative strain tensor
f_1, f_2	- coefficients of exponential damping function
G'	- storage modulus
G''	- loss modulus
h	- damping function
I_1	- first invariant
I_2	- second invariant
I_3	- third invariant
\underline{I}	- identity matrix
k	- dimensionless parameter in the power law model
L	- length of a part
m	- parameter in the power law model
\underline{M}_n	- number average molecular weight
\underline{M}_w	- weight average molecular weight
n	- damping constant
n_0	- index of refraction in unstressed state
n_1, n_2	- damping constants
n_1, n_2, n_3	- indices of refraction in stressed state associated with principal stress directions
Δn	- birefringence in 1,2 direction

NOMENCLATURE (Cont.)

P	- pressure
	- hydrostatic pressure
P_i	- initial pressure
P_f	- final pressure
P_{atm}	- atmospheric pressure
Q	- volume flow rate
R	- material property
t	- thickness of a part
	- current time
t_{fill}	- time to fill the cavity
t'	- past time
t''	- dummy variable
$t-t'$	- relative time
T	- temperature
T_0	- initial temperature
T_i	- initial temperature
T_f	- final temperature
T_g	- glass transition temperature
V	- specific volume
V_i	- initial volume
V_f	- final volume
v_x	- velocity in x-direction
W	- width of a part

NOMENCLATURE (Cont.)

x	- same as 1-direction
y	- same as 2-direction
α	- thermal diffusion coefficient
α_I	- thermal diffusivity of insulation
α_P	- thermal diffusivity of plastic
$\gamma_{t,t'}$	- relative shear strain
$\dot{\gamma}$	- shear rate
$\dot{\gamma}_0$	- initial steady shear rate
η	- viscosity
η^*	- complex viscosity
$\sigma_1, \sigma_2, \sigma_3$	- principal stresses at a point
$\underline{\sigma}_i$	- stress tensor corresponding to i-th relaxation mode
$\underline{\sigma}(t)$	- stress tensor
${}^o\mu$	- linear memory function
μ	- nonlinear memory function
π	- material property
ρ	- density
τ_{12}	- shear stress
$\tau_{11} - \tau_{22}$	- primary normal stress difference
τ_i	- relaxation time constant of i-th mode
τ_{yx}	- shear stress
ω	- angular frequency
	- material property

CHAPTER IFUNDAMENTALS OF INJECTION MOLDINGI.1 Introduction

Injection molding is one of most commonly used methods of processing polymers. The process allows rapid, automated production of a wide variety of complicated, three-dimensional parts in large production volumes. The process is capable of producing compound curvatures, snaps, hinges, bosses, threaded holes, gear teeth and many other features. With proper design, these complex parts can be produced in a single molding operation.

The advantages of the injection molding process have made the process a very important manufacturing method. In 1981 more than 7.8 billion pounds of thermoplastic material was injection molded in the United States [I-1].

I.2 The Injection Molding Process

Injection molding is a process in which some malleable material is forced under pressure into a mold cavity with subsequent solidification to retain the shape of the mold. Although the term injection molding is most often used referring to thermoplastic injection molding, thermosetting materials and ceramic materials can also be processed by injection molding. Throughout this thesis thermoplastic injec-

tion molding will be discussed even though many of the concepts presented apply not only to injection molding of other materials but also to many other molding processes such as blow molding, transfer molding, compression molding, and casting.

There are two basic types of injection molding machines, the plunger and the reciprocating screw types. The most common type of injection unit today is a reciprocating screw machine which is shown in Figure I.1. Due to its general acceptance the reciprocating screw machine will be treated as the conventional molding machine in this thesis.

An injection molding process is characterized by four successive stages: plastication, injection of molten polymer, packing, and part cooling. During plastication, polymer pellets are fed by gravity from the hopper to the screw and pushed through the barrel and toward the nozzle by this rotating screw. As the plastic is transported along the barrel, heat is generated from the shear work done on the material and heat is conducted into the material from electric heater bands which surround the barrel. The combination of the heat conduction and the heat generation causes the polymeric material to melt as it moves along the screw. The screw moves back due to the accumulation of plasticated material in front of the screw until a limit switch is tripped. At this point plastication is completed and the screw stops turning. During injection the screw is pushed forward by a hydraulic ram and the molten polymer is pushed into the mold

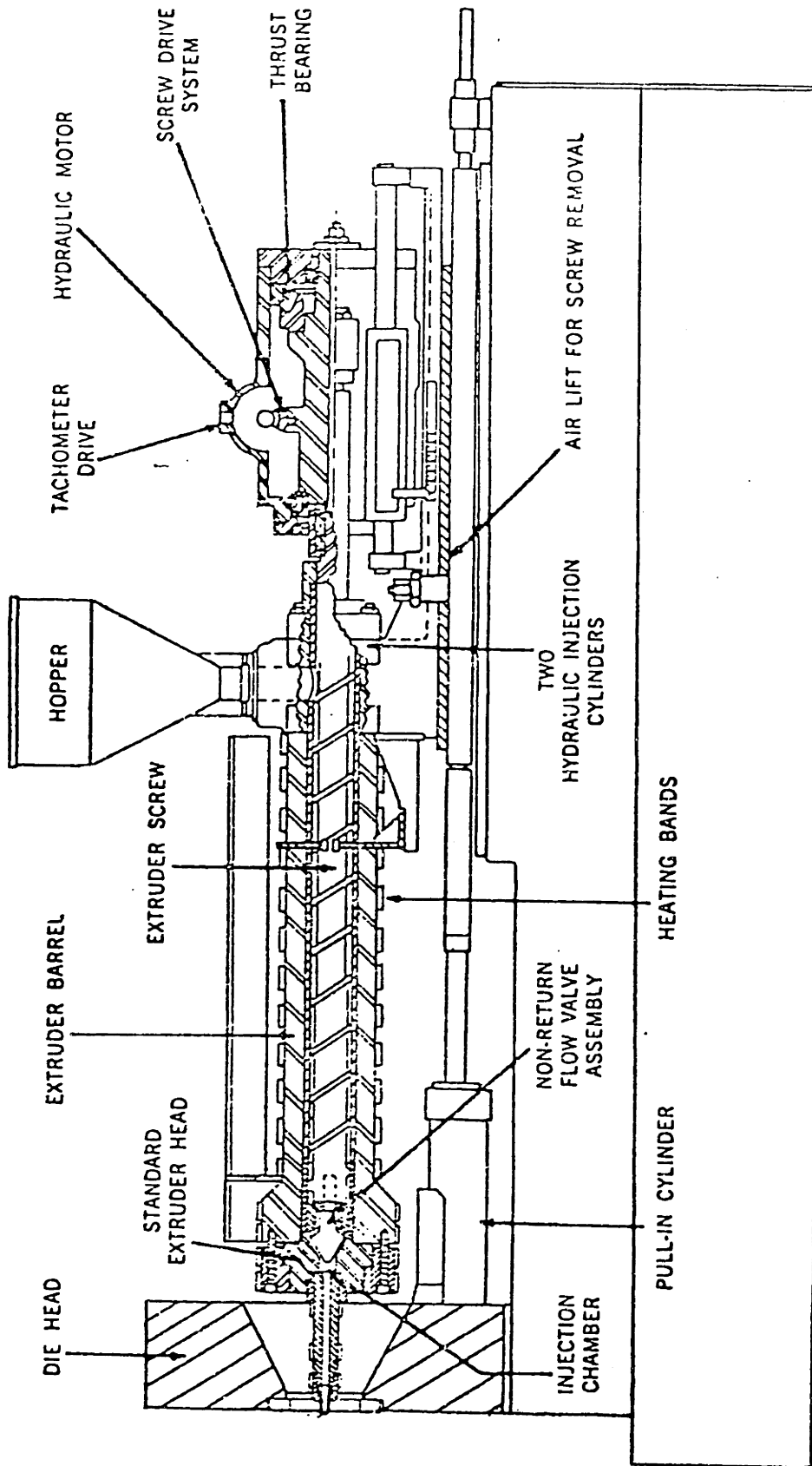


Figure I.1 Schematic drawing of the injection end of a reciprocating screw machine. (Courtesy Van Nostrand Reinhold Company)

cavity. A non-return valve near the screw tip limits the polymer back flow so that the screw effectively becomes a plunger. After the mold cavity is filled, continued pressure on the hydraulic ram forces more polymer into the cavity during the packing stage. As the molten polymer in the cavity is trapped due to freezing of the polymer at the mold gate, the screw begins turning, preparing the molten polymer for the next shot while the molten polymer in the cavity solidifies to the shape of the cavity. The mold opens after solidification and the part is ejected. When the mold closes the next injection cycle begins.

A typical cavity pressure curve for an injection cycle is shown in Figure I.2. The cavity pressure is an important process variable since it affects the state of the molding part directly. The four stages of the injection molding cycle can be readily inferred from the cavity pressure curve.

A more complete introduction to the injection molding process has been written by Rubin [I-2]. Several polymer processing books include the subject of injection molding, and detailed descriptions of the process are available [I-3,4,5,6].

I.3 Evaluation of Controls in Injection Molding

The injection molding process is fast and can be completely automated. Recently some injection molding machines have been automated extensively to include programmable

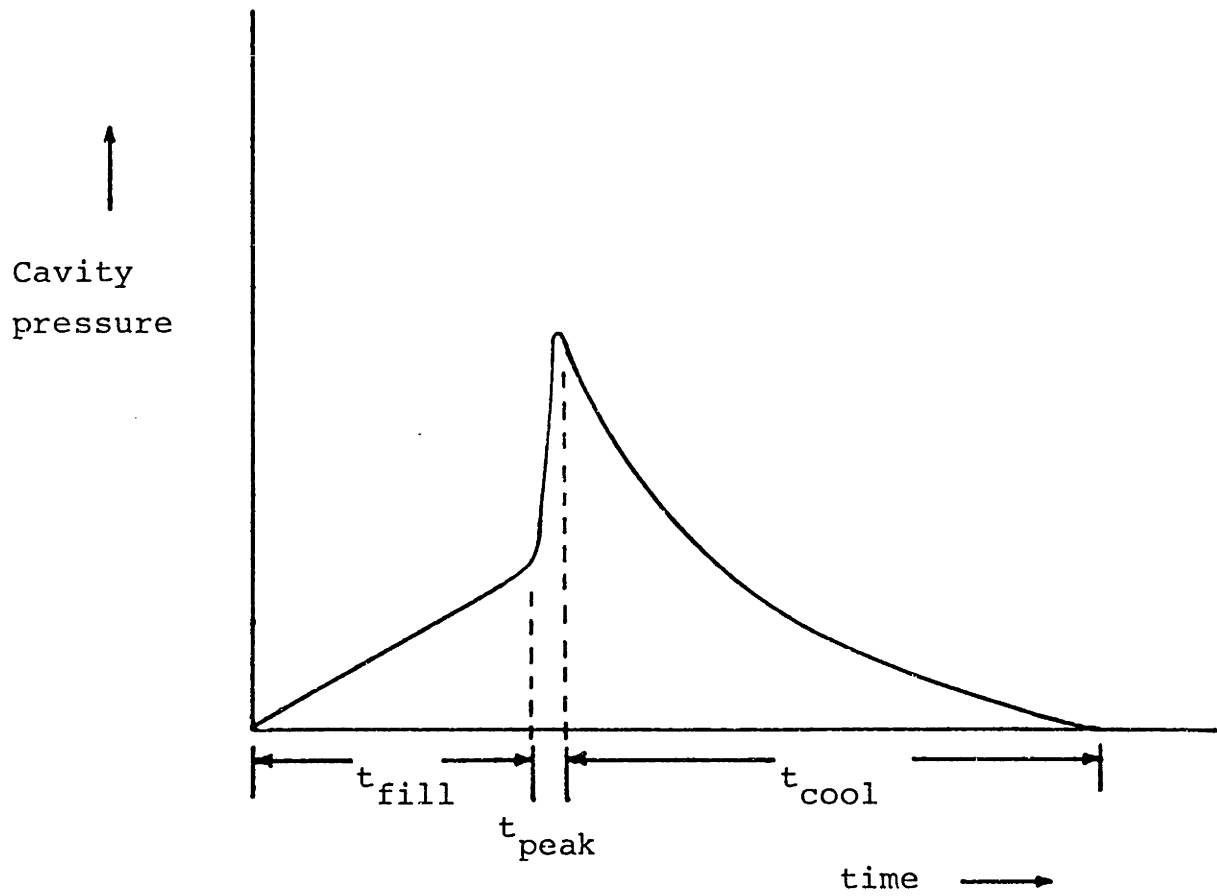


Figure I.2 : A typical cavity pressure curve for an injection cycle.

process control. For example, Maco IV made by Cincinnati Milacron is capable of controlling the velocity of the ram and peak cavity pressure control.

Preliminary evaluation of this modern injection molding control system, Maco IV, indicated that it can handle a 20% variation of molecular weight of incoming material. The test results are reported in Appendix A. The three types of polystyrene materials specifically prepared for this investigation by American Hoechst Co. have been processed successfully by the control system, Maco IV, to produce parts of the same weight. With an open-loop type control machine, it is impossible to process these materials due to the change in the melt viscosity.

J.N. Border [I-7] attempted to control the viscosity by changing the back pressure to produce a change in melt temperature. He found the relationship between a change in back pressure and a change in viscosity to be independent of material. Although his viscosity control scheme was inconclusive due to problems in obtaining a consistent measurement of the viscosity, his control scheme can be used to make an intelligent injection molding machine.

Based on the preliminary evaluation of modern injection molding systems and J.N. Border's work, it may be concluded that the melt viscosity can be adjusted with the current technology in modern injection molding equipment to produce acceptable parts.

J.R. Rinderle [I-8] has indicated that a high quali-

ty, precision part can be produced if the mold is preheated, filled at high pressures, and cooled at a variable rate. He presented a possible mold configuration and techniques for constructing such a mold. His method of heating the mold surface is by encapsulated resistance heaters. He tested a volume-controlled variable-conductance heat pipe as a means of providing controlled mold cooling. Since his mold surface is made of electroformed shell, the mold will deform inevitably under the molding pressure. He presented an analysis of mold deflections as a guide for the design of mold structures.

I.4 Project Goal

The goal of this project is to develop an injection molding system that can improve quality of the molded part. The research effort has been focused on development of a low thermal inertia mold to achieve the goal. Although the modern control schemes in the molding process do provide an adequate control of the process variables, it is difficult to achieve consistency due to coupling of the variables. It is hoped that the low thermal inertia mold uncouples the variables, and thus allows independent control of the process resulting in consistency of the improved part quality.

References for Chapter I

- I-1 Modern Plastics, Vol. 59, No. 1, (January, 1982)
pp. 77-87.
- I-2 Rubin, Irvin I. Injection Molding of Plastics,
John Wiley and Sons, Inc., New York, 1973.
- I-3 Middleman, Stanley Fundamentals of Polymer Processing,
McGraw-Hill Book Co., New York, 1977.
- I-4 McKelvey, James M. Polymer Processing, John Wiley
and Sons, Inc., New York, 1962.
- I-5 Tadmore and Gogos Principles of Polymer Processing,
John Wiley and Sons, Inc., New York, 1979.
- I-6 Bernhardt, E.C. Processing of Thermoplastic Materials,
Robert E. Krieger Publishing Co., New York, 1959.
- I-7 Border, J.N., "Intelligent Injection Molding,"
Master of Science Thesis, M.I.T., June 1981.
- I-8 Rinderle, James R., "A Method for Precision Injec-
tion Molding," Master of Science Thesis, M.I.T.
June 1979.

CHAPTER IIPROBLEMS IN INJECTION MOLDINGII.1 Introduction

Although the injection molding process has many advantages, there are some inherent problems.

One serious flaw of the conventional injection molding process is that the filling process is coupled with the cooling process. As the molten polymer fills the cold mold cavity it starts to cool from the mold surface where the melt comes in contact. Since the polymer cannot be injected into the mold instantaneously, the melt at every point undergoes different thermal history due to cooling while it is being injected. This temperature change within the melt changes the thermodynamic state of the melt. Because of the coupling it is difficult to control the state of the melt in the conventional injection molding process. This coupling, therefore, directly results in inconsistency of the molded part.

Another major problem is that it requires high temperature and pressure to mold a thin part. As the melt comes in contact with a cold mold surface during the injection stage, a thin layer of frozen plastic called "skin" is formed. In molding a thin part the thickness of the skin layer approaches the half thickness of the part. In order to overcome the freezing of the melt which blocks the flow path, extremely

high pressure and temperature are used so that the cavity is rapidly and completely filled.

The high temperature causes high thermal shrinkage and therefore requires high packing pressure to compensate elastically the thermal shrinkage. This subject is discussed in detail in Section III.2.

The high pressure causes high flow-induced molecular orientation which in turn increases residual stresses. The orientation freezes as the melt vitrifies. This frozen-in molecular orientation imparts anisotropic residual stresses.

Molded parts with anisotropic residual stresses exhibit not only anisotropic mechanical and optical properties, but also poor impact strength and poor resistance to heat-shrinkage. Moreover, the condition of parts is often not stable. Dimensions and other properties of parts can change for weeks after molding due to relaxation of residual stresses.

To eliminate these molding problems it is necessary to understand how the properties of a molded part depend on the condition or state of a molding. This topic is discussed in Section II.2. In the section which follows it, some inherent problems associated with the injection molding process are summarized.

II.2 The Effect of the Molded Condition on Mold Part Properties

In 1950, Spencer and Gilmore [II-1] published a paper on residual strains in injection molded polystyrene. The authors discussed the origin of residual strain in injection molded pieces, means of relieving or preventing residual strains, and their effect on crazing and on the mechanical properties of the molding. They stated that reduction in the amount of frozen orientation resulted in improved crazing resistance, dimensional stability on heating, and consistency.

Jackson and Ballman [II-2] wrote an article which discussed the effect of molding conditions on orientation and the effect of orientation on the mechanical properties of moldings. They reported the strong influence of molecular orientation on tensile strength, elongation at failure, and notched impact strength.

Johnson [II-3] conducted experiments to investigate strain-free injection molding and published his findings in 1963. He found that relatively strain-free parts can be obtained by heating the mold near to the melt temperature to relieve molding strains within the mold.

Koda [II-4] carried out statistically designed experiments to study the effects of molding conditions on the properties of polycarbonate. He found that reduction of frozen orientation resulted in improved abrasion resistance and decreased heat shrinkage. He stated that moldings with low

residual stresses could be molded at a high mold temperature and at a low holding pressure. He also stated that the extension of molecular orientation can be controlled by the initial temperature of the melt or its cooling rate.

Menges and Wubken [II-5] studied the influence of processing conditions on molecular orientation in injection moldings. They concluded that the main direction of orientation in plane-shaped moldings is the flow direction. They also found that the orientation is highly biaxial at the surface of the molding and that there is very little orientation in the center of moldings. The frozen orientation is reduced when the melt temperature is increased. Increasing cavity wall temperature has a similar effect in relaxing the orientation. An increase in injection rate results in a slightly higher surface orientation while the internal orientation is significantly reduced.

Y.T. Koita [II-6] considered the effect of packing and discharge on the injection molded parts. Photoelastic stress patterns suggested that packing and discharge give rise to high frozen stresses due to molecular orientation in the gate area. Degradation of mechanical properties of the specimen resulted in the high frozen stress region at the gate.

Tadmor [II-7] proposed a semiquantitative model to explain the complex molecular orientation distribution observed in injection moldings of amorphous polymers. The bead and spring macromolecular theory was used to calculate root mean end to end distances of macromolecules in the various

flow fields and the relaxation process. The model assumes that the orientation in the surface skin is related to steady elongational flow in the advancing front and the orientation in the core is related to the shear flow.

Burkle [II-8] used a modified milling method to measure inherent stresses in molded thermoplastic materials. His data on fourteen different samples does not correlate well with the theory he presents to estimate residual stress. He states that the inherent stress decreases with increasing mold temperature. He also states that the injection temperature has almost no significant effect on residual stress. This seems contradictory to earlier works [II-5].

In 1976, Menges et al. [II-9] published a study on relaxation of molecular orientation in plastics. They found that the relaxation process in an injection molding die is governed by the WLF (Williams, Landel, Ferry) equation [II-10]. They reported a method to estimate the relaxation of molecular orientation from a knowledge of the temperature-time history of the material.

Han and Villamizar [II-11] carried out an experimental study to investigate the development of stress birefringence patterns of molten polymer during the mold filling and cooling operation. Their study showed how molding conditions influence the distribution of stress birefringence patterns. They showed that mold temperature influences the amount and distribution of residual stress in the molded part and that the residual stress is intimately related to its mechanical

properties and dimensional stability of heating.

Bakerdjian and Kamal [II-12] studied anisotropic physical properties of injection-molded parts. They reported the three-dimensional variation of density, heat shrinkage, birefringence and tensile strength. The lowest heat shrinkage values, for example, are found near the center of the molding, where the polymer chains have the greatest chance to relax and assume a more random configuration.

Hoare and Hull [II-13] studied the effect of orientation on the mechanical properties of injection molded polystyrene. They regarded the molding as a composite structure of materials with different degrees of anisotropy and orientation. They concluded that the crazing behavior and crack mechanism can be predicted from the properties of hot drawn sheet.

Dietz, White, and Clark [II-14] presented a study of the development of orientation distribution and relaxation of the orientation in injection molding of amorphous polymers. Their predictions of orientation development are based on the assumption that the stress-optical laws are valid in the molten state. They also assumed that the melt relaxes in a Maxwellian manner. Their analysis predicts the birefringence distribution in injection molded parts fairly well.

In 1982, Isayev [II-15] reported a study of a coupled effect of the flow induced and thermally induced orientation in the molded part. He measured three components of birefringence and related these to the processing conditions.

His work is based on the constitutive equation of Leonov [II-16]. The experimental results are in good agreement with Leonov's theory.

Crouthamel et al. [II-17] studied the effects of processing conditions on the residual stresses of the molded part using the layer-removal technique of Treuting and Read [II-18]. They found that residual stresses in the molded part depend on the orientation with respect to flow during cavity filling, and on the distance from the gate. They concluded that injection rate and mold temperature have a minor effect on the level and distribution of molding stress, while melt temperature has a significant effect. Their mold temperature, however, varies only from 40°C to 60°C.

Hubbauer [II-19] stated that physical properties of a molded part can be improved by optimizing processing conditions such as injection pressure, melt temperature, injection rate and mold temperature. He did not, however, mention a method of optimizing processing conditions.

Fritch [II-20] studied the effect of mold temperature on impact strength. He concluded that mold temperature influences the molded part properties to a significant degree. However, he pointed out a need to compromise in raising mold temperature and in minimizing cycle time. He showed that the improvement of impact strength is greatest at low melt temperature and at high mold temperature.

Burke and Newcome [II-21] made an assessment of the mold temperature influence on molded part quality of semicrys-

talline polymer. Mold temperature can directly influence the physical properties of semicrystalline material since it affects the degree of crystallinity. They recommended higher mold surface temperature for a thinner part to ensure full crystallinity.

II.3 Summary

In the previous section, literatures of many investigators regarding the effects of processing conditions on the properties of injection molded parts were surveyed. Most of the researchers indicated that processing conditions are interrelated to molded part properties in a complex manner. Common processing variables were mold temperature, melt temperature, and injection rate. Most of the works related molded part properties to the level and distribution of molecular orientation. Many investigators attempted to predict an anisotropical residual stress distribution resulting from the flow-induced orientation. Although the relationship between part properties and processing conditions is complicated, quality of the molded part can be improved by increasing mold temperature.

Mold temperature, of all the process variables, can have the greatest influence on reducing residual stresses of molded parts. The general properties of the molded part are improved when the residual stress is reduced. In other words, an isotropic and homogeneous part has, in general, improved

part qualities. The main cause of the residual stresses is the frozen-in molecular orientation in the molded part. It can be concluded, therefore, that the minimization of residual stress through the relaxation of molecular orientation improves the molded part quality.

References for Chapter II

- II-1 Spencer, R.S. and G.D. Gilmore, "Residual Strains in Injection Molded Polystyrene," Modern Plastics, (December 1950).
- II-2 Jackson, G.B. and R.L. Ballman, "The Effect of Orientation on the Physical Properties of Injection Molding," SPE Journal, (October 1960), p. 1147.
- II-3 Johnson, L.I., "Strain-free Injection Molding," Modern Plastics, 40, (June 1963), p. 111.
- II-4 Koda, Hiroyuki, "Effects of Molding Conditions on Properties of Injection Molded Polycarbonates," Journal of Applied Polymer Science, 12, (1968), p. 2257.
- II-5 Menges, G. and G. Wubken, "Influence of Processing Conditions on Molecular Orientation in Injection Moldings," presented at the Society of Plastics Engineers 31st Annual Technical Conference, Montreal, May 1973.
- II-6 Koita, Y.T., "Packing and Discharge in Injection Molding," Polymer Engineering and Science, 14, 12, (December 1974).
- II-7 Tadmor, Z., "Molecular Orientation in Injection Molding," Journal of Applied Polymer Science, 18, (1974), p. 1753.
- II-8 Burkle, Dieter, "Measurement of Inherent Stresses in Plastic Mouldings," Kunststoffe, 6, (January 1975).
- II-9 Menges, G., P. Thienel and G. Wubken, "A Method to Estimate the Relaxation of Molecular Orientation in Plastics," Kunststoffe, 66, (January 1976), p. 42-48.
- II-10 Williams, M.L., R.F. Landel and J.D. Ferry, Journal of the American Chemical Society, 77, (1955), p. 3701.
- II-11 Han, C.D. and C.A. Villamizar, "Measurement of Pressure and Stress Birefringence Patterns During the Mold Filling and Cooling Operation," presented at the Society of Plastics Engineers 35th Annual Technical Conference, Montreal, 1977.

- II-12 Bakerdjian, Z. and M.R. Kamal, "Distribution of Some Physical Properties in Injection Molded Thermoplastic Articles," Polymer Engineering and Science, 17, 2, (February 1977).
- II-13 Hoare, Linda and Derek Hull, "The Effect of Orientation on the Mechanical Properties of Injection Molded Polystyrene," Polymer Engineering and Science, 17, 3, (March 1977).
- II-14 Dietz, White, and Clark, "Orientation, Development and Relaxation in Injection Molding of Amorphous Polymers," Polymer Engineering and Science, 18, 4, (March 1978), p. 273.
- II-15 Isayev, A.I., "Orientation Development in the Injection Molding of Amorphous Polymers," presented at the Society of Plastic Engineers 40th Annual Technical Conference, San Francisco, 1982, p. 288.
- II-16 Leonov, A.I., Rheol. Acta, Vol. 15, 1976, p. 85.
- II-17 Crouthamel, Isayev, and Want, "Effect of Processing Conditions on the Residual Stresses in the Injection Molding of Amorphous Polymers," presented at the Society of Plastics Engineers 40th Annual Technical Conference, San Francisco, 1982, p. 295.
- II-18 Treuting and Read, Journal of Applied Physics, Vol. 22, 1951, p. 130.
- II-19 Hubbauer, P., "Effects of Processing Conditions on Plastic Parts," presented at the Society of Plastics Engineers 40th Annual Technical Conference, San Francisco, 1982, p. 302.
- II-20 Fritch, L.W., "How Mold Temperature and Other Molding Variables Affect ABS Falling Part and Izod Impact," presented at the Society of Plastics Engineers 40th Annual Technical Conference, San Francisco, 1982, p. 332.
- II-21 Burke and Newcome, "Essential Parameters for Molding Modified PET Resins: An Assessment of Their Influence on Molded Part Quality," presented at the Society of Plastics Engineers 40th Annual Technical Conference, San Francisco, 1982, p. 336.

CHAPTER IIIMETHODS OF IMPROVING THE MOLDED PART QUALITYIII.1 Introduction

In reviewing literature on injection molding (Chapter II), it is clear that anisotropical residual stress in the molded piece is the single most important cause of degraded part quality. For example, impact strength, crazing resistance, dimensional stability, abrasion resistance, and resistance to heat shrinkage will be improved by minimizing the residual stress. In order to eliminate many molding problems, the residual stress must be minimized.

In the injection molding process, development of stresses due to molecular orientation during the injection stage is unavoidable. Reduction of the developed stress can be achieved by heating the mold, thereby allowing the relaxation of the stress before the vitrification of the melt. Since the same mold must be heated and cooled quickly to shorten the injection cycle time and to improve the molded part quality, a low thermal inertia mold is needed. Development of a low thermal inertia mold is discussed in Chapter V.

A low thermal inertia mold is quite useful in improving the molded part quality. Isothermal filling and differential cooling processes can be achieved with the low thermal inertia mold. Unique advantages of the isothermal filling

process and the differential cooling process will be described in Sections III.2 and III.3, respectively.

III.2 Isothermal Filling Process

When the surface of a mold is at the same temperature as the incoming molten polymer, the filling process can be done isothermally. Upon the completion of filling, the surface temperature of the mold is lowered to cool the part. A plot of the temperature curve of the mold surface for an isothermal filling process is shown in Figure III.1. When the parts are produced this way, the quality of the molded part is improved due to the relaxation of the flow-induced molecular orientation. In conventional molding, however, the molecular orientation is frozen before it relaxes completely, thereby producing an anisotropically oriented part. This anisotropical molecular orientation degrades the mechanical and the optical properties of the molded part. Therefore, an isothermal filling process can improve the general quality of the part.

There are other advantages in injection molding with the isothermal filling process. For example, the process is capable of producing a high quality optical part. An optical part must have a uniform index of refraction across the whole section of the part. In conventional injection molding, however, molding a part with a uniform index of refraction is very difficult to achieve due to frozen-in molecular orienta-

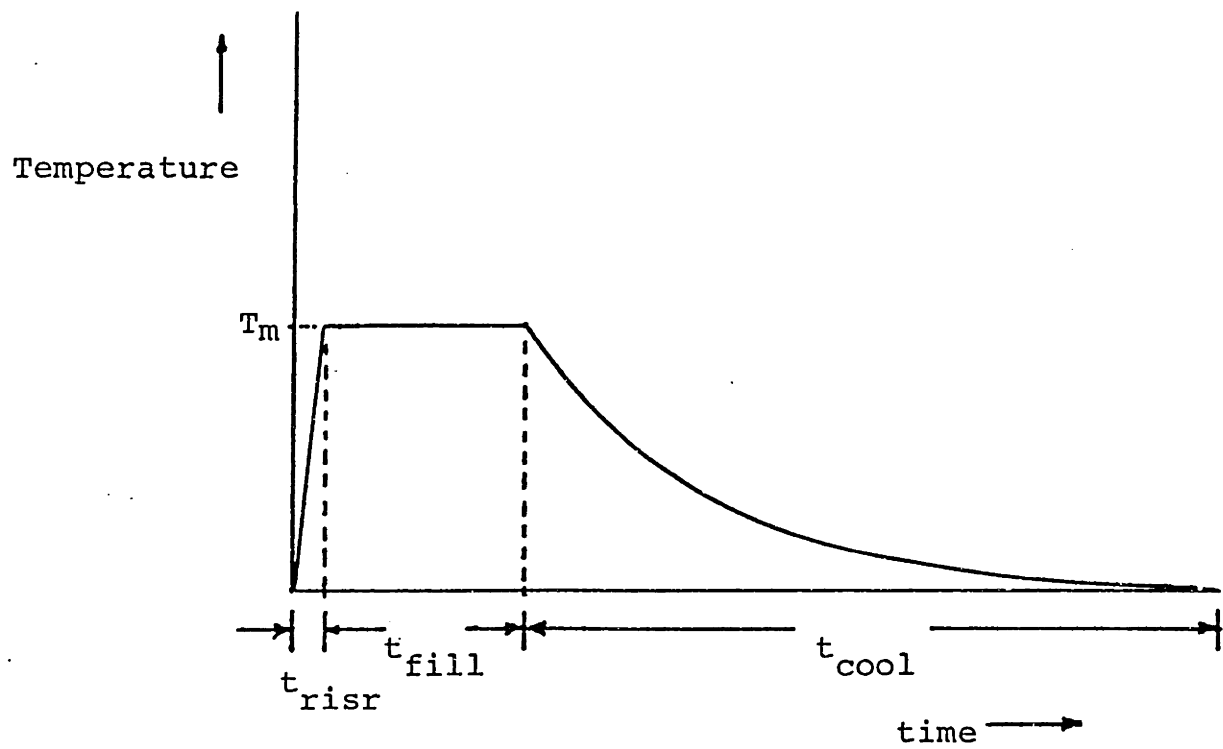


Figure III.1 : A plot of temperature curve of the mold surface for an isothermal filling process.

tion near the surface of the part. Figure III.2 depicts a schematic comparison between the conventional process and the isothermal filling process in molding an optical part. In conventional molding, the macromolecules, elongated due to shear stress near the surface, freeze when they come in contact with the cold mold surface; consequently, the index of refraction at the surface and the core section is different as shown in Figure III.2, part a. In order to make a part without frozen-in molecular orientation, it is necessary to relax the orientation. The relaxation process can occur simultaneously as the molten polymer fills the cavity isothermally. A complete relaxation of the flow-induced orientation is possible if the surface temperature of the mold remains the same for some time after the isothermal filling has been completed. A detailed analysis of stress relaxation of the isothermal filling process is written in Chapter IV.

Since there is no solidification layer along the surface of the mold during the isothermal filling process, the required pressure to fill the mold is less than that of the conventional mold filling process. As the L/t ratio (L = length, t = thickness of the part) increases, the solidification layer buildup increases in the conventional process and thus the area that the molten polymer passes through to fill the mold decreases. The reduction of the area directly results in an increase of the pressure requirement to fill the mold at the same filling rate. When the L/t ratio is too large such that the reduction of the area completely closes

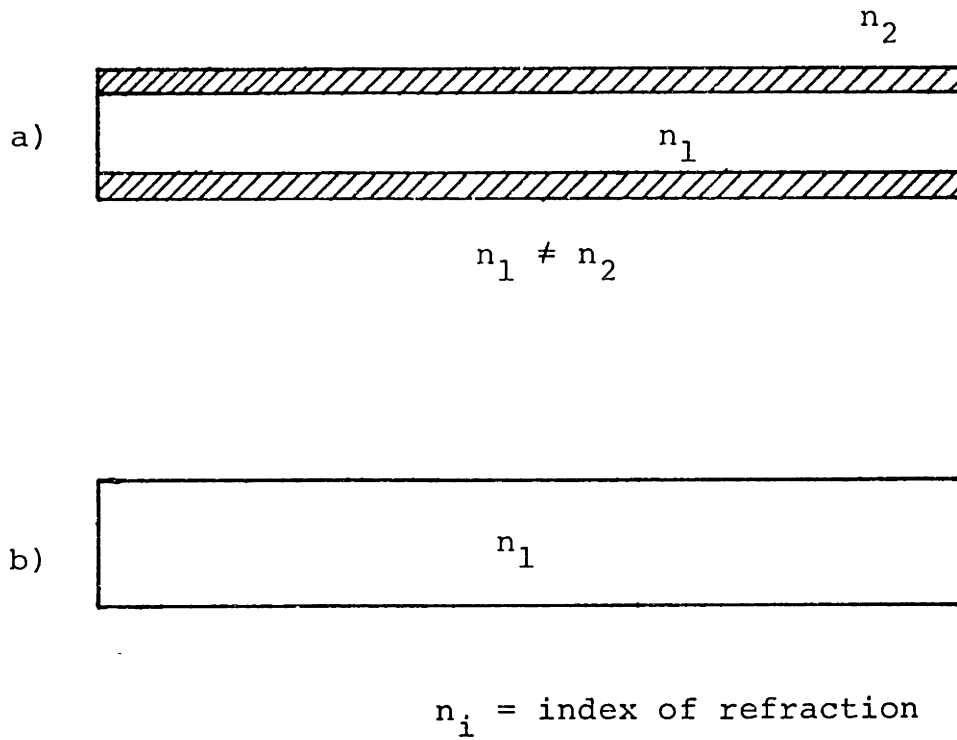


Figure III.2 : Schematic comparison between a) conventional and b) isothermal filling process in molding an optical part.

off the polymer passage, the mold cavity cannot be filled completely; this is termed "short shot." In the isothermal filling process there is no pressure drop due to the reduction of the area in the mold cavity. Moreover, shear stress will be reduced because of the lesser pressure gradient. The reduced shear stress results in a decrease of flow-induced molecular orientation.

Another advantage of the isothermal filling process is the lower packing pressure requirement for zero thermal shrinkage. The density of polymeric material at solid state is higher than that of molten polymer. In other words, the volume of polymeric material becomes smaller when the molten polymer solidifies. Therefore, in injection molding process a high packing pressure is needed for elastic deformation to compensate for the thermal shrinkage. However, with the isothermal mold filling process, the pressure required to compensate for thermal shrinkage can be reduced if initial melt temperature can be lowered.

Spencer and Gilmore [III-1,2] proposed a state equation to relate the temperature, pressure, and volume of polymer materials. The equation they proposed:

$$(P + \pi) (v - \omega) = RT \quad (1)$$

where

P = pressure
 T = temperature
 v = specific volume
 π, ω, R = material properties

is only valid for amorphous materials above the glass transition temperature. We can use the Spencer-Gilmore equation (1) to estimate the pressure required to compensate for thermal shrinkage.

Rinderle [III-3] has considered the elastic and thermal expansion of steel molds and plastics, and concluded that the volume changes of the mold can be neglected to obtain an approximate solution of the volume changes in plastics during the molding process. Rearranging equation (1), and substituting the injection temperature, T_i , and the average final temperature, T_f , the following two equations can be written:

$$P_i = \frac{RT_i}{(v_i - \omega)} - \pi \quad (2)$$

$$P_f = \frac{RT_f}{(v_f - \omega)} - \pi \quad (3)$$

For zero volume change:

$$v_i = v_f \quad (4)$$

and

$$P_f = P_{atm} \quad (5)$$

$$P_f \ll \pi \quad (6)$$

Equations (2) and (3) can be combined to determine the injection pressure for zero volume change in terms of the injection temperature and the average final temperature:

$$P_i = \left(\frac{T_i}{T_f} - 1 \right) \pi \quad (7)$$

The pressure required, P_i , can be reduced in the isothermal filling process because the injection temperature, T_i , in equation (7) can be lowered since the freezing of plastic during the filling stage is no longer an issue. With the decreased injection temperature, the time required to cool the part is correspondingly shortened.

One more advantage of the isothermal filling process is the consistency of the part. Since the temperature of the molten polymer in the mold cavity is the same throughout the entire cavity upon cessation of the flow and the cavity volume does not change, the pressure of the polymer melt must remain the same everywhere within the cavity. If the injection temperature and the mold surface temperature can be controlled from one injection cycle to the next, then the state of polymer in the cavity can be controlled thereby enabling one to produce consistent parts.

The low thermal inertia mold is not only capable of

handling the isothermal filling process, but also can handle the differential cooling process. Benefits from the differential cooling process are discussed in the next section.

III.3 Differential Cooling Process

A differential cooling process is defined as a controlled cooling process in which every section of the molded part is cooled uniformly so as to maintain a constant pressure throughout the molded part. In reality, the part can not be cooled uniformly by conduction since the heat transfer by conduction itself requires a temperature gradient. Although completely homogeneous parts can not be molded, one can minimize the deleterious effects of the secondary flow caused by density variations within the part. A concept of a differential cooling process that can eliminate the secondary flow of plastic from the thick to the thin sections is illustrated in this section.

Consider molding the part shown in Figure III.3. The part consists of a thin and a thick section. When the part is cooled from the molten state in a constant temperature mold, the thick section cools more slowly than the thin section because of the thermal insulation properties of the plastic. The average temperature in the thick section, therefore, is higher than that in the thin section during the cooling process. From the Spencer-Gilmore equation (1), it can be seen that the pressure of plastic is higher at higher tempera-

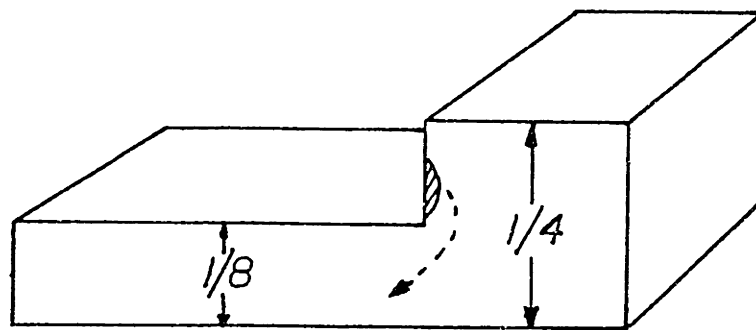


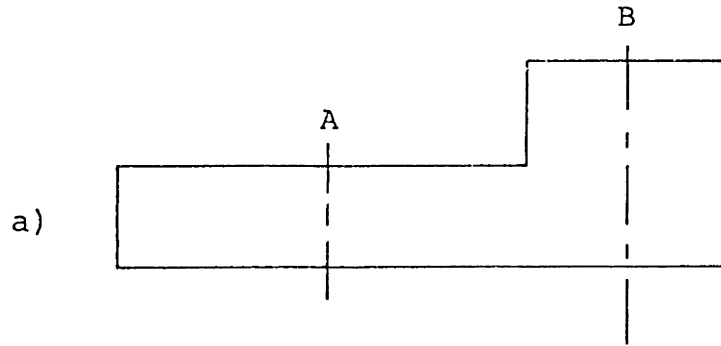
Figure III.3 : A difficult part to mold because of the change in part thickness.

tures of the plastic provided that the volume remains constant. Consequently, there is a secondary flow of plastic from thick to thin sections during the cooling process due to the pressure gradient. The secondary flow results in surface depressions known as "sink marks".

The differential cooling process minimizes the secondary flow of plastic from one section to another. There are two approaches to differential cooling of the part. One is to change the heat transfer rate by controlling the surface temperature of the mold. The other is to change the heat transfer coefficient through the thickness variation of the insulation which surrounds the part. The first method will be referred to as an active control method, and the latter will be referred to as a passive control method. Each method has its own advantages and disadvantages.

It is advantageous to use the active control method for a geometrically simple part. The simplest geometry of a part which requires the differential cooling process to prevent the secondary flow is shown in Figure III.3. A two-dimensional drawing of the part is shown in Figure III.4a. An active differential cooling for the part is shown in Figure III.4b. The effect of the active control method is simulated by one dimensional heat conduction analysis along the sections A and B shown in Figure III.4a.

When the vitrification rates are the same the temperature gradient between the two sections is minimized and thereby reduces the pressure gradient. Consequently the



Temperature of the
mold surface

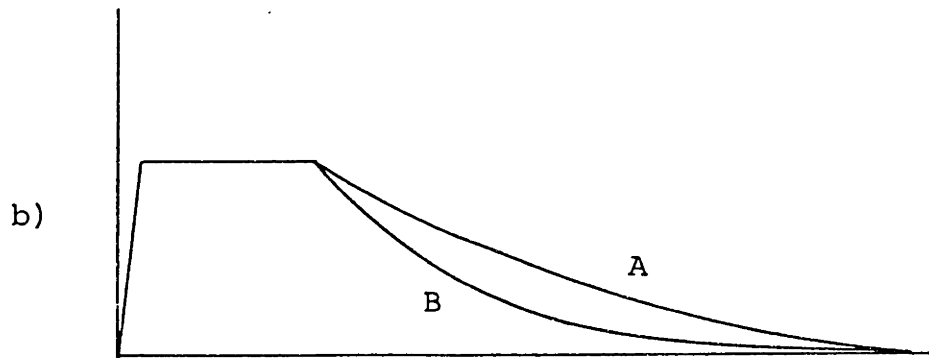


Figure III.4 : a) Two dimensional drawing of the part.
b) Differential cooling for the part.

secondary flow from thick to thin sections can be minimized. The surface temperature at the thin section is lowered more slowly than that at the thick section in order to minimize the vitrification rate difference between the two sections.

It is advantageous to use a passive control method for a part of continuously varying cross section. The passive method controls the rate of vitrification by varying the insulation thickness. The rate of vitrification is slower through the thicker insulation layer. Therefore, a thin section of the part can be cooled at the same rate as a thick section, if an appropriate insulation layer is applied around the thin section.

The passive control of vitrification rates of plastic along the thin and thick sections have been simulated, and the results are shown in Figure III.5. The program first computes the optimum insulation thickness for which the average difference in the vitrification rates along the thin and thick sections is minimized. Then, it plots the vitrification rates using the optimum insulation layer thickness. The results indicate that the vitrification rates can be controlled reasonably well with the passive control method.

Some injection molded parts have a continuously changing cross section. For example, optical parts such as lenses must have a smoothly varying cross section. The vitrification rates in the varying cross section can be passively controlled by applying an appropriate insulation layer along the varying cross section. For simplicity, a linearly varying

cross section has been simulated with the passive control method to minimize the vitrification rate differences. The results are shown in Figure III.6.

Neither the active nor the passive control method increases the injection cycle time. Both methods control the vitrification rates at the thinner sections so that they are the same as those at the thicker sections. The cycle time, therefore, does not increase since the thickest section of the part must also vitrify before ejecting the part.

The effects of an isothermal filling and a differential cooling process on the quality of the molded part have been discussed in this chapter. The part quality can be improved with the low thermal inertia mold because the isothermal filling and the differential cooling processes can be achieved with the mold. These processes affect the residual stresses in the final part. A detailed study of the stress relaxation is presented in the next chapter.

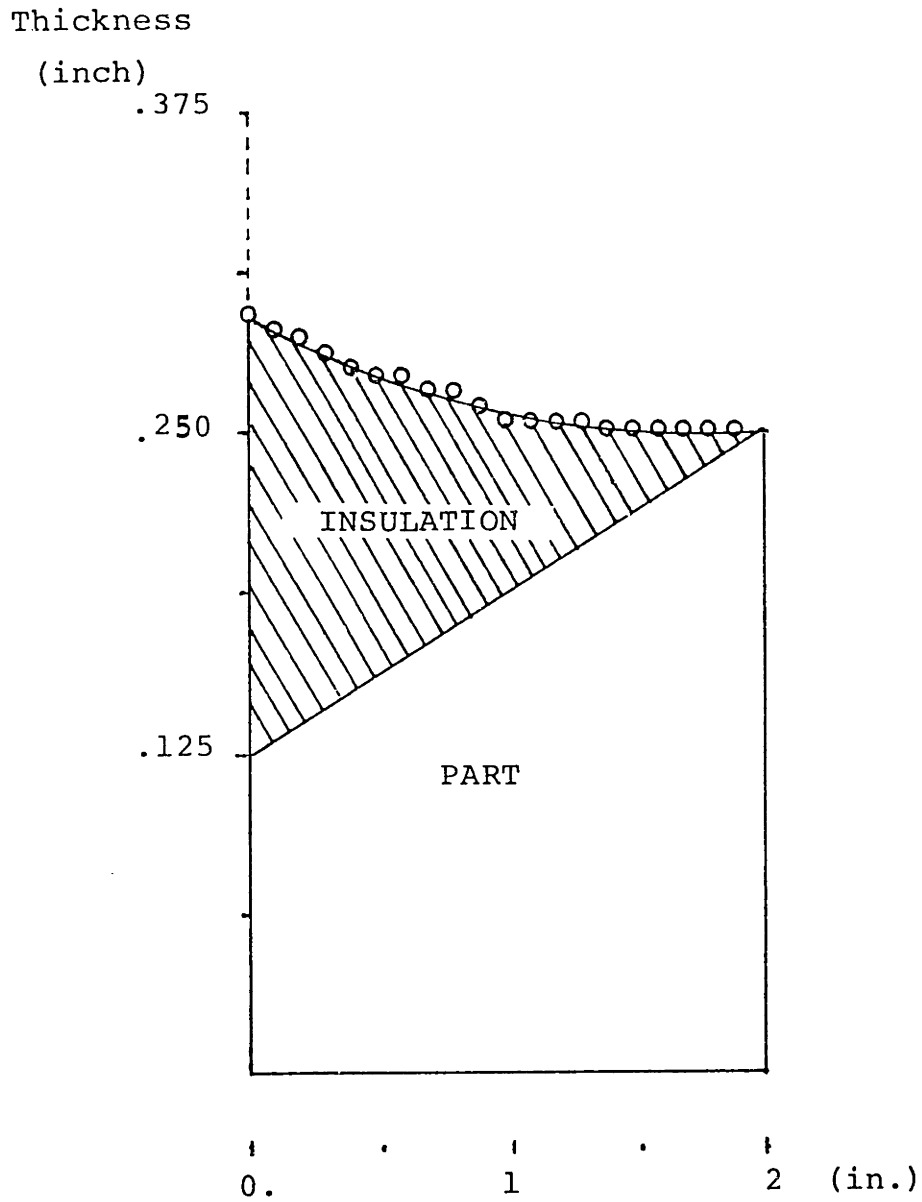


Figure III.6 : The insulation thickness required to minimize the vitrification rate difference along the linearly varying thickness of the part. ($\alpha_p = .01 \text{ in}^2/\text{s}$, $\alpha_I = .1 \text{ in}^2/\text{s}$)

References for Chapter III

- III-1 Spencer, R.S. and G.D. Gilmore, "Equation of State for Polystyrene," Journal of Applied Physics, 20, (1949), p. 502.506.
- III-2 Spencer, R.S. and G.D. Gilmore, "Equations of State for High Polymers," Journal of Applied Physics, 21, (June 1950)
- III-3 Rinderle, James R., "A Method for Precision Injection Molding," Master of Science Thesis, M.I.T., June 1979.

CHAPTER IVANALYSIS OF STRESS RELAXATIONIV.1 Introduction

In order to predict the residual stresses in the injection molded part, a rheological constitutive equation that can characterize the nonlinear viscoelastic flow behavior of the polymer melt must be used. In this thesis the Wagner's [IV-1,2] integral type constitutive equation is employed. Using the Wagner's model the stress relaxation is predicted from the instant the mold is filled by fully developed simple shear flow. Although a differential type constitutive equation developed by Leonov [II-16,IV-3] is quite successful in describing the nonlinear viscoelastic behavior [IV-4,5], it is not used in this research. The origin of Leonov's model is based on nonequilibrium thermodynamics, and it is difficult to understand its derivation.

The Wagner's constitutive equation and the stress-optical law will be described in detail in Sections IV.2 and IV.3, respectively. In the next section, IV.4, a prediction of isothermal stress relaxation upon cessation of fully developed simple shear flow will be made. A nonisothermal stress relaxation of an injection molded part will be discussed in Section IV.5.

IV.2 The Wagner Model

(a) Background

The Wagner's constitutive equation is a straight-forward generalization of the rubberlike-liquid constitutive equation given by Lodge [IV-6,7]:

$$\underline{\sigma}(t) + P\underline{I} = \int_0^{\infty} \circ\mu(t-t') \underline{C}^{-1}(t-t') d(t-t') \quad (1)$$

where $\underline{\sigma}$ is the stress tensor at the current time t , P the hydrostatic pressure, \underline{C}^{-1} the Finger relative strain tensor between the states t and t' , and $\circ\mu$ is the memory function describing the linear viscoelastic behavior specific for the material. Lodge's equation is based on the molecular network theories. He modeled the polymers as a network of interacting chains that form a junction. The junction is defined as a temporary entanglement between two chains constraining it. The network segment is defined as part of a chain between any two successive junctions. During deformation, the junctions, being impermanent, are created and lost thereby forming new segments.

The Wagner model makes two additional assumptions starting from Lodge's equation [IV-8]:

1) The Disentanglement Assumption: There are two independent decay mechanisms for a segment of type i . One is through time dependent relaxation with probability $1/\tau_i$ as in Lodge's formulation. The other is through additional disentanglement

with increasing deformation. The probability that a network segment will survive during a deformation between its created time t' and the present time t is equal to a so-called damping function $h(I_1, I_2)$ and independent of the types of the segment. $h(I_1, I_2)$ is equal to 1 in the linear viscoelastic range because h is a deformation-dependent survival probability. In the nonlinear viscoelastic range, h is less than 1.

2) The Irreversibility Assumption: Segments are lost irreversibly during a nondecreasing deformation, and are not reformed or retardation of deformation. The deformation-dependent survival probability h is therefore a function of the strain:

$$h(I_1, I_2) = \text{Min}_{t'}^t (h[I_{1_{t,t'}}, I_{2_{t,t'}}]) \quad (2)$$

where $h(I_1, I_2)$ is the survival probability, and Min is a functional operator which gives the minimum value attained by h between t' and t .

Wagner proposed the memory function for the nonlinear viscoelastic behavior (μ), and expressed as a product of the memory function for the linear behavior ${}^\circ\mu$ and a so-called damping function $h(I_1, I_2)$. The damping function depends on the first and second invariants of the Finger tensor:

$$\mu = {}^\circ\mu(t-t') h(I_1, I_2) \quad (3)$$

(b) Steady Shear Flow

A unidirectional steady shear flow at constant shear rate and constant volume may be described in terms of the relative shear strain $\gamma_{t,t'}$ for the relative Finger strain tensor $\underline{C}_t^{-1}(t')$ [IV-9]:

$$\underline{C}_t^{-1}(t') = \begin{bmatrix} 1 + \gamma_{t,t'}^2 & \gamma_{t,t'} & 0 \\ \gamma_{t,t'} & 1 & 0 \\ 0 & 0 & 1 \end{bmatrix} \quad (4)$$

The relative shear strain $\gamma_{t,t'}$ is the difference between the shear strain at the current time t and the past time t' .

The invariants of $\underline{C}_t^{-1}(t')$ are given as follows:

$$I_1 = I_2 = 3 + \gamma_{t,t'}^2 \quad (5)$$

$$I_3 = 1 \quad (6)$$

The shear stress τ_{12} and the primary normal stress difference $[\tau_{11} - \tau_{22}]$ for simple shear flow can be obtained from equations (1) and (4).

$$\tau_{12}(t) = \int_0^t \mu(t-t') \gamma_{t,t'} d(t-t') \quad (7)$$

$$[\tau_{11} - \tau_{22}](t) = \int_0^\infty \mu(t-t') \gamma_{t,t'}^2 d(t-t') \quad (8)$$

The linear memory function is approximated by a sum of exponential functions with time constants τ_i and weight factors a_i [IV-8,9,10]:

$$\sigma_{\mu}(t-t') = \sum_i a_i \exp\left[-\frac{t-t'}{\tau_i}\right] \quad (9)$$

The time constants τ_i and the weighting factors a_i in equation (9) can be obtained from a small-amplitude oscillatory shear flow experiment. Details of obtaining these parameters are discussed in Section IV.2, part (c).

Wagner proposed a single exponential function for the approximation of the damping function $h(\gamma_{t,t'})$:

$$h(\gamma_{t,t'}) = \exp[-n\gamma_{t,t'}] \quad (10)$$

A more accurate description of the damping function has been obtained by a sum of two exponential functions, as proposed by Osaki [IV-11]:

$$h(\gamma_{t,t'}) = f_1 \exp[-n_1\gamma_{t,t'}] + f_2 \exp[-n_2\gamma_{t,t'}] \quad (11)$$

Equation (11) is characterized by three parameters; n_1 , n_2 , and $f_1 = 1-f_2$.

The shear stress and the primary normal stress difference calculated for the single exponential damping function can easily be generalized for a damping function represented by a sum of exponential functions. For example, the shear stress for a damping function represented by a sum of two exponential functions can be obtained by a linear superposition of shear stress given by each of the single exponential damping functions.

$$\tau_{12}(t, n_1, n_2) = f_1 \tau_{12}(t, n_1) + f_2 \tau_{12}(t, n_2) \quad (12)$$

Thus, calculations will be made with the single exponential damping function for simplicity.

The following relations for the shear stress and the primary normal stress difference are obtained from equations (7), (8), (9), and (10).

$$\tau_{12}(t) = \sum_i a_i \int_{t-t'=0}^{\infty} \exp\left[-\frac{(t-t')}{\tau_i}\right] \exp[-n\gamma_{t,t'}] \gamma_{t,t'} d(t-t') \quad (13)$$

$$[\tau_{11} - \tau_{22}](t) = \sum_i a_i \int_{t-t'=0}^{\infty} \exp\left[-\frac{(t-t')}{\tau_i}\right] \exp[-n\gamma_{t,t'}] \gamma_{t,t'}^2 d(t-t') \quad (14)$$

One can calculate stress relaxation after the stop of steady shear flow. The shear history is defined as follows:

$$\gamma_{t,t'} = \begin{cases} 0 & \text{for } t-t' < t \\ \dot{\gamma}_0 \cdot (t-t') - \dot{\gamma}_0(t) & \text{for } t-t' \geq t \end{cases} \quad (15)$$

where t stands for the time after stop of steady shear flow, and $\dot{\gamma}_0$ is the initial shear rate before the relaxation takes place. By substituting $\gamma_{t,t'}$ in equation (15) into equations (13) and (14), the following relations are obtained:

$$\tau_{12}(t, \dot{\gamma}_0) = \dot{\gamma}_0 \sum_i \frac{a_i \tau_i^2 \exp[-t/\tau_i]}{(1 + n \dot{\gamma}_0 \tau_i)^2} \quad (16)$$

$$[\tau_{11} - \tau_{22}](t, \dot{\gamma}_0) = 2 \dot{\gamma}_0 \sum_i \frac{a_i \tau_i^3 \exp[-t/\tau_i]}{(1 + n \dot{\gamma}_0 \tau_i)^3} \quad (17)$$

A detailed derivation of equation (16) is shown in Appendix B.

(c) Evaluation of Model Parameters

Model parameters must be evaluated for each material to be used. The material used for tests in this thesis is polystyrene (Styron[®] 685D, Dow Chemical Company).

The time constants τ_i and the weighting factors a_i can be evaluated from the storage modulus (G') and the loss modulus (G'') data. The modulus data have been supplied by Eastman Kodak Co. using a rheometric mechanical spectrometer (System IV) [IV-12]. The data are shown in Figure IV.1. These data were taken using the parallel-plate configuration in a low-amplitude oscillatory mode.

The following relations are derived using equation (13), for oscillatory shear flow of angular frequency ω . The derivation is given in Reference [IV-13].

$$G'(\omega) = \sum_i a_i \tau_i \frac{\omega^2 \tau_i^2}{1 + \omega^2 \tau_i^2} \quad (18)$$

$$G''(\omega) = \sum_i a_i \tau_i \frac{\omega \tau_i}{1 + \omega^2 \tau_i^2} \quad (19)$$

The memory function, equation (9), is approximated by eight relaxation time constants τ_i . The time constants are

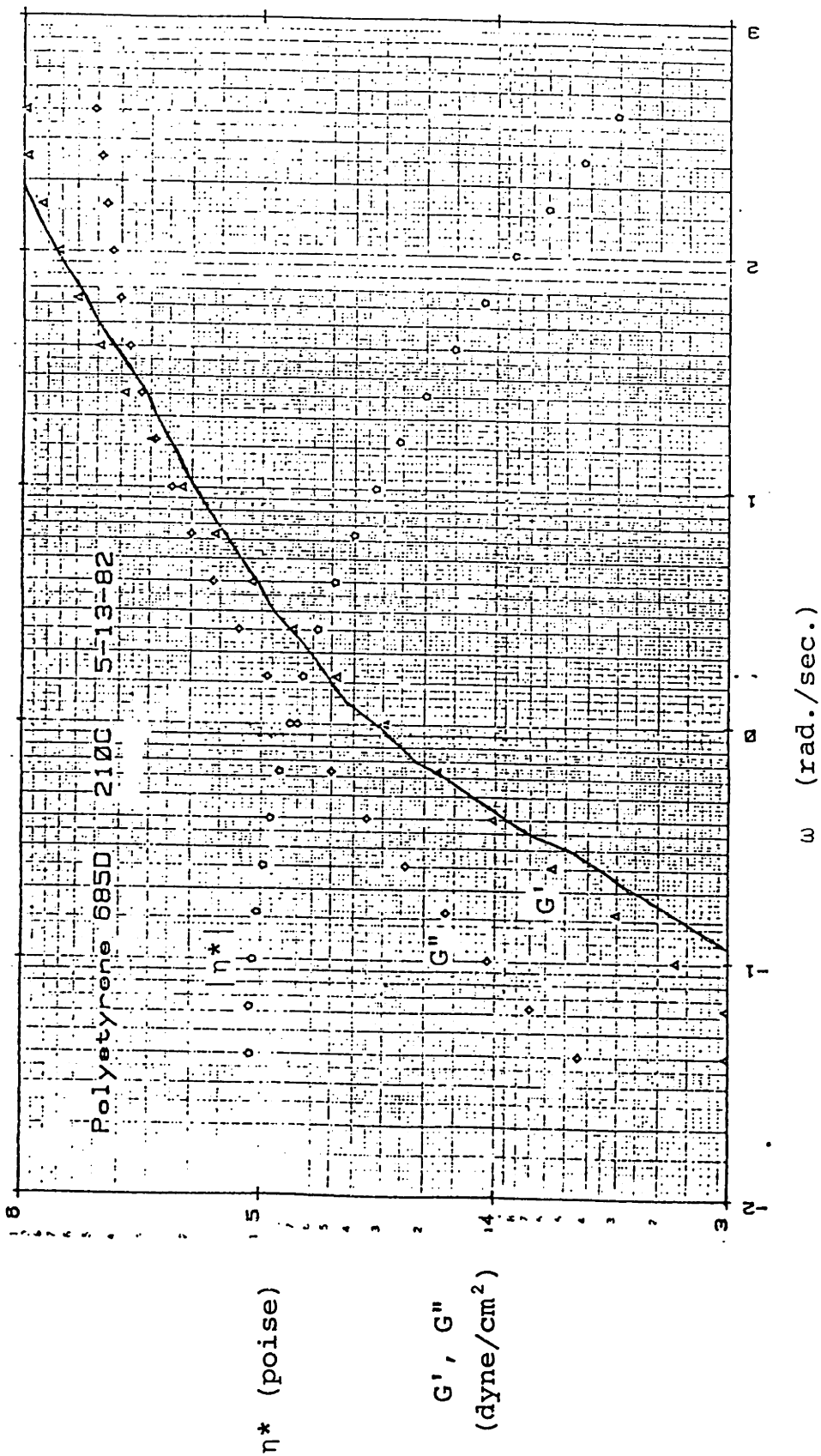


Figure IV.1 : The storage modulus (G'), the loss modulus (G''), and the complex viscosity (η^*) data.

chosen in such a way that ω varies from 9×10^{-2} (rad/sec) to 4×10^2 (rad/sec) with a half decade spacing. The weighting factors a_i are determined by a fit of equations (18) at $\omega \cdot (a_{T 170^\circ C} / a_{T 210^\circ C})$ to the data in Figure IV.1. The fitting was done by regression analysis program called Powell. A user-supplied subroutine for the program is listed in Appendix C. The set of constants which describes the linear memory function is given in Table IV.1. The storage modulus (G') has been plotted as a solid line in Figure IV.1 using these constants.

The nonlinear material function in Wagner's model is described by the damping function. If one chooses a single exponential damping function for simplicity, the damping constant n in equation (10) is the only nonlinear model parameter that needs to be determined. Although the damping constant can be determined from one nonlinear shear experiment, the constant can be evaluated without the experiment if the validity of the Cox-Merz relation [IV-14] is assumed:

$$\eta(\dot{\gamma}) = |\eta^*(\omega)|_{\omega=\dot{\gamma}} \quad (20)$$

where the absolute value of the complex viscosity $\eta^*(\omega)$ is determined from the frequency dependence of the storage and loss moduli $G'(\omega)$ and $G''(\omega)$, respectively:

$$|\eta^*(\omega)| = \frac{1}{\omega} \sqrt{G'^2(\omega) + G''^2(\omega)} \quad (21)$$

Table IV.1 : Set of constants which describes the linear memory function of Polystyrene (Dow 685D) at 170°C.

i	τ_i (s)	a_i ($\text{Nm}^{-2}\text{S}^{-1}$)
1	69.8	86
2	15.7	442
3	6.98	1640
4	1.57	16560
5	0.698	58000
6	0.157	564000
7	0.0698	1940000
8	0.0157	18600000

The complex viscosity $\eta^*(\omega)$ is plotted in Figure IV.1.

The steady state shear viscosity $\eta(\dot{\gamma}_0)$ is determined from equation (16) and is utilized to determine the damping constant n :

$$\eta(\dot{\gamma}_0) = \frac{\tau_{12}(\dot{\gamma}_0)}{\dot{\gamma}_0} = \sum_i \frac{a_i \tau_i^2}{(1 + n \dot{\gamma}_0 \tau_i)^2} \quad (22)$$

The value of $n = 0.25$ is determined from the fit of the viscosity plot. Unfortunately, nonlinear experimental data were not available to test the value of n directly. The Cox-Merz relation is useful, because a complete set of the model parameters, namely the relaxation time constants (τ_i), weighting factor (a_i), and the damping constant (n) can be determined from one oscillatory shear experiment.

IV.3 The Stress-Optic Law

The theory which relates changes in the indices of refraction of a material to the anisotropical state of stress in the material is known as the stress-optic law. Maxwell [IV-15] reported that the changes in the indices of refraction were linearly proportional to the loads. The relationships are expressed as follows:

$$\begin{aligned} n_1 - n_0 &= c_1 \sigma_1 + c_2 (\sigma_2 + \sigma_3) \\ n_2 - n_0 &= c_1 \sigma_2 + c_2 (\sigma_3 + \sigma_1) \\ n_3 - n_0 &= c_1 \sigma_3 + c_2 (\sigma_1 + \sigma_2) \end{aligned} \quad (23)$$

where $\sigma_1, \sigma_2, \sigma_3$ = principal stresses at a point
 n_0 = index of refraction
 in unstressed state
 n_1, n_2, n_3 = indices of refraction in
 stressed state associated
 with principal stress directions
 c_1, c_2 = constants known as
 stress-optic coefficients

Although equations (23) provide the complete state of stress at a point, practical application has been limited because of the difficulty in measuring absolute changes in the index of refraction. However, the more widely used method of photoelasticity makes use of relative changes in the indices. The following equations are obtained by eliminating n_0 from equations (23):

$$\begin{aligned} n_2 - n_1 &= c (\sigma_1 - \sigma_2) \\ n_3 - n_2 &= c (\sigma_2 - \sigma_3) \\ n_1 - n_3 &= c (\sigma_3 - \sigma_1) \end{aligned} \tag{24}$$

where $c = c_2 - c_1$ is the relative stress-optic coefficient, usually expressed in terms of brewsters (1 brewster = 10^{-13} cm²/dyn = 10^{-12} m²/N = 6.895×10^{-9} in²/lb). From Reference [II-14], c is taken as 4500 brewsters.

For plane-stress situations, equations (24) reduce to

$$\Delta n = n_2 - n_1 = c (\sigma_1 - \sigma_2) \tag{25}$$

From the Mohr's circle, the principal stress can be expressed in terms of normal stress and thus equation (25) can also be expressed as

$$\Delta n = c [4 \tau_{12}^2 + (\tau_{11} - \tau_{22})^2]^{1/2} \quad (26)$$

The relationship of birefringence (Δn) to the stress in amorphous polymers obeys the stress-optic law. Oda, White, and Clark [IV-16] found that the molecular orientation in polymeric parts is quantitatively related to the principal stress difference acting at the time of vitrification. Thus, the amount of orientation in an injection molded part can be determined by measuring the birefringences.

IV.4 Isothermal Stress Relaxation

An isothermal stress relaxation after the stop of a fully developed one-dimensional shear flow is considered in this section. Analysis of this section is useful in describing the stress relaxation behavior of the injection molded part when the isothermal condition is maintained some time after the filling stage has been completed.

Consider the situation in which a polymer melt is initially at a uniform temperature T_i and flowing as a fully-developed flow between parallel plates. From time $t=0^-$ to $t=t_{fill}$, the temperature of the plate remains the same as that of the melt, namely T_i . Thus the fully developed iso-

thermal flow condition is identical to the initial condition. At $t=t_{fill}$, the flow stops and the flow-induced stress starts to relax while the melt temperature remains constant at T_i , assuming that viscous heating is negligible.

A schematic representation of isothermal filling is shown in Figure IV.2. The gap distance between the plates is $2a$.

The steady shear rate $\dot{\gamma}_0(y)$ must be determined in order to predict the relaxation of shear stress, primary normal stress difference, and birefringence as a function of y . To describe the steady shear rate the equations of continuity and momentum have been utilized. The continuity equation has the simple form:

$$\frac{\partial v_x}{\partial x} = 0 \quad (27)$$

or in the integral form:

$$Q = 2W \int_0^a v_x dy \quad (28)$$

where Q is the volume flow rate of plastic, and W is the width of the rectangular mold. The momentum equation is simply a balance between the pressure gradient which drives the motion of plastic and the viscous shear stress which resists it:

$$\frac{\partial p}{\partial x} = \frac{\partial \tau_{yx}}{\partial y} \quad (29)$$

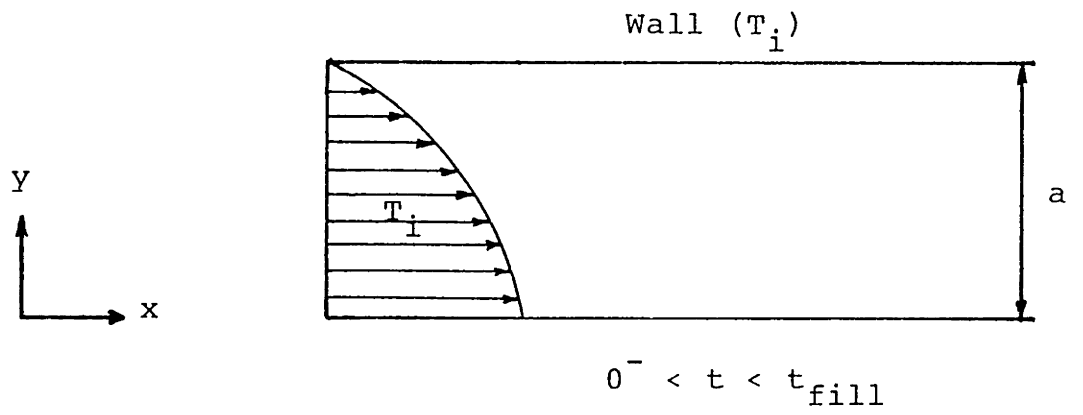


Figure IV. 2 : Schematic representation of isothermal filling

The boundary conditions for this equation are:

$$\frac{\partial v_x}{\partial y} = 0 \quad \text{at } y = 0 \quad (30)$$

$$v_x = 0 \quad \text{at } y = a \quad (31)$$

In equation (29) the total differential of P can be used, since pressure is a function of x only when the gravity effect has been neglected. Equation (29) must be valid for all values of x and y. This requires that:

$$\frac{d\tau_{yx}}{dy} = \frac{dP}{dx} = \text{constant} \quad (32)$$

Integrating this momentum equation,

$$\tau_{yx} = \left(\frac{dP}{dx} \right) y \quad (33)$$

and from the Wagner model,

$$\tau_{yx} = \dot{\gamma} \sum_i \frac{a_i \tau_i}{(1 + n \dot{\gamma}_0 \tau_i)^2} \quad (34)$$

From equation (33) and (34), the implicit expression for shear rate is given by

$$\dot{\gamma} = \left(\frac{dP}{dx} \right) y \frac{1}{\left[\sum_i \frac{a_i \tau_i^2}{(1 + n \dot{\gamma} \tau_i)^2} \right]} \quad (35)$$

The shear rate is determined solving equation (35) by an iterative scheme outlined in Figure IV.3. The initial guess of the shear rate for a given y is determined from the power law model, that is

$$\tau_{yx} = m (\dot{\gamma})^{k-1} \dot{\gamma} \quad (36)$$

where m (with units of $N \cdot s^k / m^2$) and the dimensionless parameter k are constants characteristic of the fluid. Combining equations (33) and (36) gives the initial guessed value for the shear rate based on the power law fluid.

$$\dot{\gamma} = \left(\frac{dP}{dx} \right) \cdot \left(\frac{y}{m} \right)^{1/k} \quad (37)$$

The shear rate obtained in this way for two pressure gradients are plotted in Figure IV.4.

The isothermal relaxation of shear stress (τ_{12}), primary normal stress difference ($\tau_{11} - \tau_{22}$), and birefringence (Δn) for the two pressure gradients are shown in Figures IV.5, IV.6 and IV.7, respectively.

IV.5 Nonisothermal Stress Relaxation

In practice, the stress will relax nonisothermally. The molten polymer in the mold cavity must be cooled below the glass transition temperature before it can be ejected. The stress relaxation rate at a lower temperature is slower. In

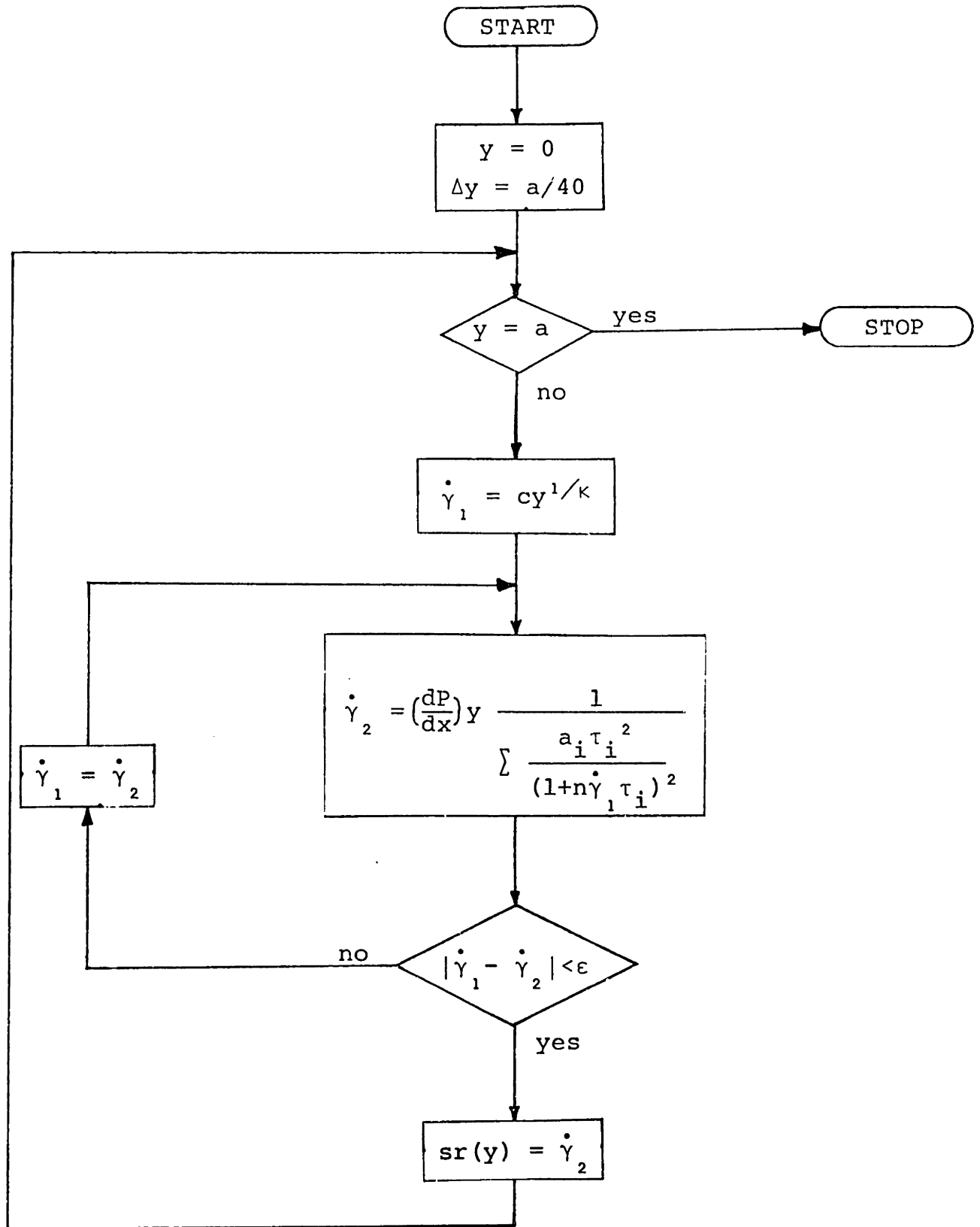


Figure IV.3 : Flow chart to determine the shear rate as a function of the pressure gradient.

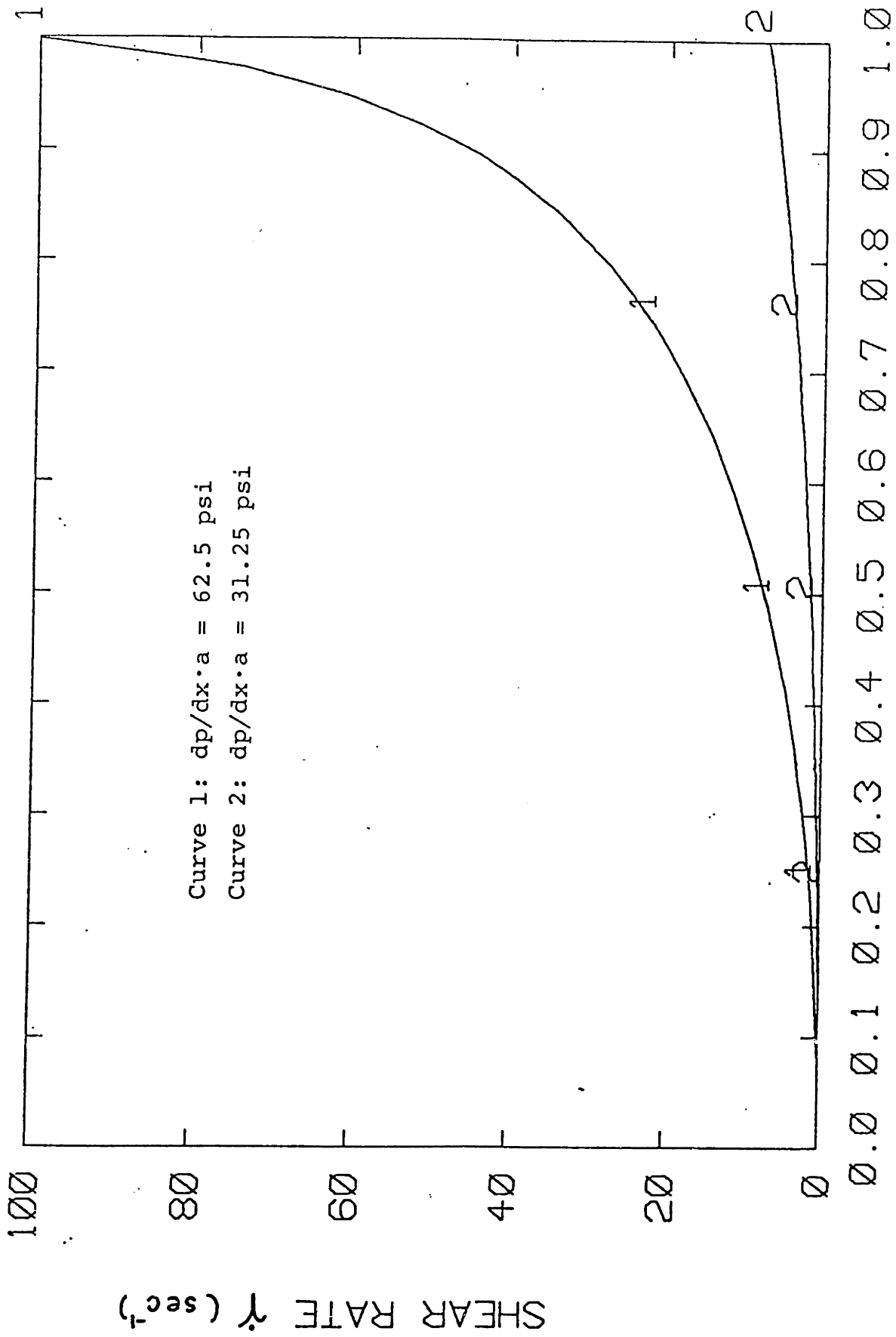
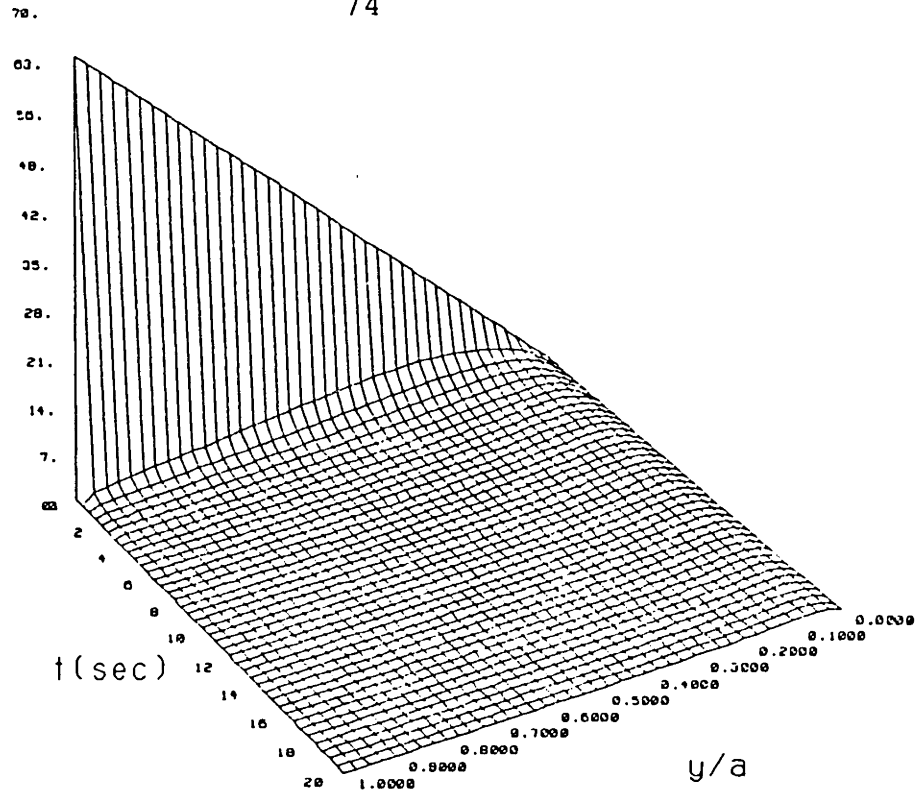


Figure IV.4 : Shear rates for the two pressure gradients as a function of the gap distance.

(a)

 τ_{12} (psi)

(b)

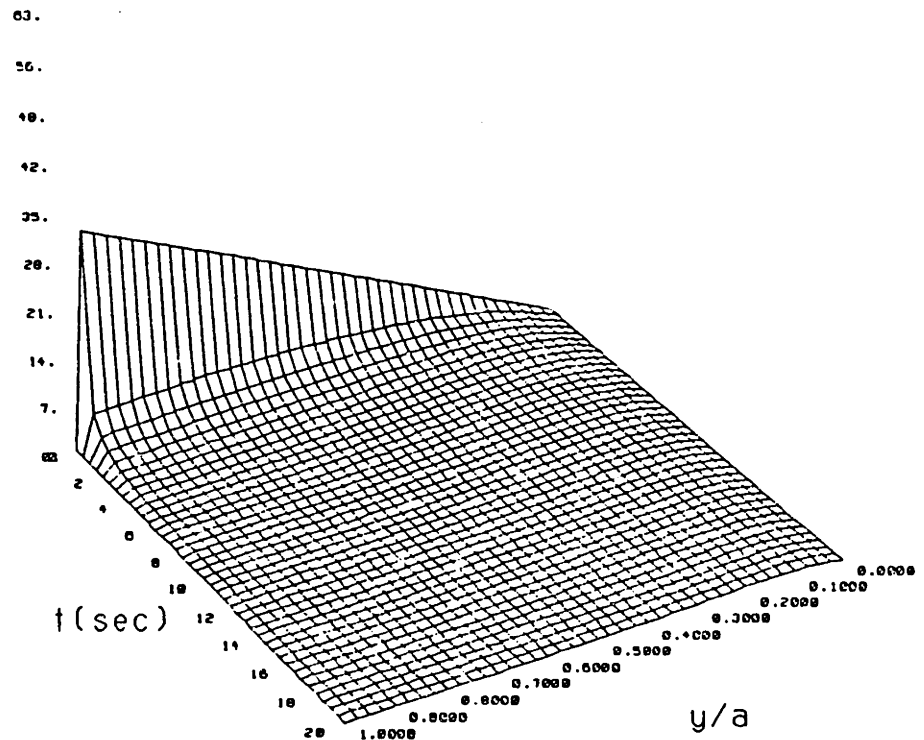
 τ_{12} (psi)

Figure IV.5 : Isothermal relaxation of the shear stress for
 (a) $dP/dx \cdot a = 62.5$ psi and
 (b) $dP/dx \cdot a = 31.25$ psi.

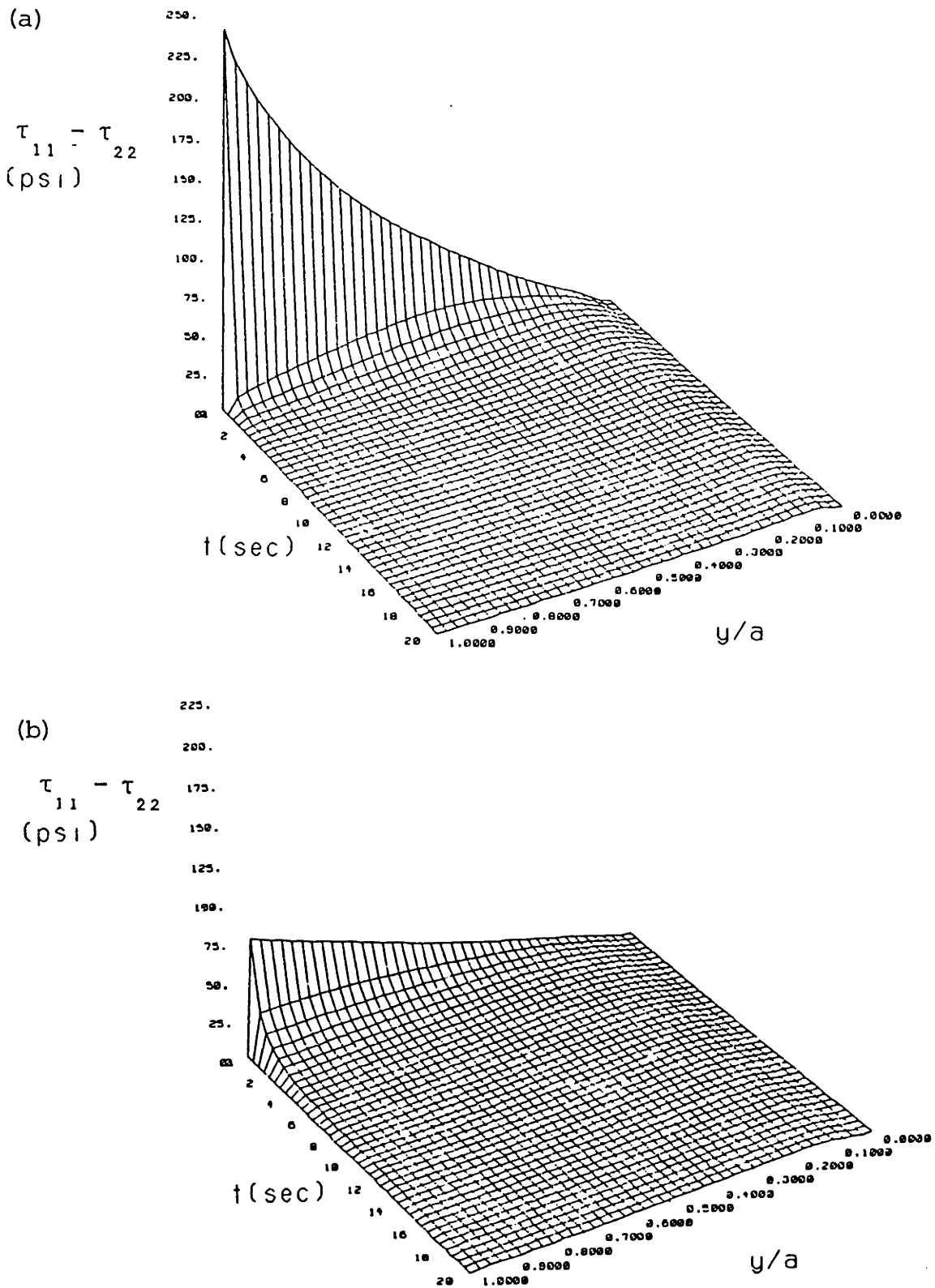
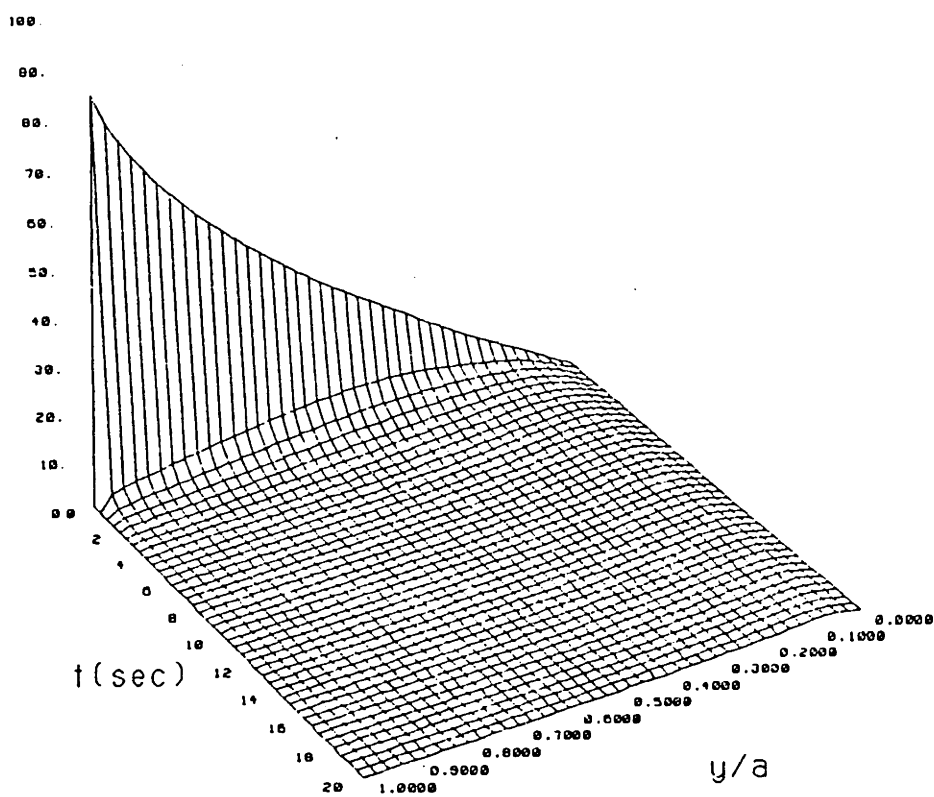


Figure IV.6 : Isothermal relaxation of the primary normal stress difference for
 (a) $dP/dx \cdot a = 62.5$ psi and
 (b) $dP/dx \cdot a = 31.25$ psi.

(a)

 $\Delta n \cdot e^4$ 

(b)

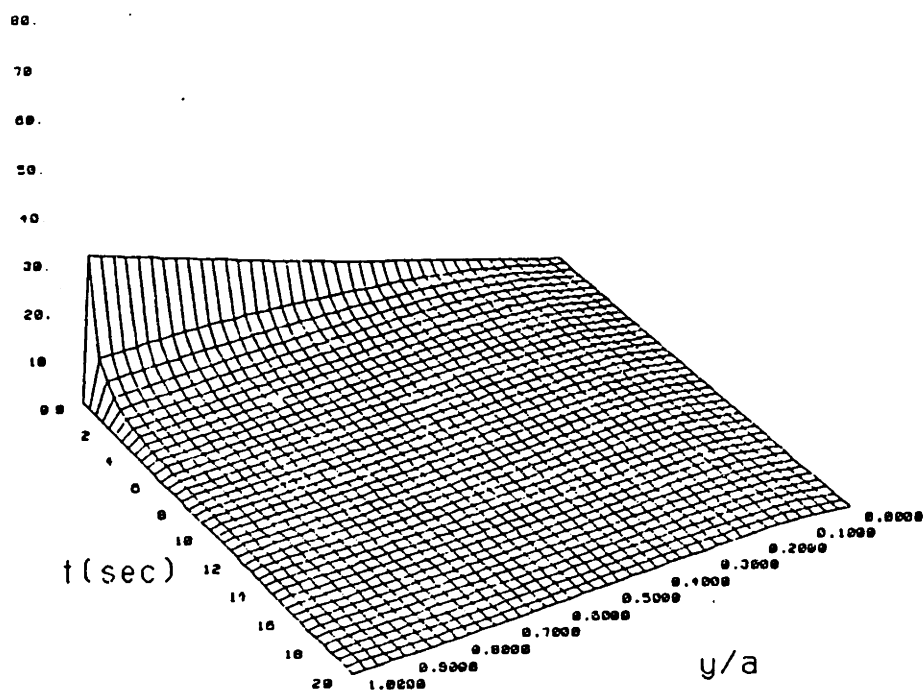
 $\Delta n \cdot e^4$ 

Figure IV.7 : Isothermal relaxation of the birefringence for
 (a) $dP/dx \cdot a = 62.5$ psi and
 (b) $dP/dx \cdot a = 31.25$ psi.

analyzing the nonisothermal stress relaxation, one must take this variation of the relaxation rate due to temperature changes into account. In thermoplastic materials, however, the changes in temperature can be easily compensated for by the appropriate changes in the relaxation time using the WLF temperature-shift factor (38),

$$a_T = \begin{cases} a_{T_g} & , \quad T \leq T_g \\ \exp_{10} \left[\frac{-17.44 (T-T_g)}{51.6 + (T-T_g)} \right] & , \quad T > T_g \end{cases} \quad (38)$$

in which T_g is the glass transition temperature.

Since a variation of temperature corresponds to a shift in time scale, all relaxation time changes with temperature proportional to the shift factor are as in equation (39).

$$\tau_i(T) = \frac{a_T}{a_{T_0}} \cdot \tau_i(T_0) \quad (39)$$

An equivalent differential form for the Lodge constitutive equation neglecting density changes is given as follows [IV-17].

$$\underline{\sigma} = \sum_i \underline{\sigma}_i \quad (40)$$

$$\underline{\sigma}_i + \tau_i \frac{\partial \underline{\sigma}_i}{\partial t} = a_i \tau_i^2 \underline{\dot{\gamma}} \quad (41)$$

Note that $\underline{\sigma}_i$ is not the i -th component of the stress tensor; rather, it is the stress tensor corresponding to the i -th re-

laxation mode.

For the stress relaxation upon the cessation of flow $\dot{\underline{Y}}=0$, and equation (41) reduces to

$$\underline{\sigma}_i + \tau_i \frac{\partial \underline{\sigma}_i}{\partial t} = 0 \quad (42)$$

It can be shown that equation (42) also holds for the Wagner equation, although a differential form of the Wagner in general does not exist.

For the nonisothermal stress relaxation, the relaxation time is a function of temperature which in turn depends on time. Thus, changes in the relaxation time due to the temperature change can be determined. Integrating equation (42) with the following initial condition,

$$\underline{\sigma}_i(0) = \underline{\sigma}_i(\text{steady shear}) \quad (43)$$

gives

$$\underline{\sigma}_i(t) = \underline{\sigma}_i(\text{steady shear}) e^{-\int_0^t \frac{1}{\tau_i(t'')} dt''} \quad (44)$$

The values of the steady shear tensor for the shear stress and the primary normal stress difference are given by equations (16) and (17) with $t=0$. With these initial conditions and equation (44), the following relations for nonisothermal stress relaxation are obtained:

$$\tau_{12}(t, \dot{\gamma}_0) = \dot{\gamma}_0 \sum_i \frac{a_i \tau_i^2 \exp \left[-\int_0^t \frac{1}{\tau_i(t')} dt' \right]}{(1 + n \dot{\gamma}_0 \tau_i)^2} \quad (45)$$

$$[\tau_{11} - \tau_{22}](t, \dot{\gamma}_0) = 2 \dot{\gamma}_0 \sum_i \frac{a_i \tau_i^3 \exp \left[-\int_0^t \frac{1}{\tau_i(t')} dt' \right]}{(1 + n \dot{\gamma}_0 \tau_i)^3} \quad (46)$$

In order to verify the model's prediction of the viscoelastic behavior, $\tau_{12}(t)/\tau_{12}(0)$ has been plotted as a function of shear rate. Figure IV.8 shows that the rate of shear stress relaxation increases as shear rate increases.

Temperature variation within the plastic part has been determined by the one dimensional heat conduction equation (47).

$$\alpha \frac{\partial^2 T}{\partial x^2} = \frac{\partial T}{\partial t} \quad (47)$$

The boundary conditions in using equation (47) for the low thermal inertia molding simulation are as follows:

$$T(t, \pm a) = \begin{cases} 170 e^{-0.24t} & , \quad 0 \leq t < 3.5 \\ 72 e^{-0.085(t-3.5)} & , \quad 3.5 \leq t < 9 \\ 45 e^{-0.02(t-9)} & , \quad 9 \leq t \leq 20 \end{cases} \quad (48)$$

Conditions in equation (48) are obtained from the cooling experiments of the low thermal inertia block itself. This temperature condition is the lower limit, since the effect of plastic is excluded, and therefore results in predicting the

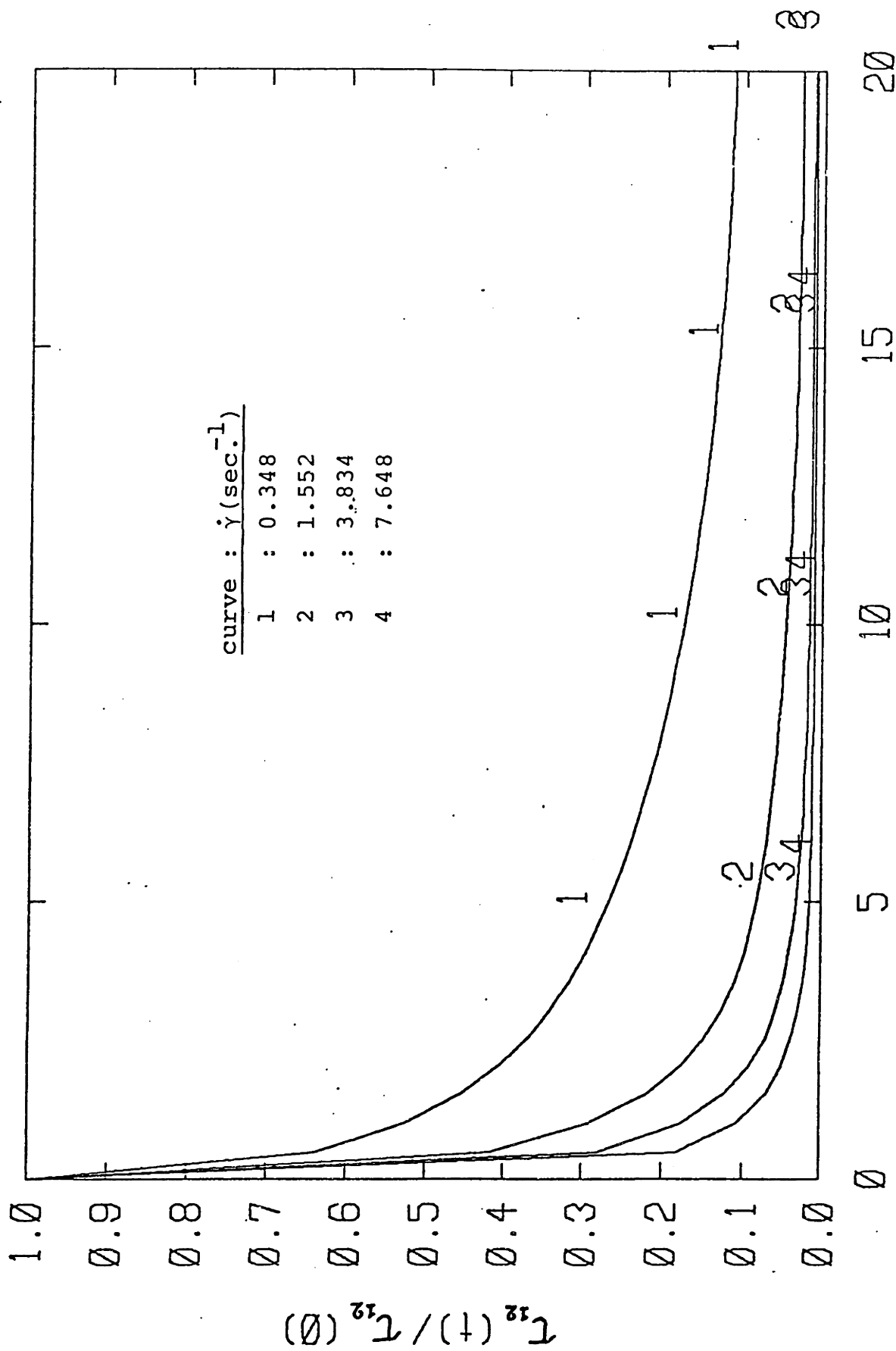


Figure IV.8 : Shear stress relaxation as a function of shear rate for the condition A in Table IV.2

upper limit stress relaxation value.

The nonisothermal relaxation of the stresses have been simulated with conditions shown in Table IV.2. A flow chart for the simulation and the program listings are shown in Figure IV.9 and Appendix D, respectively.

The nonisothermal relaxation of shear stress (τ_{12}), primary normal stress difference ($\tau_{11} - \tau_{22}$), and birefringence (Δn) for the condition (A) in Table IV.2 are shown in Figure IV.10, IV.11, and IV.12. The relaxation of the stresses for the other conditions in Table IV.2 are shown in Appendix E.

It has been found from the simulation that the flow-induced stresses relax on the order of a second for the isothermal filling and nonisothermal cooling process, and the residual stresses can be minimized without difficulty. Because of the viscoelastic nature of the polymer melt, the more strain the melt undergoes within the longest relaxation time period the faster it will relax. Hence the cavity should be filled as rapidly as possible for molecular relaxation and for decreasing total cycle time. If the molding machine, however, can not provide the rapid filling then the isothermal condition may be maintained beyond the completion of filling to relax slowly relaxing orientation due to small strain from the slow filling process. Therefore, molding a part with the minimum residual stress can be achieved if molecular relaxation takes place before vitrification by using a heated mold surface.

Table IV.2 : Conditions for the simulated low thermal inertia injection molding with Polystyrene (Dow 685D).

Molding Condition	Half Channel Depth a (inch)	Pressure Gradient dP/dx (psi/in.)
A	0.0075	8336
B	0.0075	4168
C	0.015	4168
D	0.015	2084
E	0.030	2084
F	0.030	1042
G	0.060	1042
H	0.060	521
I	0.125	500
J	0.125	250

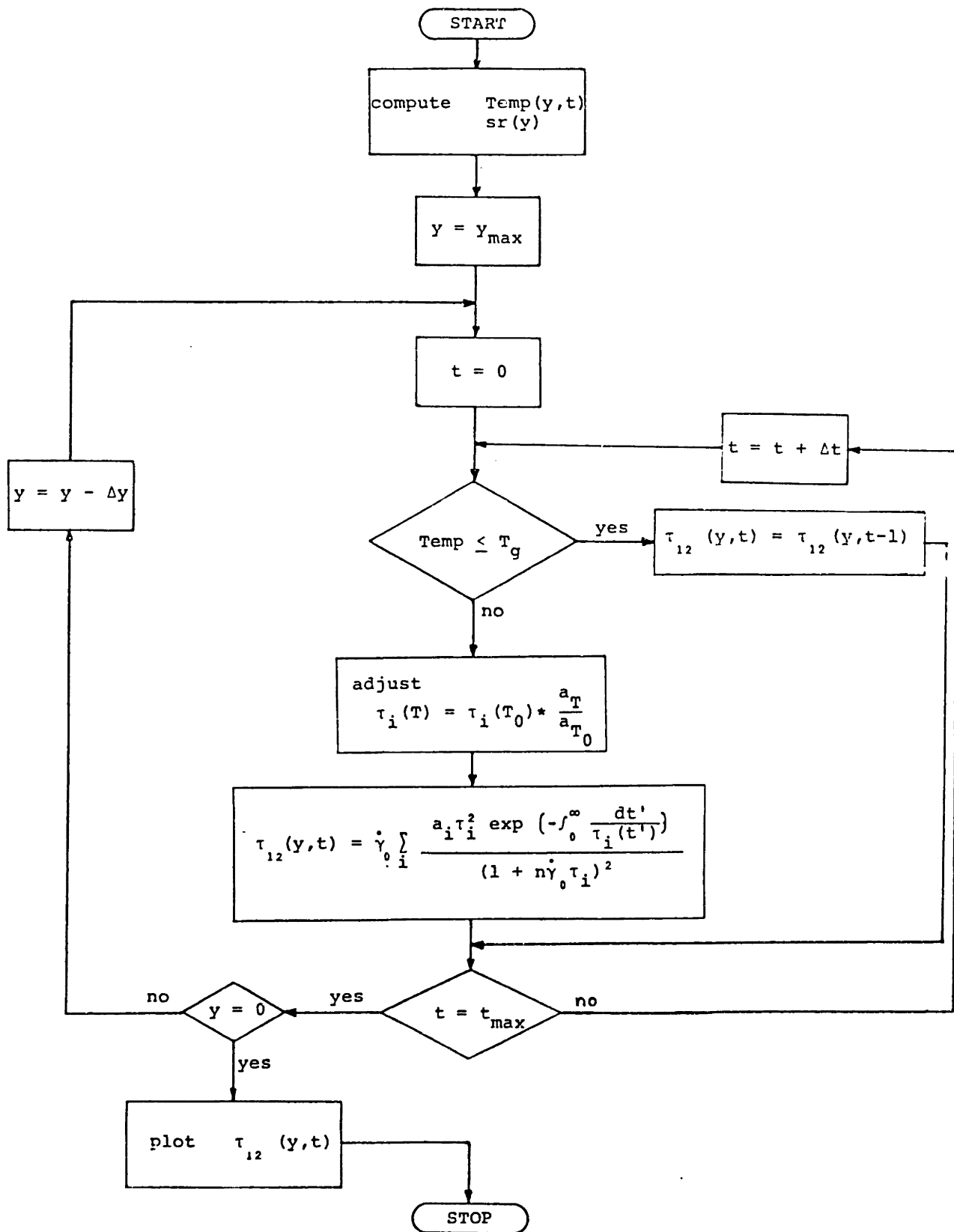


Figure IV.9 : Flow chart for nonisothermal shear stress relaxation.

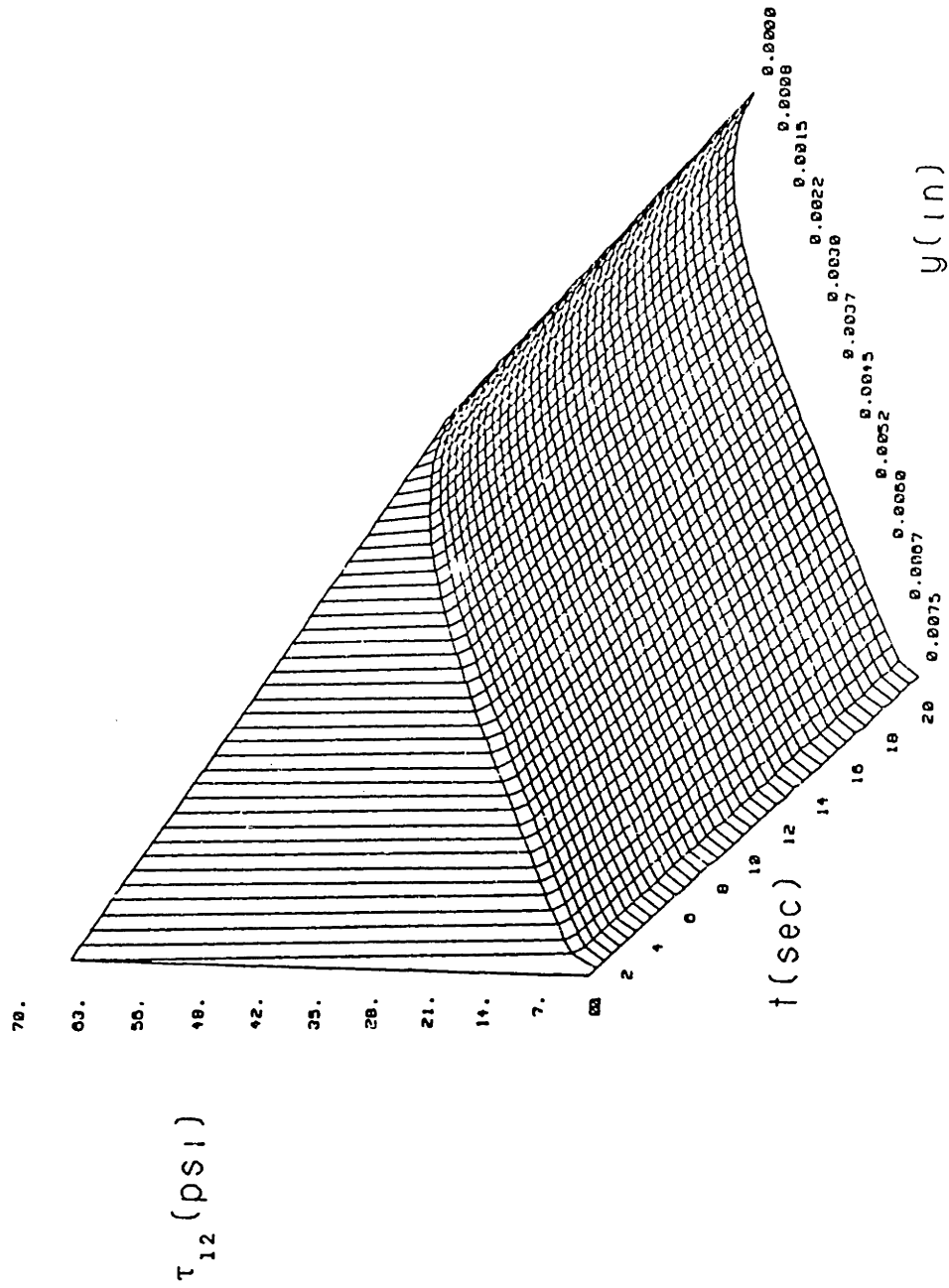


Figure IV.10 : Nonisothermal relaxation of the shear stress for $dP/dx = 8336$ psi/in. (condition A in Table IV.2).

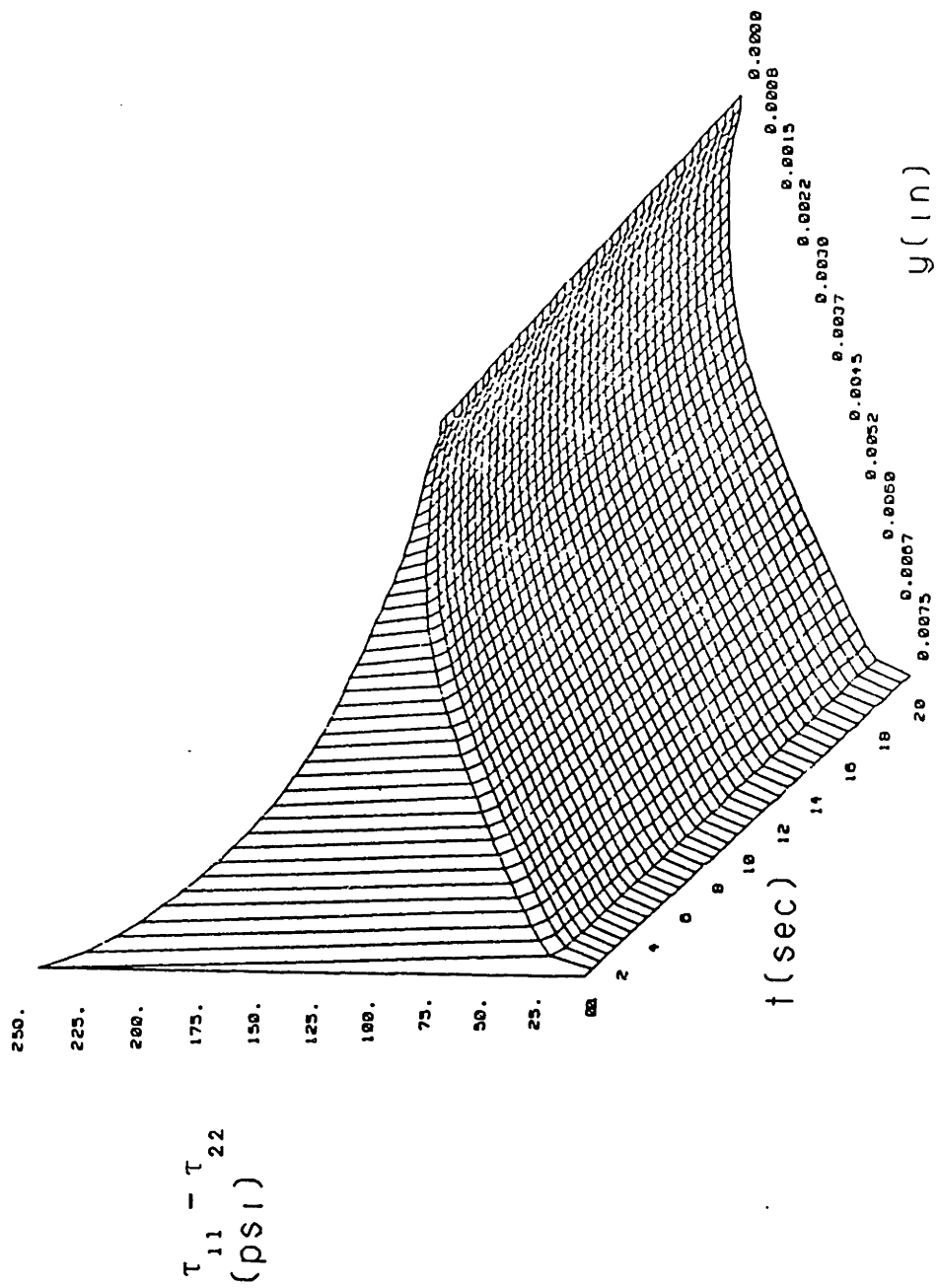


Figure IV.11 : Nonisothermal relaxation of the primary normal stress difference for $dP/dx = 8336$ psi/in. (condition A in Table IV.2).

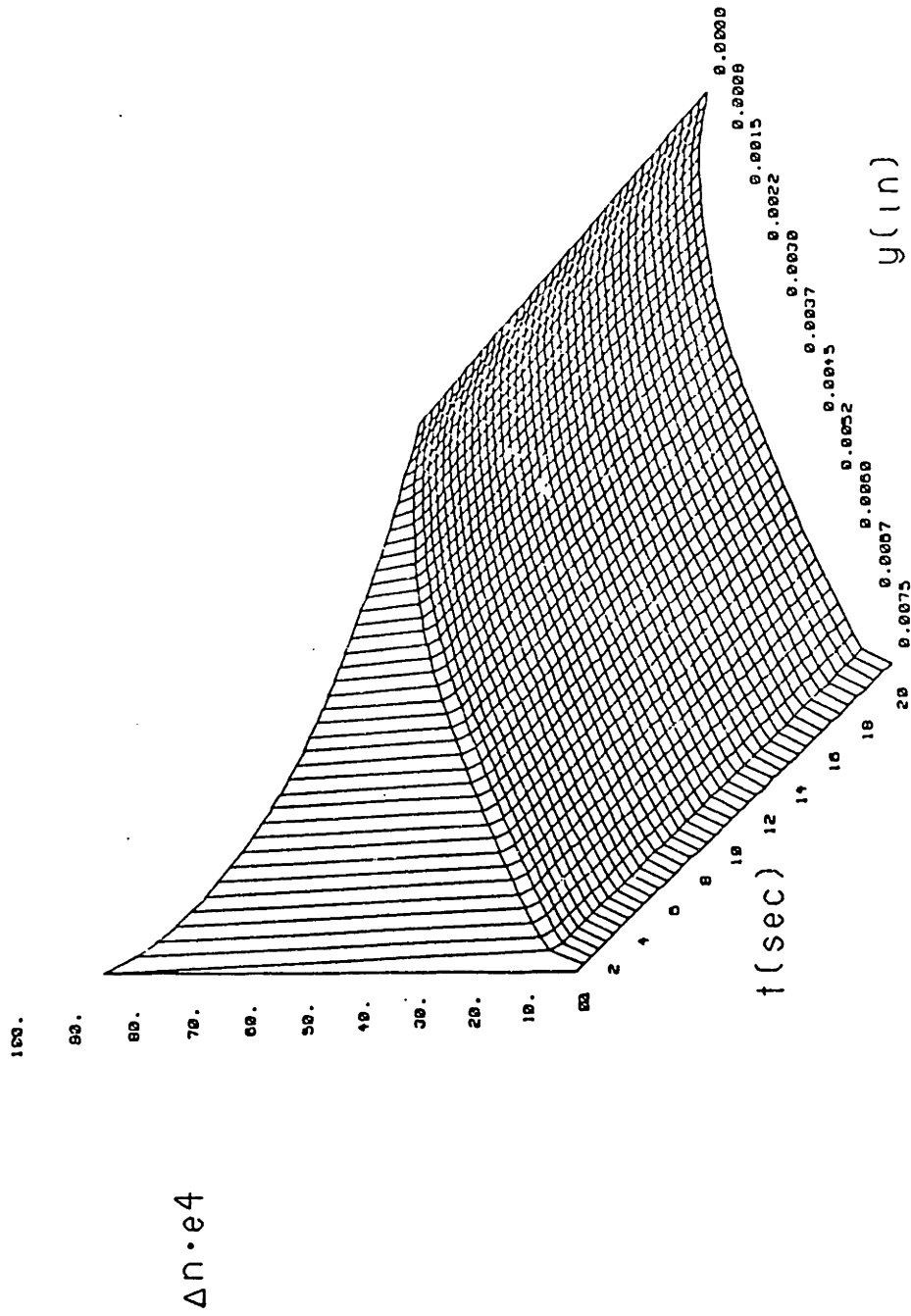


Figure IV.12 : Nonisothermal relaxation of the birefringence for $dP/dx = 8336 \text{ psi/in.}$ (condition A in Table IV.2).

References for Chapter IV

- IV-1 Wagner, M.H., Rheol. Acta, 15, 1976, p. 136.
- IV-2 Wagner, M.H., Rheol. Acta, 16, 1977, p. 43.
- IV-3 Leonov, A.I., E.H. Lipkina, E.D. Paskhin, A.N. Prokunin, Rheol. Acta, 15, 1976, p. 411.
- IV-4 Isayev and Hieber, Rheol. Acta, 19, 1980, p. 168.
- IV-5 Wang, K.K., S.F. Shen, C. Cohen, C.A. Hieber, A.I. Isayev, "Computer Aided Injection Molding Systems," Progress Reports Nos. 6-8, Cornell University for NSF under grant APR74-114990.
- IV-6 Lodge, A.S., Elastic Liquids (London-New York), 1964.
- IV-7 Lodge, A.S., Body Tensor Fields in Continuum Mechanics, (London-New York), 1974.
- IV-8 Laun, H.M. Rheol. Acta, 17, 1978, p. 1.
- IV-9 Wagner, M.H. and H.M. Laun, Rheol. Acta, 17, 1978, pp. 138-148.
- IV-10 Chang, H., A.S. Lodge, Rheol. Acta, 11, p. 127.
- IV-11 Osaki, K., Proc. VIIth Int. Congr. Rheology, 104, (Gothenburg, Sweden), 1976.
- IV-12 Rheometrics Inc., 2438 U.S. Highway 22, Union, New Jersey 07083.
- IV-13 Weinberg, M., "The Rheology of Carbon Black Filled Elastomers," Ph.D. thesis, MIT, January 1981.
- IV-14 Cox, W.P., E.H. Merz, J. Polym. Sci., 28, 1958, p. 619.
- IV-15 Maxwell, J.C., "On the Equilibrium of Elastic Solids", Trans. R. Soc. Edinburgh, XX, part 1, 1853, p. 87-120.
- IV-16 Oda, K., J.L. White, and E.S. Clark, Polym. Eng. Sci., 18, no. 1, 1978, p. 53.
- IV-17 Lodge, A.S., R.C. Armstrong, M.H. Wagner, H.H. Winter, Pure & Appl. Chem., vol. 54, no. 7, pp. 1349-1359, 1982.

CHAPTER VDEVELOPMENT OF A LOW THERMAL INERTIA MOLDV.1 Introduction

The purpose of developing a low thermal inertia mold is to shorten the injection molding cycle and to reduce the energy consumption in molding high quality parts. The surface of the mold must be heated and cooled rapidly to make the part in a short time. A low thermal inertia mold is needed to provide the rapid change in the surface temperature of the mold. The mold must also have the mechanical integrity necessary to withstand the cyclic load of injection molding. The development of a mold with these design considerations is discussed in this chapter.

The mold has been constructed with three elements: an electrically conducting layer, a metal oxide insulation layer, and a metal mold base. The conducting layer is heated by passing the electric current through it. The heated layer is insulated electrically from the mold base by the oxide layer. A detailed discussion of the mold design is given in Section V.2. Experimental results of the low thermal inertia block are discussed in Section V.3.

V.2 Design of a Low Thermal Inertia Mold

There are several important design considerations in making a low thermal inertia mold. The part of the mold which is being heated and cooled must have a low thermal mass in order to have a rapid change in temperature. The mold should withstand not only the stress caused by thermal expansion and contraction but also the high number of thermal cycles. Temperature distribution within the mold surfaces should be uniform.

In order to design a durable mold a low-cycle fatigue failure must be avoided. Low-cycle fatigue failure occurs when the stress level for each cycle is greater than the elastic stress limit [V-1].

A new method has been developed to avoid the low-cycle fatigue failure. This method reduces the interfacial thermal stress between the heating layer and the mold base by using a heating material with a low thermal expansion coefficient. Graphite¹ fibers fit this description well; therefore woven graphite was chosen as the material. The properties of the graphite used are listed in Table V.1. To go one step further in reducing interfacial thermal stress RTV silicone rubber was chosen as a bonder because of its elastic properties.

A thin layer (0.02 inch) of zirconium oxide (ZrO_2)

¹ The use of graphite resulted from our collaboration with Intelitec Corp. of Billerica, Mass.

Table V.1 : Properties of magnamite graphite fibers.*

Property	Fiber Type		
	AS	HTS	HMS
Tensile modulus (psi x 10 ⁶)	Carbon 34	Carbon 36	Graphite 53
Ultimate strength (psi x 10 ³)	450	400	320
Tensile elongation (%)	1.3	0.9	0.6
Thermal conductivity (Btu-ft/hr-ft ² -°F)	15	17	70
Specific heat (Btu/lb/°F)	0.17	0.17	0.17
Longitudinal coefficient of thermal expansion (in./in./°F x 10 ⁻⁶)	-0.2	-0.2	-0.3
Electrical resistance (ohm) (10,000-filament tow)(1-ft length)	12	8	6
Weight per foot (lbs/in. x 10 ⁻⁶) (10,000-filament tow)	48	46	46
Density (lb/in. ³)	0.065	0.060	0.066

* Hercules Incorporated product brochure.

has been plasma sprayed onto the aluminum mold base. The layer provides both electrical insulation from the heating material and moderate thermal insulation.

There must be an optimum thickness for the insulation layer to achieve the minimum injection cycle time. Suppose that the insulation layer is thicker than the optimum, then the cooling time is lengthened due to the excessive thermal insulation. On the other hand, the cooling time is also lengthened when the insulation layer is thinner than the optimum thickness. The reason is that the rest of the mold is also heated during the heating cycle when the insulation layer is too thin. Since the molten polymer cools by conduction heat transfer through the insulation layer and the mold, the excessively heated mold reduces the temperature gradient thereby slowing the cooling process. Because the optimum insulation layer thickness varies with each application, it must be determined for each case.

To attach the 0.01 inch thick woven graphite to the insulated aluminum block, a series of steps were taken. First, the surface of the block, and the woven graphite fibers were vapor degreased using trichloroethylene. Then, RTV silicon rubber was applied approximately 0.2 inch thick to the aluminum block's insulated surface. The woven graphite fibers were placed over the RTV silicon rubber, and even pressure was applied on the surface. To achieve even pressure, a female counterpart to the mold was made as in Figure V.1. This assembly was clamped down producing a final RTV silicon rubber

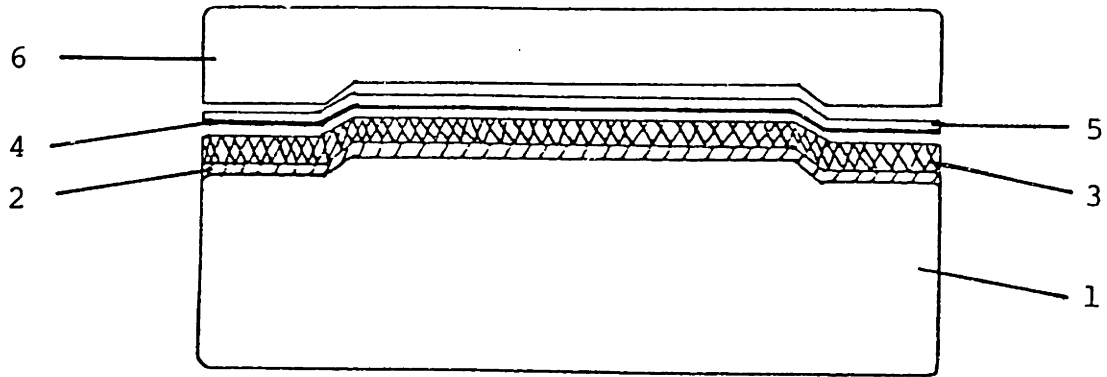


Figure V.1 : Configuration of layers to be pressed to form mold.

1. aluminum mold
2. zirconium oxide insulation
3. RTV silicon rubber
4. woven graphite fibers
5. teflon sheet
6. female counterpart to mold

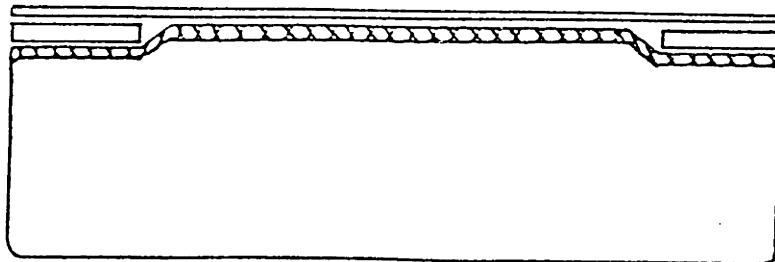


Figure V.2 : Assembly of mold showing electrodes and mold release layer.

thickness of 0.01 inch.

After the mold assembly was clamped for thirty minutes, the assembly was taken apart and the brass electrodes were put into place. A thin layer of RTV silicon rubber was applied to the entire surface, as in Figure V.2, to allow proper mold releasing. To cure the RTV silicon rubber, it was heated in an oven with steam at 95°F for one hour, followed by two hours without steam at 150°F.

V.3 Experimental Results of the Low Thermal Inertia Mold

(a) Temperature Response Experiment

To test the temperature response of the mold, the apparatus was set up using a sample block as in Figure V.3. The Omega Chromel-Alumel thermocouple (response time 10-20 milliseconds) was laid on the surface with maximum surface contact. The electrodes were placed on small brass plates then clamped. The brass plates distribute the current across the surface of the block. While the electrodes heat the mold surface, the mold is cooled by water flow. As the current goes through cycles of 5.3 seconds on and 12.3 seconds off, the water is constantly cooling the aluminum. In this experiment, the mold is attached to a cooling block. The cooling block is an aluminum block with a constant flow of water through it. The electrodes and the timer each have their own power supply. The signal from the timer and the positive

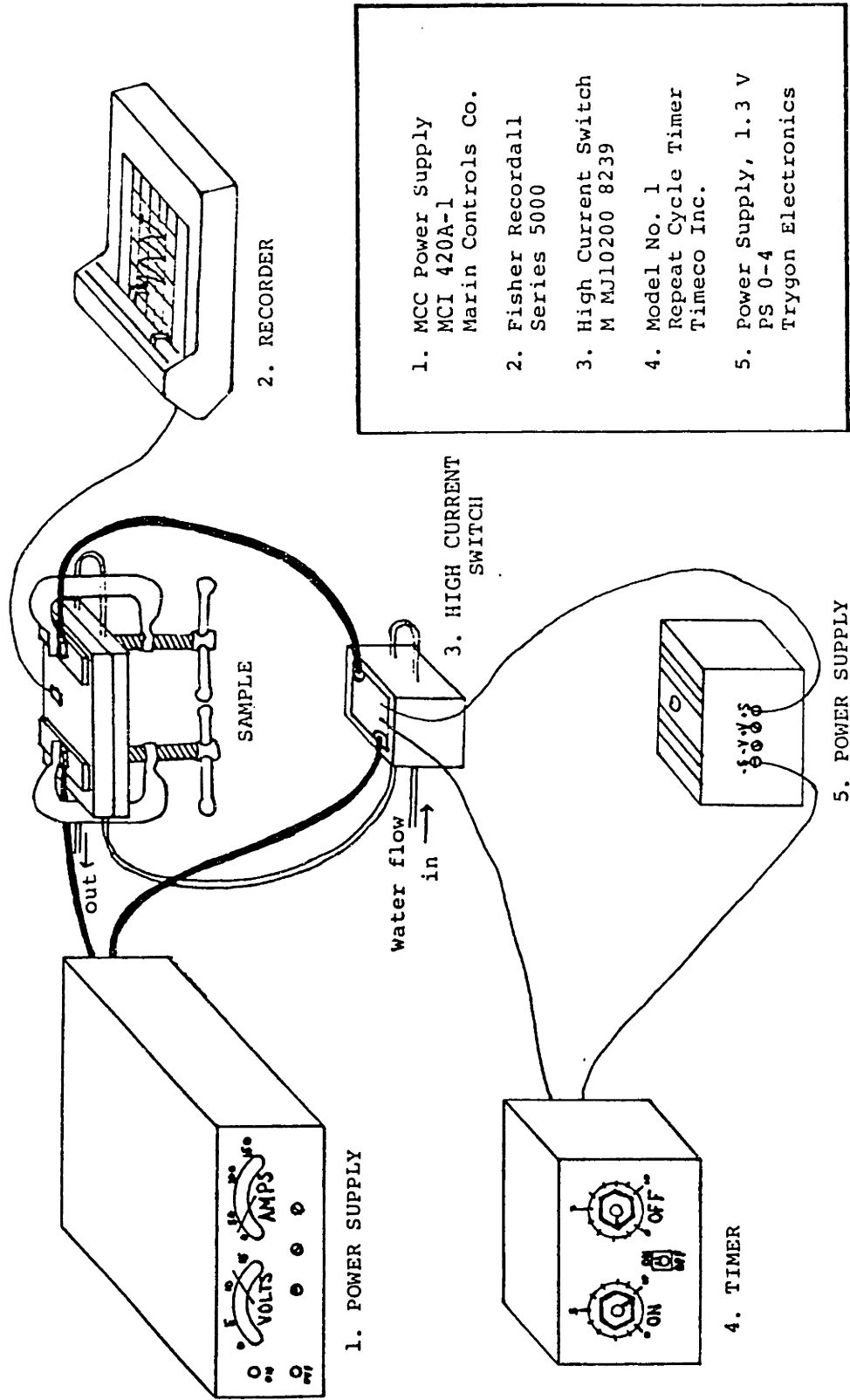


Figure V.3 : Experimental set-up for temperature response and thermal cycle endurance tests.

electrode are attached to a high-current switchmode device manufactured by Darlington.

To heat the mold surface, a current of 20 amps, and a voltage of 11.5 volts are used. Since the area being heated was 2" x 2.38", the power density was 48.3 watts/in². After a few cycles, the response stabilizes, and is as in Figure V.4. While the current is on, the surface temperature changes from 100°F to 300°F in 5.3 seconds. The 12.3 second off cycle decays exponentially with a time constant of .21 second for the temperature range 300°F to 145°F.

(b) Endurance Experiment

Once the temperature response test was satisfactorily completed, the endurance of the mold was tested. The same set-up was used as for the temperature response. Over 20,000 cycles were run from 100°F to 300°F with cycles of 5.3 seconds on and 12.3 seconds off, without any sign of deterioration.

The combination of RTV silicon rubber and graphite can endure many cycles due to the particular properties of these materials. Because graphite has a very small coefficient of thermal expansion, and since RTV silicon rubber can give if the surfaces it is bonded to expand differently, this mold can withstand many cycles.

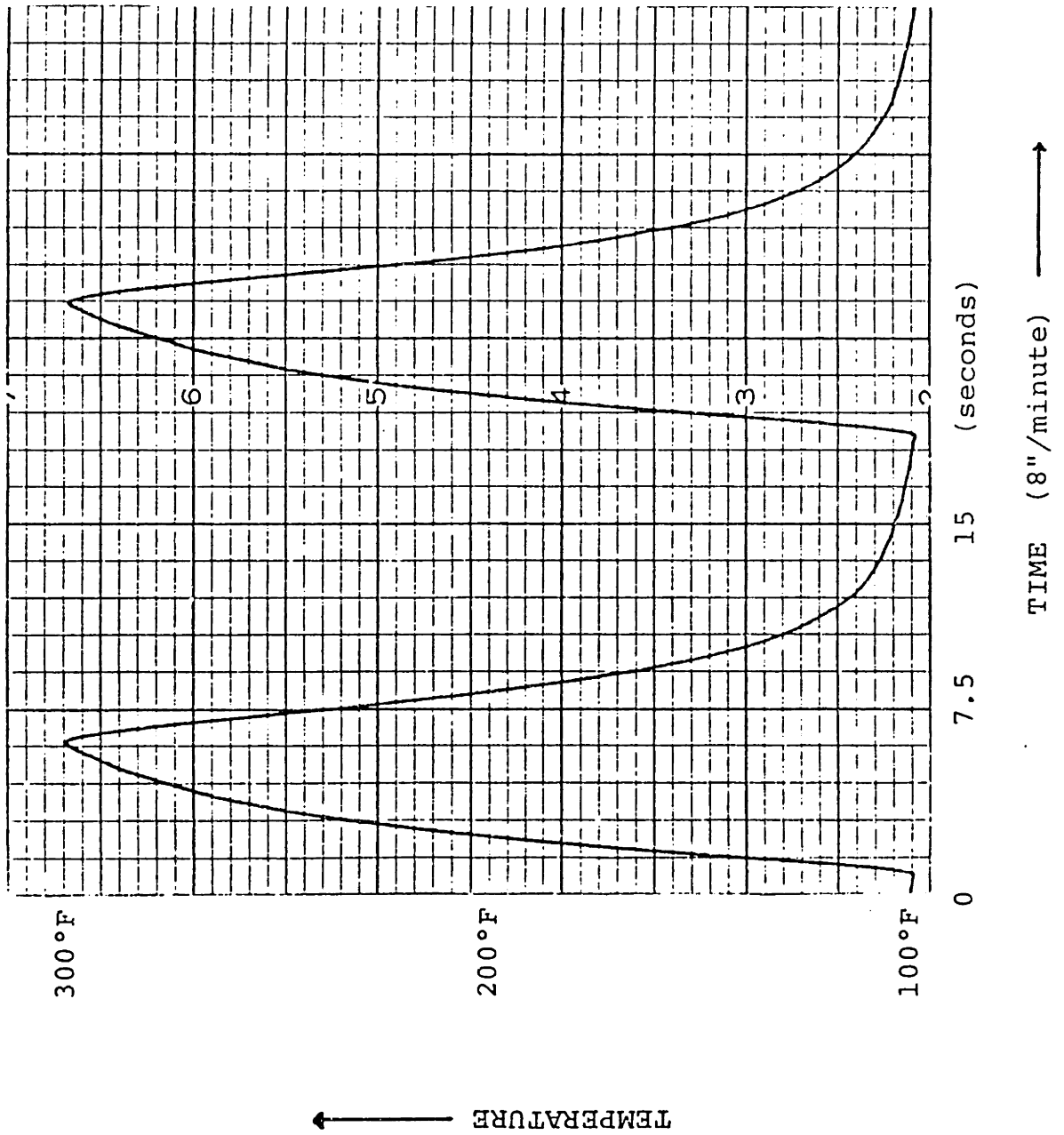


Figure V.4 : Two cycles of temperature response.

References for Chapter V

- V-1 Suh, N.P. and A.P.L. Turner, Elements of the Mechanical Behavior of Solids, McGraw-Hill Book Co., New York, 1975, pp. 477-479.

CHAPTER VIEXPERIMENTAL RESULTS OF LOW THERMAL INERTIA MOLDINGVI.1 Introduction

The aim of experimental investigation of the low thermal inertia molding (LTIM) process is to demonstrate the feasibility of molding a part with minimum residual stresses without increasing the total injection cycle time. The evaluation of the new molding concept consists of a comparison of a conventionally molded part with a part molded by the LTIM. Experimental procedures and results are discussed for conventional molding and the LTIM in Section VI.2 and Section VI.3, respectively.

VI.2 Conventional Molding(a) Experimental Procedure

Parts were molded conventionally at the Eastman Kodak Company. A 125 ton Farrel mechanical clamp injection molding machine with an 8 ounce shot size and Barber-Colman Maco IV process control was used to mold the parts. Two polystyrene materials were used: 3350 Monsanto and 685D Dow. The part dimensions were 3" x 5" x 0.030". The closed loop process control which established an injection velocity rate and switch point pressure using the runner transducer was used.

The material's melt temperatures, mold temperatures, and ram injection rates were varied. The three melt temperatures were 470°F, 520°F, and 570°F. The three mold temperatures were 70°F, 120°F, and 170°F. The five ram rates were 2, 3, 4, 5, and 6 inches per second.

In order to observe birefringences, a thin section along the filling direction was cut and polished. The samples were then placed under a cross polarized microscope to be observed along the thickness direction.

(b) Results

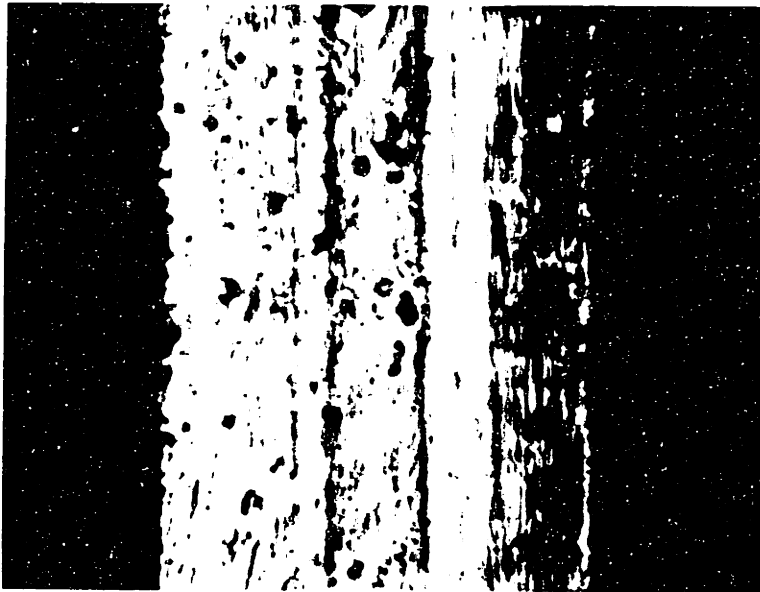
The conventional molding method was not capable of filling a 0.015" part thickness cavity completely even with 570°F melt temperature and 170°F mold temperature. An incomplete filling known as "short shot" occurred in making the 0.030" part thickness with 470°F melt temperature and 70°F mold temperature as shown in Figure VI.1.

Not only short shot but also birefringences between the cross polarized plates showing the anisotropical stress distribution can be observed from Figure VI.1. Birefringences along the thickness direction of the 0.030" part thickness are shown for 470°F melt temperature with 70°F mold temperature and 570°F melt temperature with 170°F mold temperature in Figure VI.2 (a) and (b), respectively.

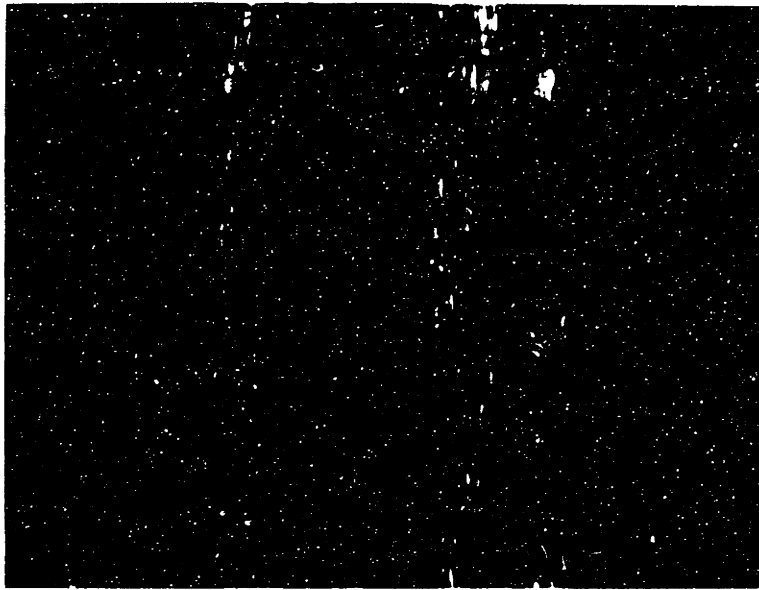
Other data for the conventional molding experiments are listed in Appendix F.



Figure VI.1 : Cross sectional view of the incomplete filler under the stress of polarized plates; part thickness = 0.03", melt temperature = 400 °F, mold temperature = 70 °F, ram rate = 3"/sec.



(a) part thickness = 0.03"
melt temperature = 470 °F
mold temperature = 70 °F
ram rate = 3"/sec.



(b) part thickness = 0.03"
melt temperature = 570 °F
mold temperature = 170 °F
ram rate = 3"/sec.

Figure VI.2 : Cross sectional view of the conventionally molded parts under the cross polarized plates

VI.3 Low Thermal Inertia Molding

(a) Preliminary Experiments and Results

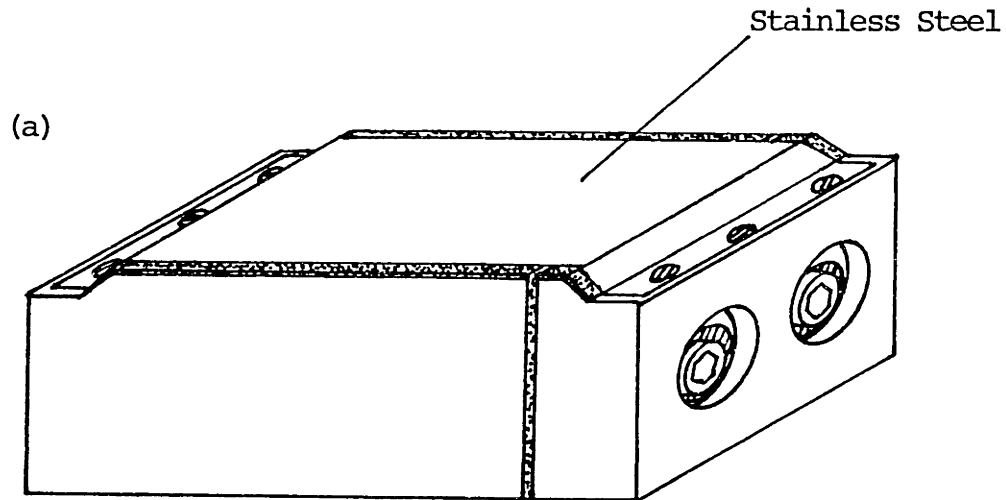
Preliminary experiments of the low thermal inertia molding were done at MIT using a thin stainless steel sheet (0.002 inch) as a heating surface. The sheets were bolted down on the aluminum mold block which had been plasma sprayed with aluminum oxide (Al_2O_3) for electrical insulation as shown in Figure VI.3.

The parts were molded using a 75 ton New Britain mechanical clamp injection molding machine with a 4 ounce shot size. The material used was Dow 687 polystyrene. The part dimensions were 2" x 4" x 0.065".

The nozzle temperature was set at 400°F. Injection pressure and holding pressure were set at 1750 psi and 500 psi, respectively. Cooling was accomplished by running tap water behind the mold, and took 25 seconds.

The mold surface temperature was raised to 350°F, then the two halves of the mold were closed for subsequent filling. The power to heat the surface of the mold was shut off, and the parts were cooled.

Parts were molded with the LTIM and without heating the surfaces of the LTIM for a comparison. Birefringences showing the anisotropical stress distribution and almost stress-free part are shown in Figure VI.4 (a) and (b), respectively. Figure VI.4 (a) and (b) shows a cross section of a part along the filling direction molded with LTIM without



Aluminum Oxide

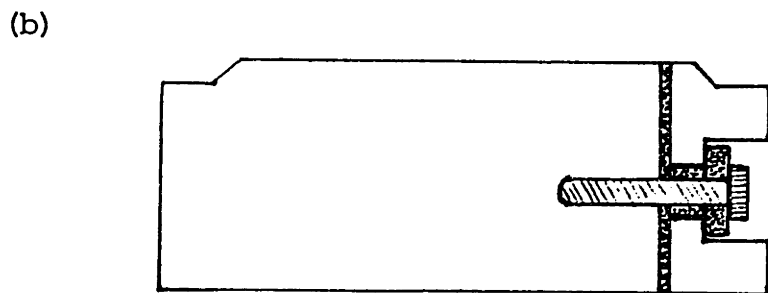
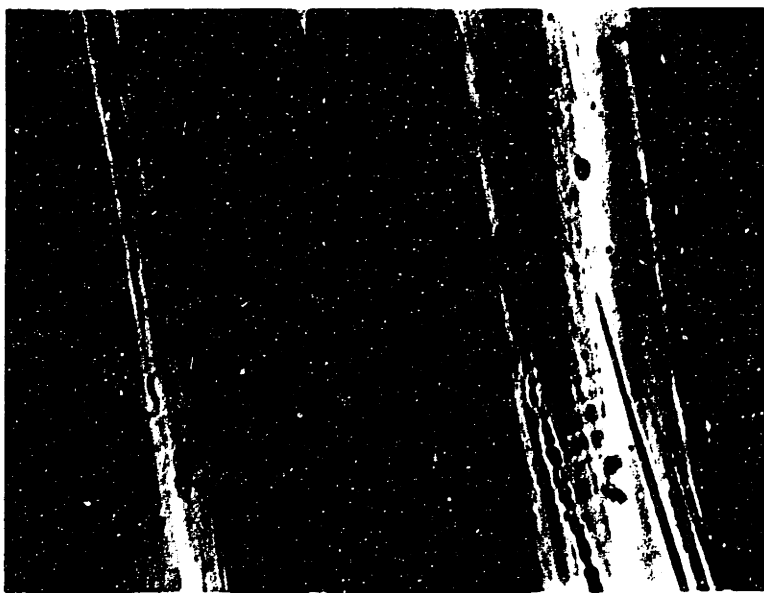
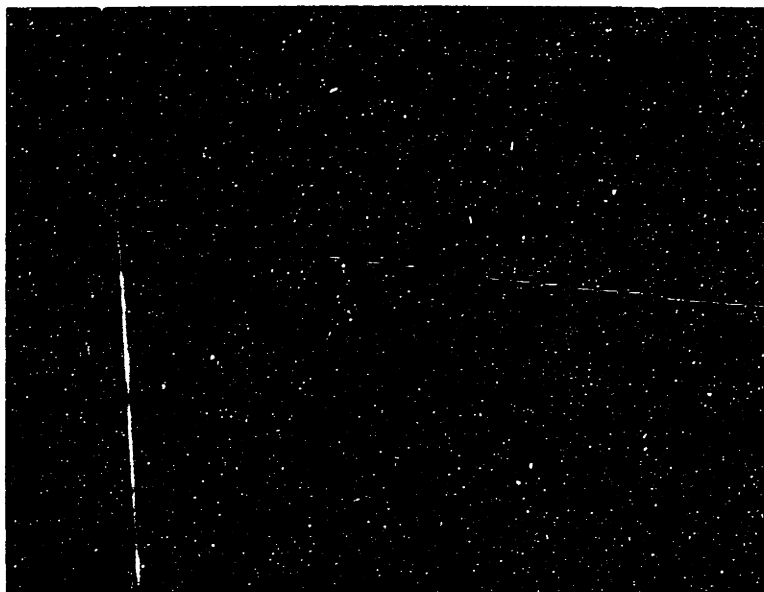


Figure VI.3 : Configuration of LTIM
(a) stainless steel as a heating surface
(b) electrical insulation of the mold



(a)



(b)

Figure VI.4 : Cross sections of the molded parts using the low thermal inertia mold with (a) heat-off and (b) heat-on under the cross polarized plates.

heating and with heating the mold surface, respectively.

(b) Low Thermal Inertia Molding and Discussion

Low thermal inertia mold inserts were prepared as described in Chapter V. The injection molding machine was the same 125 ton Farrel used in the conventional molding. The machine was operated manually.

Temperature response of the mold was taken before it was put in the machine. A non-contact temperature measurement device by Digital Heatspy Model DHS-14, a Sorensen D.C. power supply DCR 40-500A from Raytheon Company, and a Soltec 1242 two channel chart recorder were used to obtain the response curves shown in Figures VI.5 and VI.6.

The difference between the maximum temperatures in the two halves of the mold was 40°F. The two halves were connected in series and the parts were molded with the temperature difference. The area heated was 19.06 in² with 25 volts and 21.7 amps. Hence, the power density was 28.6 watts per square inch. The power density is lower than that of the mold block in Chapter V. This might be due to an increase of the insulation layers and a mild steel mold base instead of the aluminum mold base block.

Conditions of molding and the length of filling along the center of the part are listed in Table VI.1. It can be seen from the table that the length of filling is longer for the LTIM method than without heating the mold. It should be noted that turning the power off is not the same as the

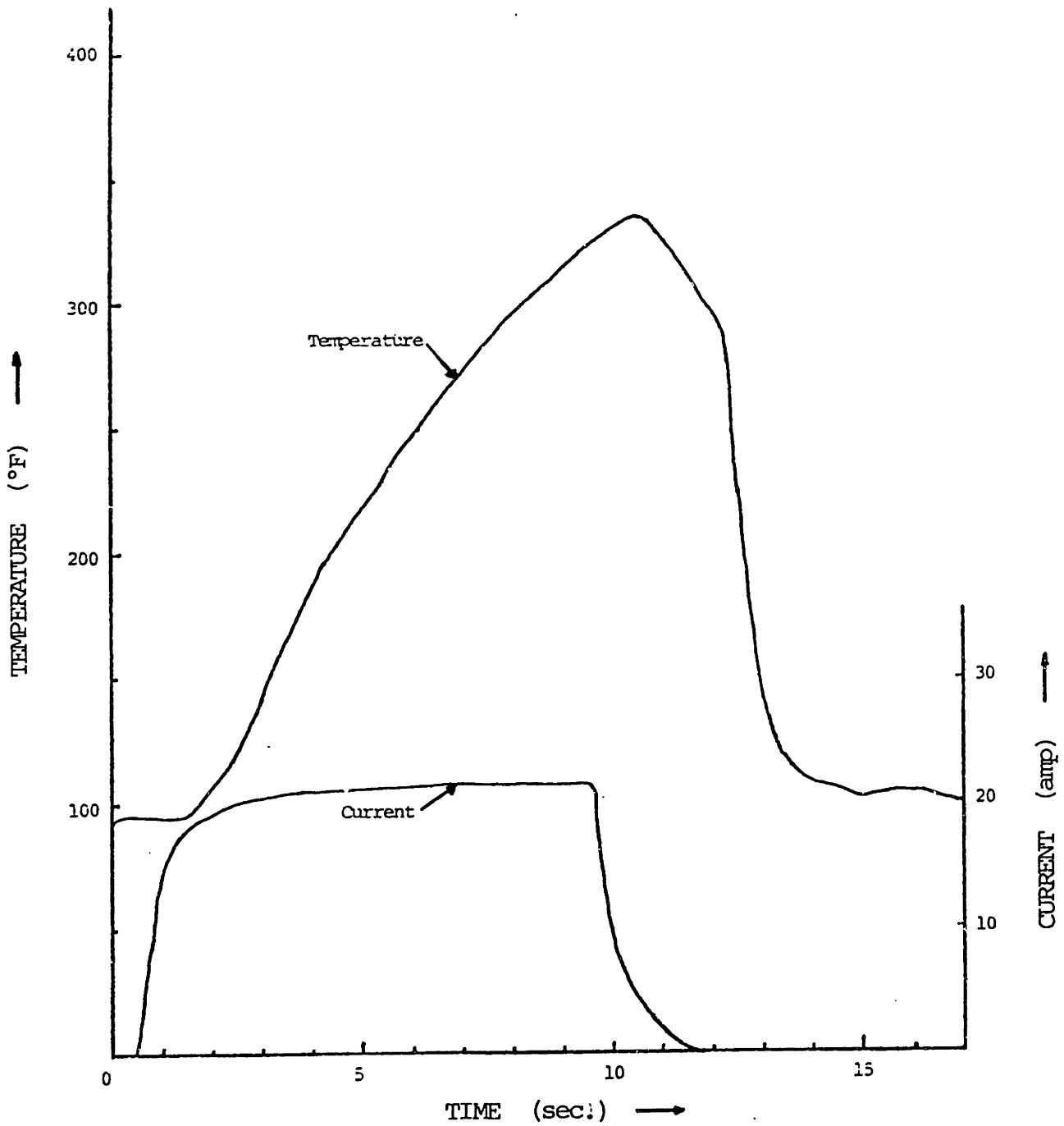


Figure VI.5 : Temperature and current response of the thin part of the mold.

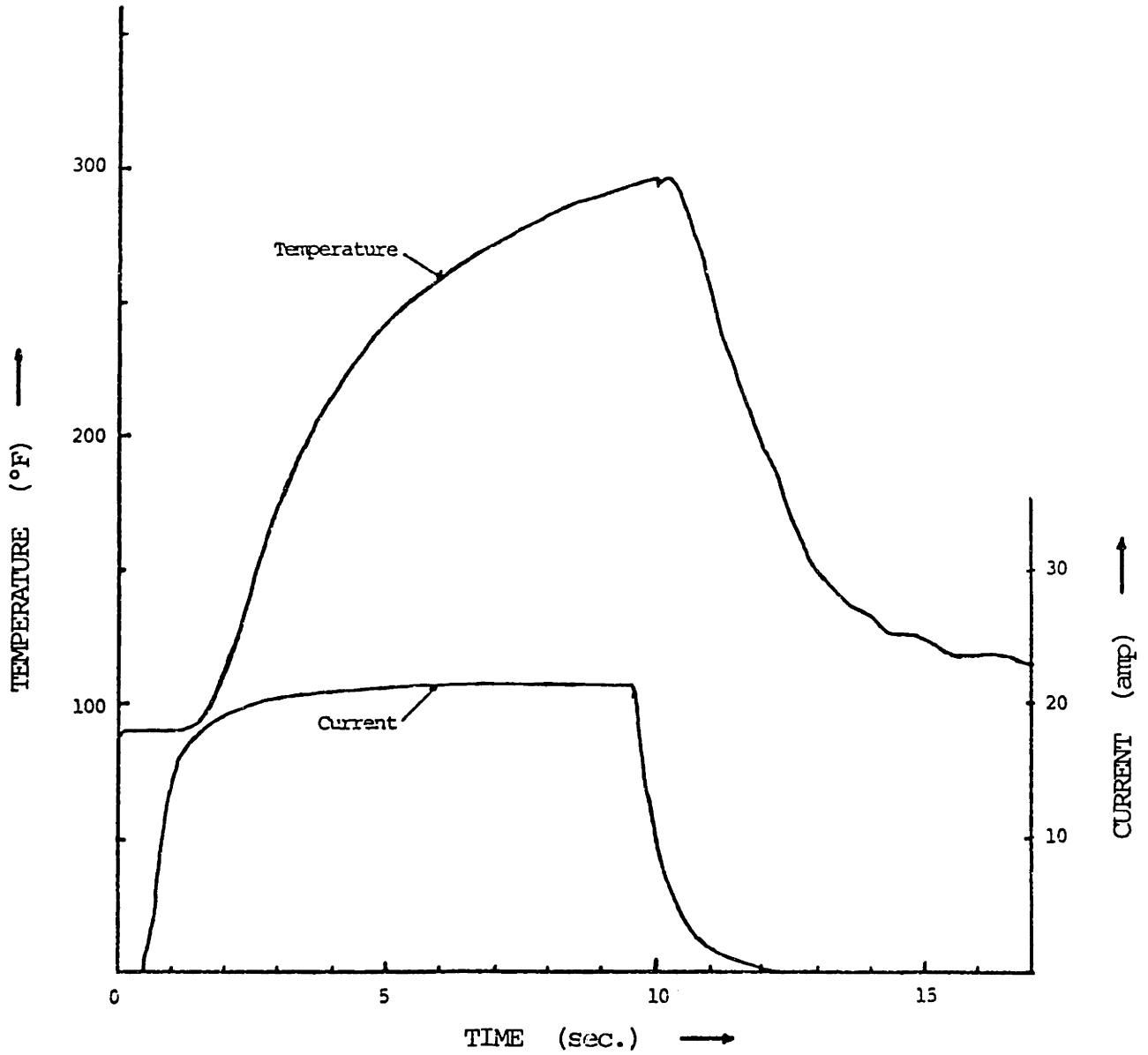


Figure VI.6 : Temperature and current response of the thick part of the mold.

Table VI.1 : Conditions of molding 0.045" x 2.5" x 5.2" part with Polystyrene (Dow 685D) by LTIM.

#	Max. Mold Surface Temperature (°F)	Melt Temperature (°F)	Hydraulic Pressure (psi)	Length of Filling (inch)	
				Heat Off	Heat On
1	275	440	1950		5.2
2	275	444	500		1.2
3	275	452	1000		5.2
4		446	750	3.0	
5	275	449	750		3.5
6	275	446	750		3.3
7	370	---	750		3.3
8	370	449	800		4.4
9		449	800	3.0	
10	370	449	850		4.6
11	370	448	900		5.0
12	370	450	925		5.1
13		450	925	3.8	
14	370	450	950		5.2
15		450	950	4.0	

conventional molding, since the multiple layers on the mold act as thermal insulation. Comparison of LTIM and power-off molding showed not as much dramatic difference as there might have been for a comparison with the conventional molding. However, the molding experiment showed that the same length can be filled with less pressure for the LTIM than the power-off molding. It can also be asserted that the same filling length can be achieved with a lower melt temperature for the LTIM than for the conventional molding.

The location of the electrode of the mold made the LTIM effect less vivid, since the brass electrode acts as a heat sink and cooled the incoming melt. The electrode can be relocated to avoid the unnecessary pressure drop due to the chilling effect.

(c) Suggestions for Future Work

Quality of the mold surface should be improved. Since the silicone rubber had been layed over the surface by hand, the mold surface was not smooth. A spray technique to apply the silicone rubber could improve the mold surface smoothness.

Temperature distribution on the mold surface should be uniform. The edge effect of the mold should be taken into account when the heat loss to the mold block is a considerable amount. The edges of the mold can be heated more to balance the extra heat loss along the edges. The edges of the mold can also be thermally insulated more to balance the loss.

The temperature of the mold surface should be controlled directly. In other words, a temperature sensing device should feed back the temperature information quickly and accurately. The temperature must be controlled even during the cooling period, when parts are differentially cooled by differentially heating the mold surface. Controlling the temperature of the mold surface is an essential task of the LTIM.

The optimum mold surface temperature during the filling process should be investigated, since the length of the part during filling appears to be the same whether the mold surface temperature is 275°F or 370°F as seen from #6 and #7 in Table VI.1. It may not be necessary to exceed the glass transition temperature of the material by more than 50°F, which could be substantially less than the temperature for isothermal filling. It would be advantageous to use this lower surface temperature in order to minimize the cycle time yet still fill the mold completely.

Other possible applications of the LTIM method should be investigated. Since there is no solidification layer during the filling, a multiple cavity mold would be easily balanced. Additionally, molding of materials over the heated mold surface can reduce the wear rate of the mold for glass fiber composite, and can improve the surface quality of structural foam materials. The heated mold surface can also be used to cure thermosetting materials.

CHAPTER VIICONCLUSIONS

- (1) Modern injection molding control systems such as the Maco IV made by Cincinnati Milacron are capable of producing parts of the same weight even when the molecular weight of incoming material varies as much as 20 percent. With an open-loop type control machine, it was impossible to process these materials due to the change in the melt viscosity. Although the modern process control can handle the variation of viscosity of incoming material, it can not produce parts with the minimum residual stress on every molding cycle. In order to make acceptable parts consistantly, controlling the viscosity may not be the only process variable that must be controlled.

- (2) The low thermal inertia molding (LTIM) method can minimize the residual stress in the molded part. The LTIM only heats the surface of the mold and not the entire mold, thereby reducing the total cycle time. Since only the surface is being heated while the melt fills the cavity, it can eliminate vitrification during the filling process and the part can be cooled rapidly. The method uncouples the cooling process from the filling process. This uncoupling allows consistancy of the modling process and low pressure molding.

- (3) The developed mold consists of a woven graphite fiber fabric as a heating element, RTV silicon rubber as an adhesive, and a plasma sprayed ZrO_2 layer on the mold surface as a moderate thermal insulation. The mold had a fast temperature response time ($100^\circ F$ to $300^\circ F$ in 5.3 seconds for heat-up using 48.3 watts/in^2 and in 12.3 seconds for cool down). Also the mold endured greater than 20,000 thermal cycles without any deterioration. The combination of RTV silicon rubber and graphite yields a durable LTIM.
- (4) Study of molecular relaxation showed that the flow-induced orientation can be relaxed on the order of a second. When the relaxation takes place before the vitrification, a part with the minimum residual stress can be molded. Because of the viscoelastic nature of the polymer melt, the more strain the melt undergoes within the longest relaxation time period the faster it will relax. Hence the cavity should be filled as rapidly as possible for molecular relaxation and for decreasing total cycle time. If the molding machine, however, can not provide the rapid filling then the mold surface may be heated beyond the filling process to relax slowly relaxing orientation due to small strain from the slow filling process. Therefore, molding a part with the minimum residual stress can be achieved with the heated mold surface.

- (5) Differential cooling by a differential heating method can minimize the secondary flow of the material within the part. Since the method heats the surfaces of thinner sections to have the same cooling rate as the thickest section of the part, it prevents secondary flow without increasing the total cycle time.
- (6) The LTIM method described in this thesis should be applicable to other molding methods, such as casting, compression molding, stamping, and thermoforming. Furthermore, injection molding thermosetting, composites and structural foam materials should all benefit from LTIM.

APPENDIX APreliminary Test Results for Modern Injection Molding

machine : 75 ton, 4 ounce barrel,
Cincinnati Milacron

control : velocity of the ram and
peak cavity pressure

material : polystyrene manufactured solely for
this test by
American Hoechst Co.

<u>Material</u>	\bar{M}_n	\bar{M}_w	<u>Polydispersity</u>	ρ (g/cm ³)
A	87167	245071	2.81	1.042
B	74954	181235	2.43	1.043
C	97182	292659	3.01	1.042

Figure A1 - A8 : Important Injection Molding Parameters
during 50 shots for each material.

Preliminary Conclusion : Although the three materials
(A, B and C) were so different
in their molecular weight
that material B flashed while
material C could not even fill
the mold with open loop control,
the velocity and peak cavity pres-
sure control produced parts with
a consistant density.

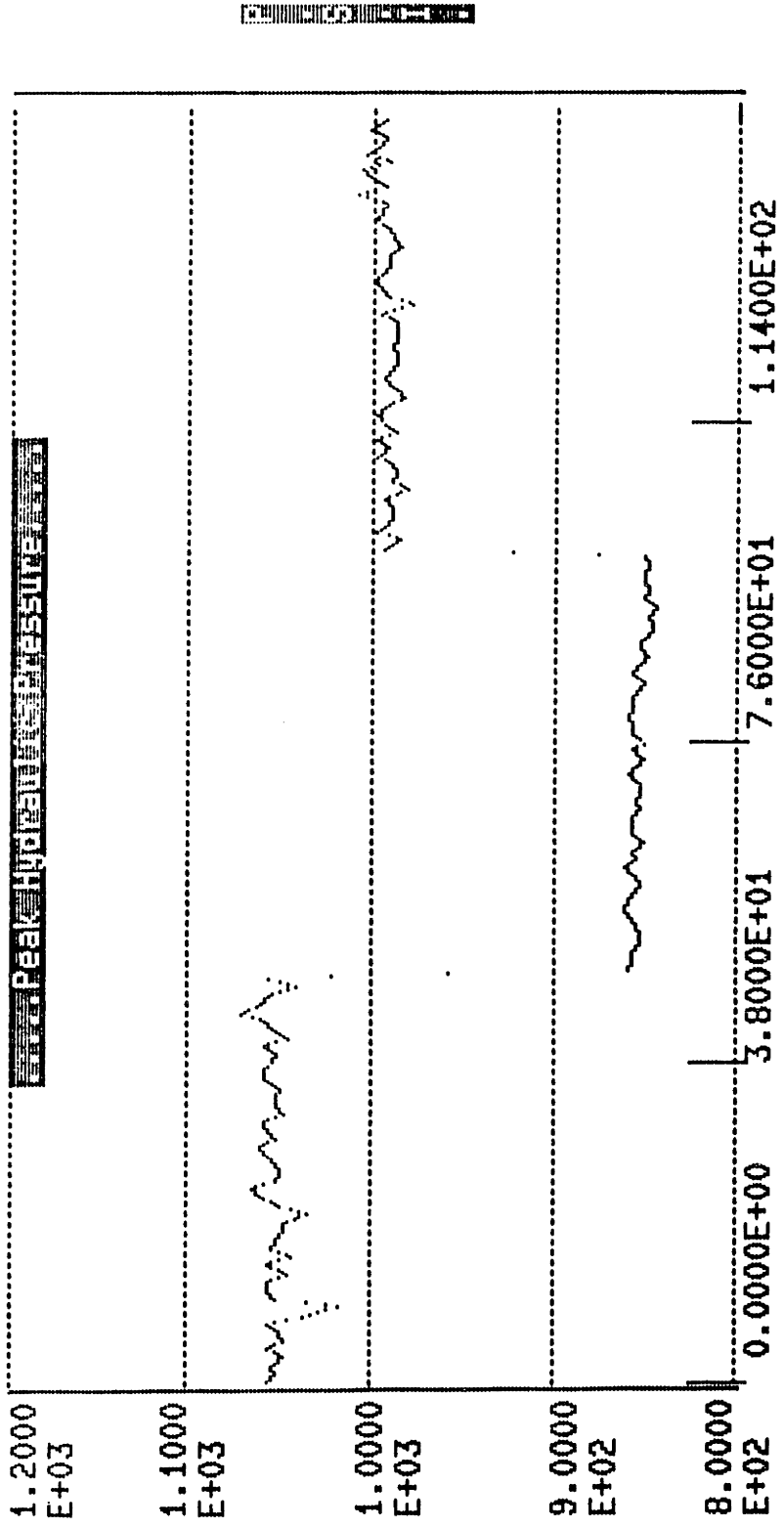


Figure A1. Hydraulic pressure for the three molecular weight materials. This is based on constant velocity with a fixed gate pressure.

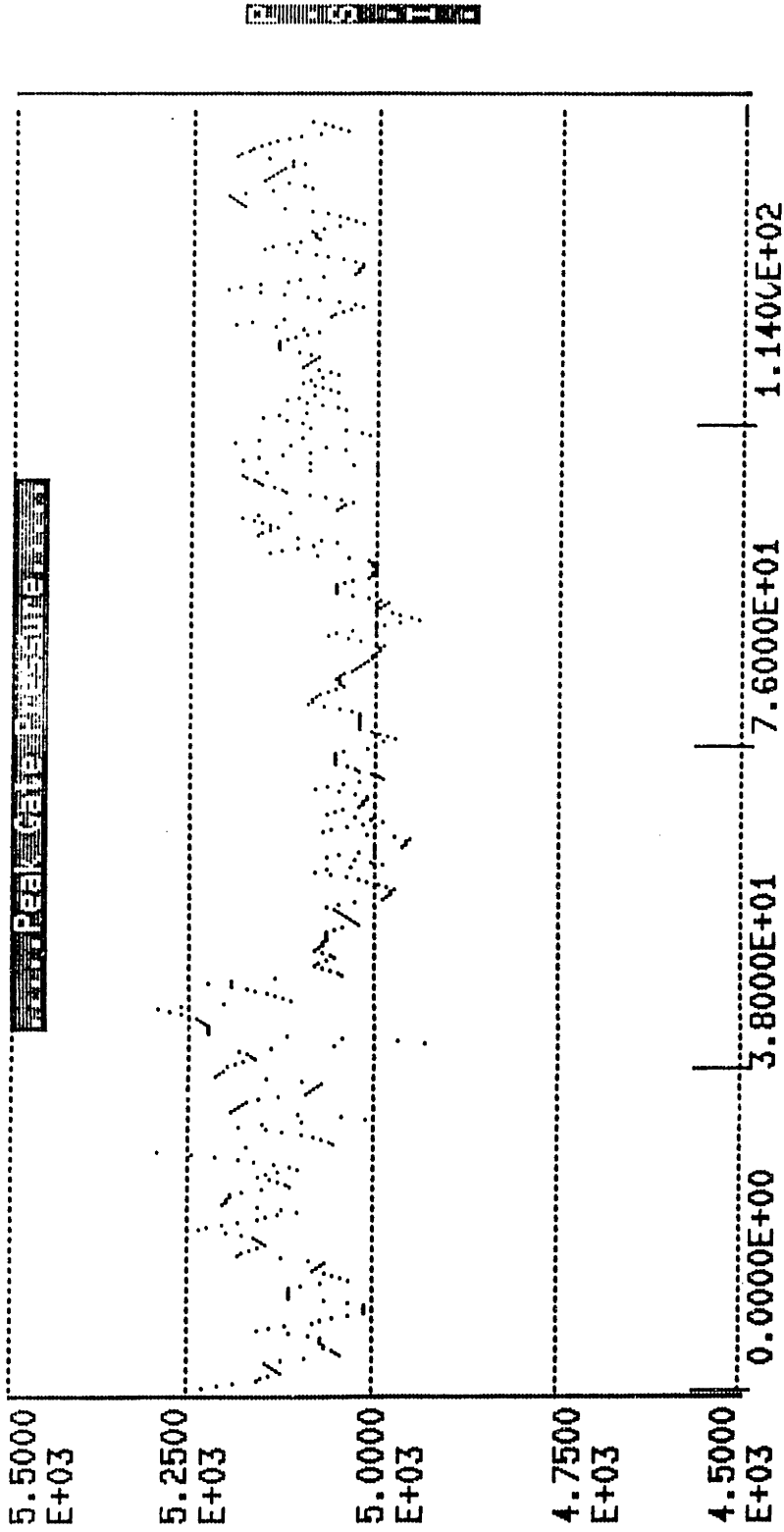


Figure A2. Gate pressure for the three molecular weight materials. This is based on constant velocity with a fixed gate pressure.

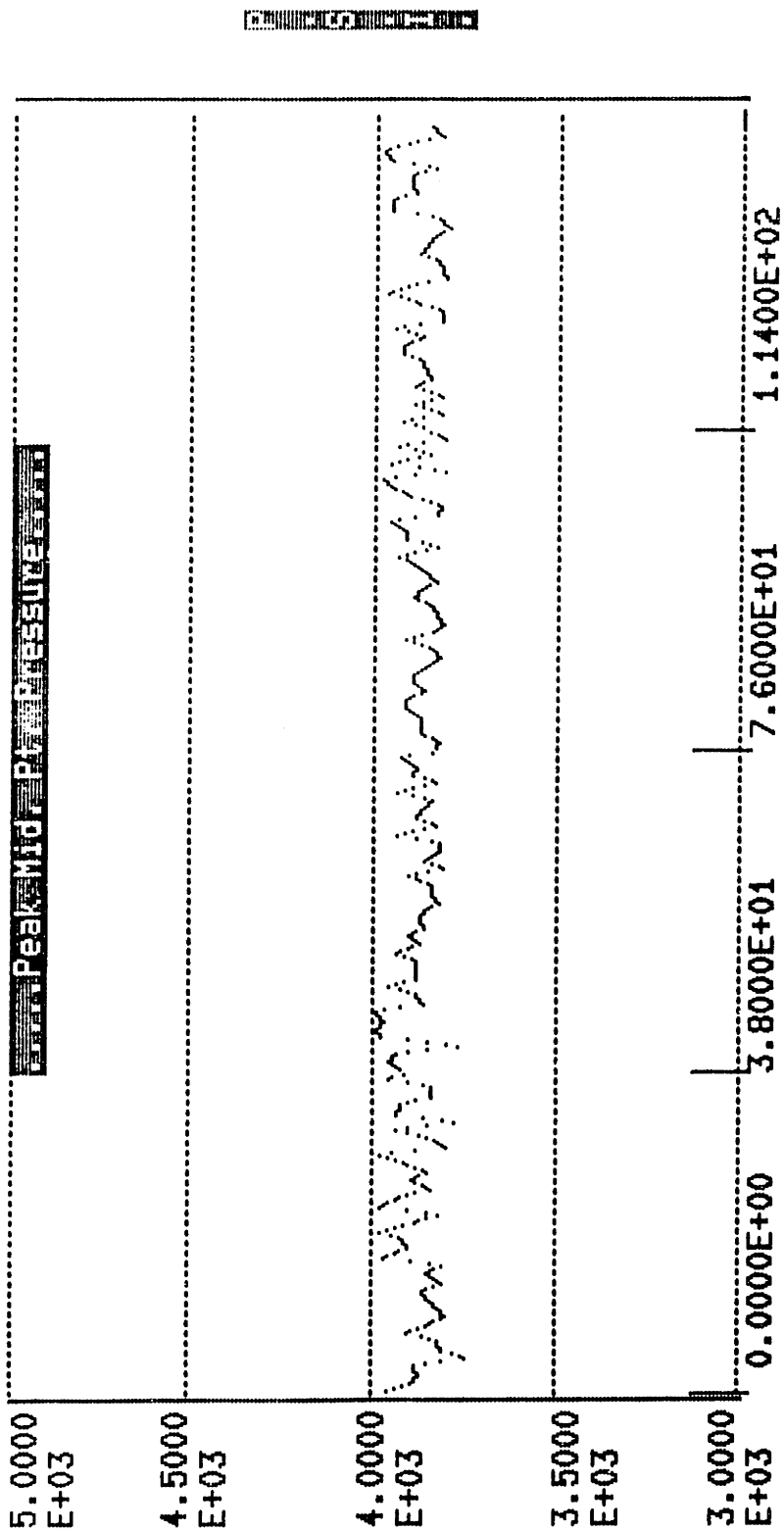


Figure A3. Mid. Pt. pressure for the three molecular weight materials. This is based on constant velocity with a fixed gate pressure.

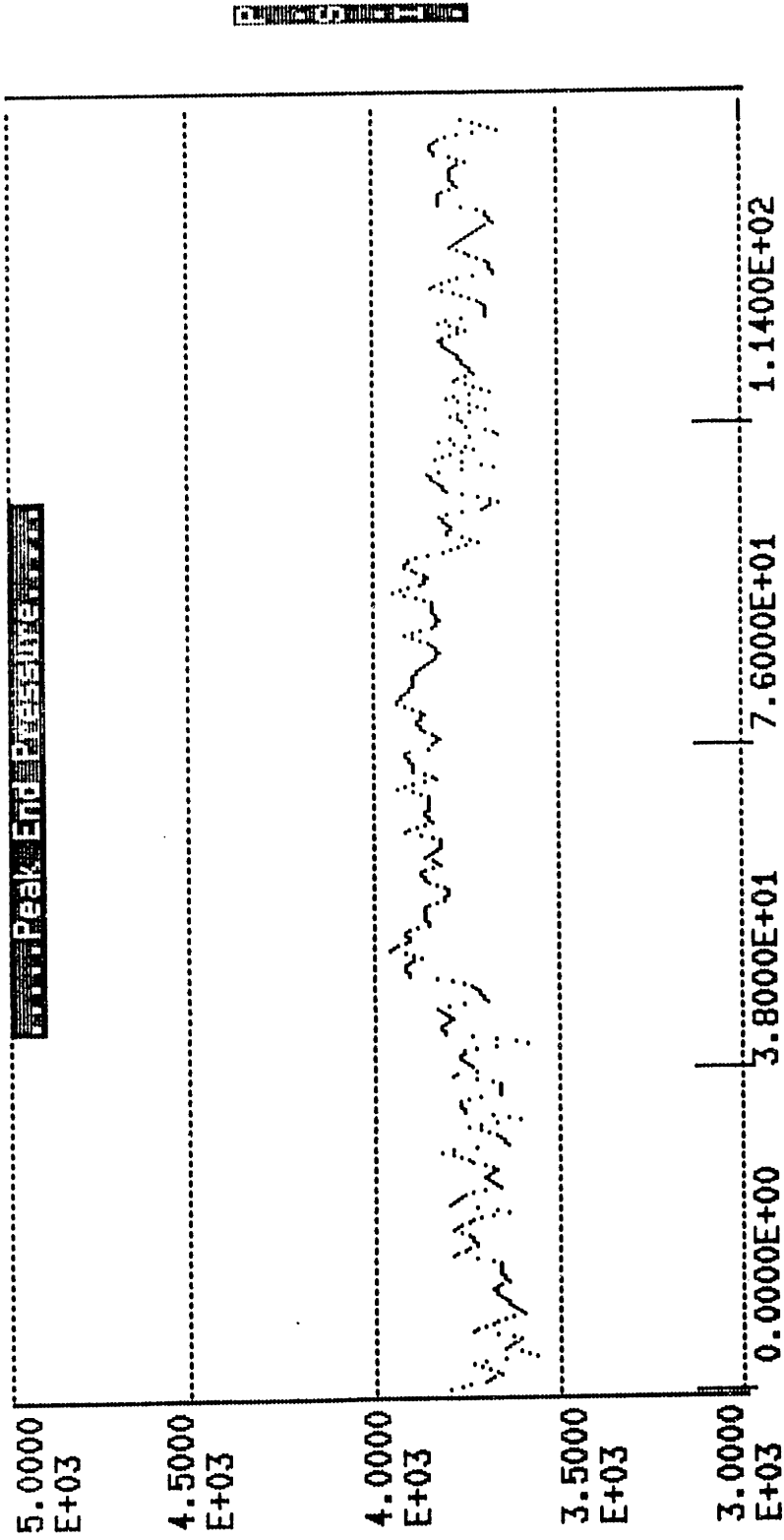


Figure A. End pressure for the three molecular weight materials. This is based on constant velocity with a fixed gate pressure.

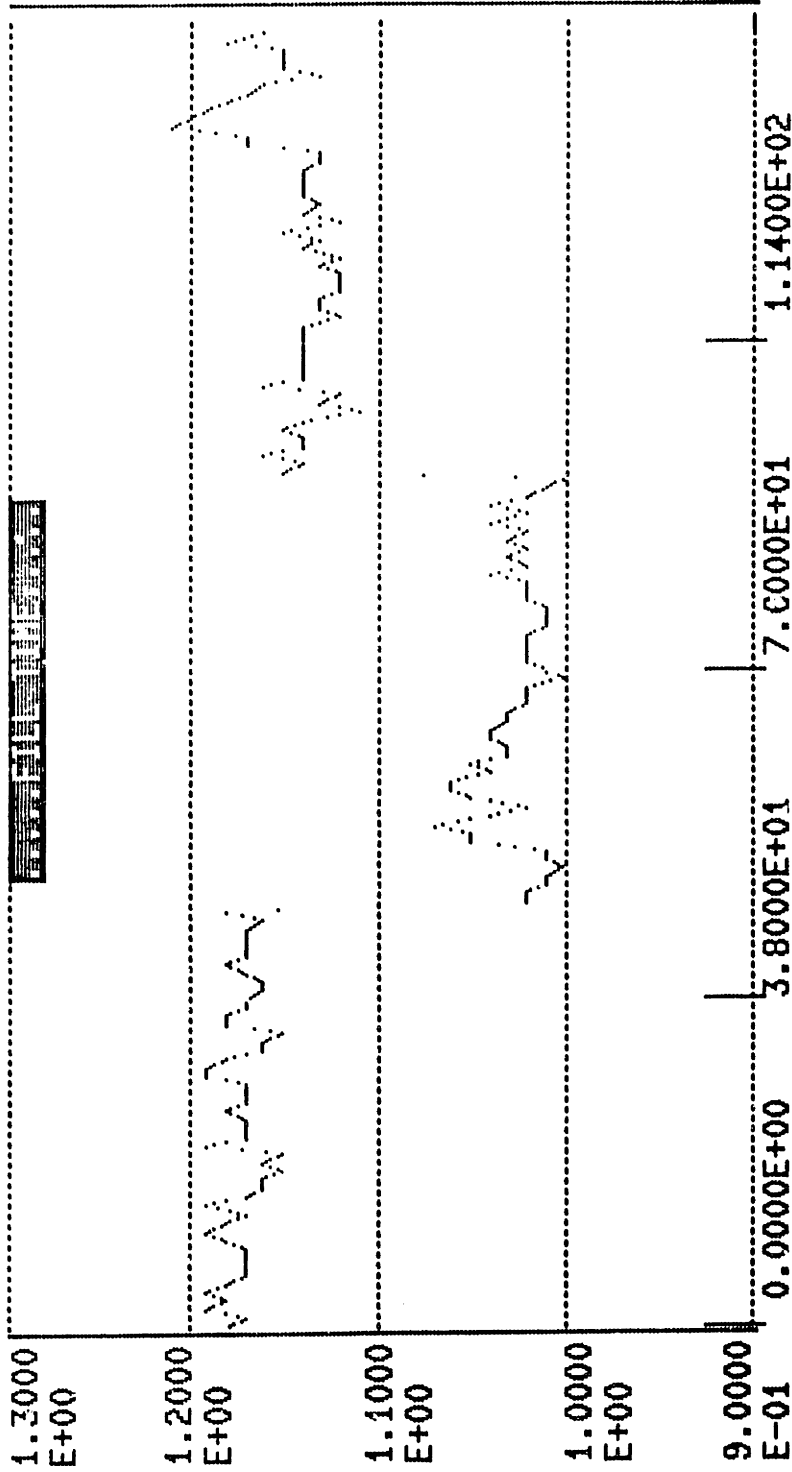


Figure 5. Fill time for the three molecular weight materials. This is based on constant velocity with a fixed gate pressure.

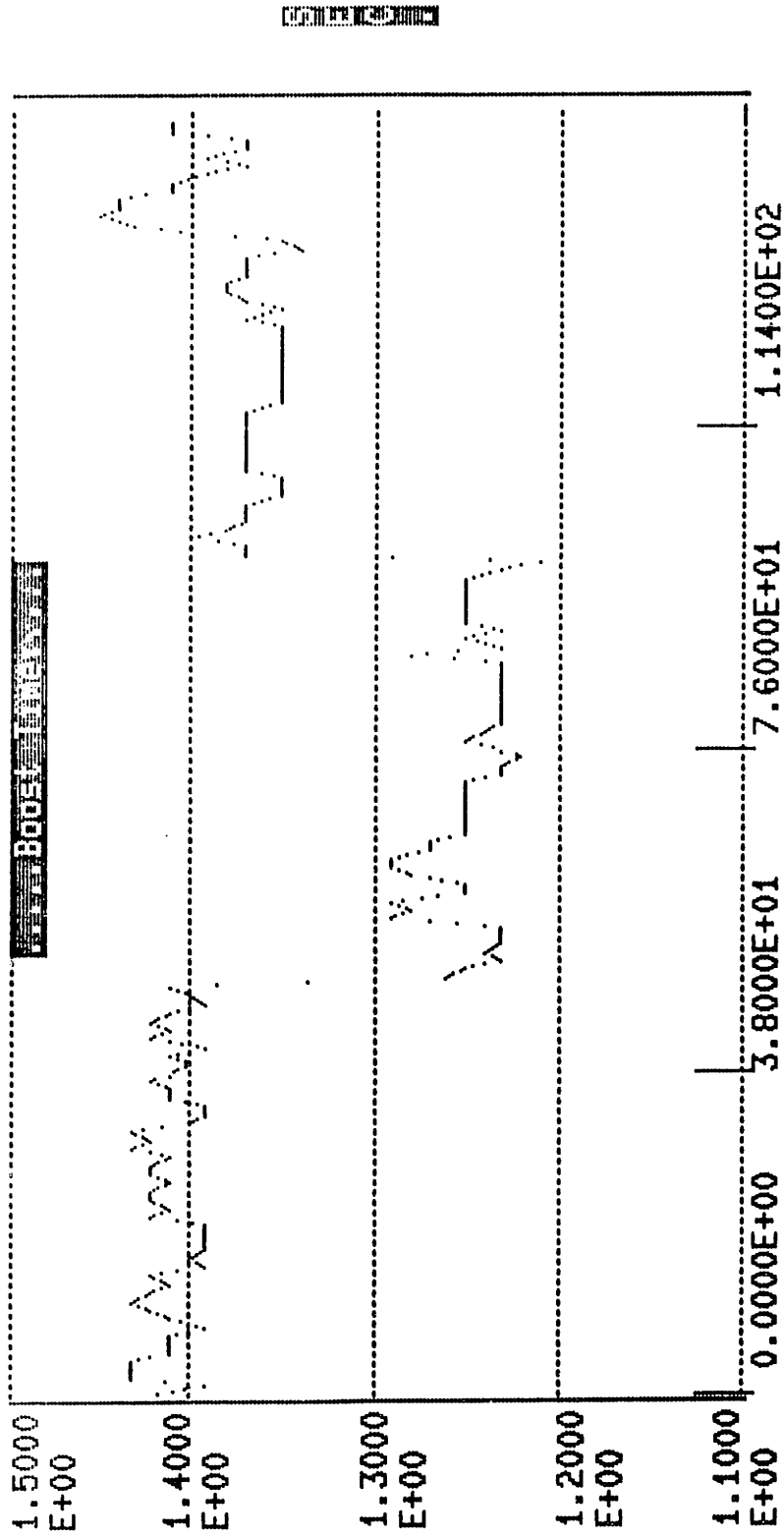


Figure A6. Boost time for the three molecular weight materials. This is based on constant velocity with a fixed gate pressure.

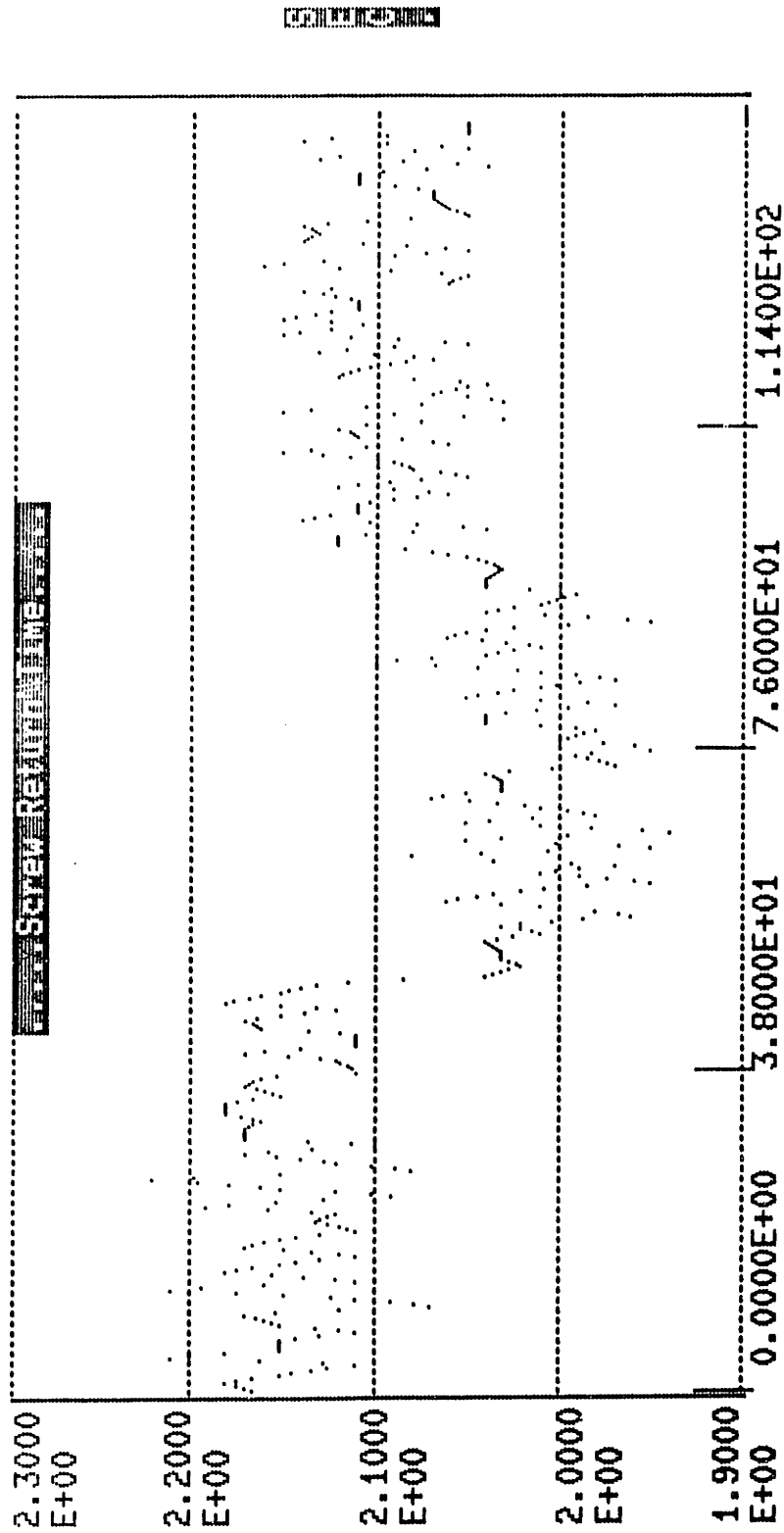


Figure A7. Screw return time for the three molecular weight materials. This is based on constant velocity with a fixed gate pressure.

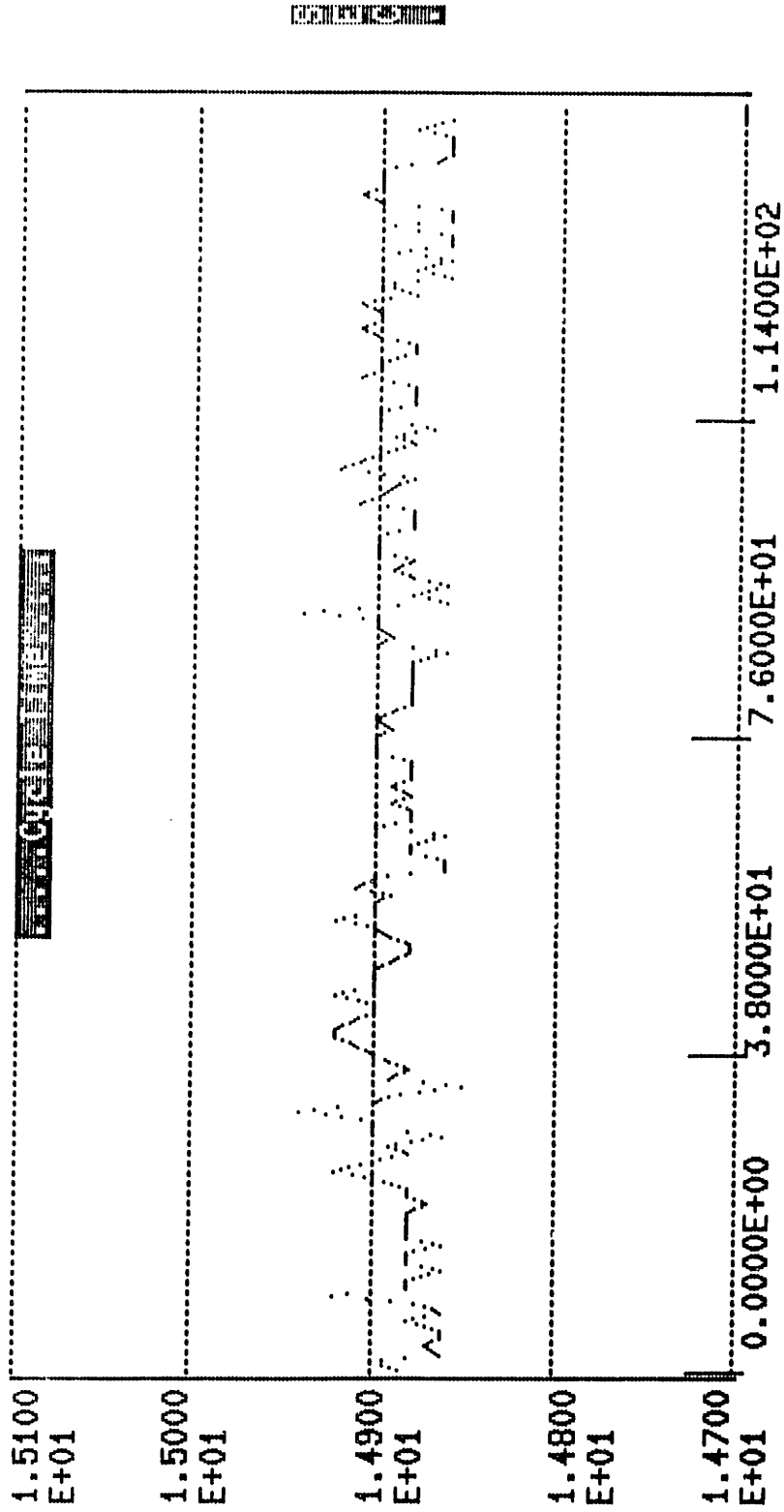


Figure A8. Cycle time for the three molecular weight materials. This is based on constant velocity with a fixed gate pressure.

APPENDIX B

Derivation of Equation (16) in Chapter IV

For convenience, equation (13) and (15) in chapter IV are rewritten.

$$\tau_{12} = \sum_i a_i \int_{t-t'=0}^{\infty} \exp \frac{-(t-t')}{\tau_i} \exp(-n \cdot \gamma_{t,t'}) \gamma_{t,t'} d(t-t') \quad (13)$$

$$\gamma_{t,t'} = \begin{cases} 0 & \text{for } t-t' < t \\ \dot{\gamma}_0(t-t') - \dot{\gamma}_0(t) & \text{for } t-t' \geq t \end{cases} \quad (15)$$

Let $t-t' = s$, then equations (13) and (15) become:

$$\tau_{12}(t) = \sum_i a_i \int_{s=0}^{\infty} \exp \frac{-s}{\tau_i} \exp(-n \cdot \gamma_{t,t'}) \gamma_{t,t'} ds \quad (13)'$$

$$\gamma_{t,t'} = \begin{cases} 0 & \text{for } s < t \\ \dot{\gamma}_0(s-t) & \text{for } s \geq t \end{cases} \quad (15)'$$

Substituting equation (15)' into equation (13)',

$$\begin{aligned}
 \tau_{12}(t) &= \sum_i a_i \int_t^{\infty} e^{-s/\tau_i} e^{-n \cdot \dot{\gamma}_o (s-t)} \dot{\gamma}_o (s-t) ds \\
 &= \sum_i a_i \int_t^{\infty} e^{-s \left[1/\tau_i + n \cdot \dot{\gamma}_o \right] + n \cdot \dot{\gamma}_o t} \dot{\gamma}_o (s-t) ds \\
 &= \sum_i a_i \int_t^{\infty} e^{-s \left[\frac{1 + n \cdot \dot{\gamma}_o \tau_i}{\tau_i} \right]} e^{n \cdot \dot{\gamma}_o t} \dot{\gamma}_o (s-t) ds \\
 &= \sum_i a_i e^{n \cdot \dot{\gamma}_o t} \dot{\gamma}_o \int_t^{\infty} e^{-s \left[\frac{1 + n \cdot \dot{\gamma}_o \tau_i}{\tau_i} \right]} (s-t) ds
 \end{aligned}$$

integrating by parts,

$$\begin{aligned}
 &= \sum_i a_i e^{n \cdot \dot{\gamma}_o t} \dot{\gamma}_o \left\{ (s-t) \left(- \frac{e^{-s \left[\frac{1 + n \cdot \dot{\gamma}_o \tau_i}{\tau_i} \right]}}{\left[\frac{1 + n \cdot \dot{\gamma}_o \tau_i}{\tau_i} \right]} \right) \right. \\
 &\quad \left. - \frac{e^{-s \left[\frac{1 + n \cdot \dot{\gamma}_o \tau_i}{\tau_i} \right]}}{\left[\frac{1 + n \cdot \dot{\gamma}_o \tau_i}{\tau_i} \right]^2} \right\} \Bigg|_t^{\infty} \\
 &= \sum_i a_i e^{n \cdot \dot{\gamma}_o \tau_i} \dot{\gamma}_o \left\{ 0 + \frac{e^{-t \left[\frac{1 + n \cdot \dot{\gamma}_o \tau_i}{\tau_i} \right]}}{\left[\frac{1 + n \cdot \dot{\gamma}_o \tau_i}{\tau_i} \right]^2} \right\}
 \end{aligned}$$

$$= \dot{\gamma}_0 \sum_i \frac{a_i \tau_i^2 e^{-t/\tau_i}}{(1 + n \cdot \dot{\gamma}_0 \tau_i)^2} ,$$

which is equation (16) in chapter IV.

APPENDIX C

User-Supplied Subroutine for the Powell Nonlinear
Regression Program

```

FUNCTION FUN(NPARAMS,PARAMS,NDATAS,DATAS)
DIMENSION PARAMS(NPARAMS),DATAS(NDATAS),TAU(8),A(8),P(8)
OPEN (3,FILE='ASUBI.DAT',STATUS='NEW')

```

```

IF (II.NE.0) GOTO 44

```

```

OPEN(5,FILE='PAT.DAT',TYPE='OLD',FORM='FORMATTED')
DO 99 I=1,8
READ(5,*) P(I)
99 CONTINUE
II=1

```

```

44 OMEGA=DATAS(9)

```

```

C

```

```

AA=PARAMS(1)
B=PARAMS(2)
C=PARAMS(3)
D=PARAMS(4)
C=P(1)*C
D=P(2)*D
GP=0.0

```

```

C

```

```

DO 51 I=1,8
TAU(I) = DATAS(I)

```

```

51 CONTINUE

```

```

C

```

```

DO 101 I=1,8
E=ALOG(TAU(I)*1000.)
G=B+AA*E+C*(E/(FLOAT(I)+1.))
F=D*(TAU(I)**2)
A(I)=EXP(G)+F
DEN = 1.0 + ((OMEGA*TAU(I))**2)
GP = GP + (A(I)*TAU(I)*((OMEGA*TAU(I))**2)/DEN)
WRITE(3,*) 'A-SUB-',I,' IS:',A(I)

```

```

101 CONTINUE

```

```

C

```

```

WRITE(3,*) 'OMEGA=',OMEGA, ' GP=',GP
FUN = GP

```

```

C

```

```

RETURN
END

```

APPENDIX D

Computer Program Listing for Nonisothermal stress
Relaxation


```

C                                PROGRAM MAIN
COMMON /ZCM/ T12(40,40),T11(40,40),BR(40,40),srm(40)
COMMON /stuff/ tem(40,40),iy,it,AT,TI(9),AI(9)
common/label/ ht,zl,xt,c
data tgt/100./
print*,'enter ht'
read*,ht
print*,'enter zl'
read*,zl
print*,'enter xt'
read*,xt
PRINT*,'ENTER px'
READ*,C

100  CALL TEMP

      ITMAX=40
      IYMAX=40
      call shear

200  DO 20 IY=IYMAX,1,-1
300    DO 30 IT=1,ITMAX
      IF (TEM(IY,IT).LE.TGT) GOTO 400
      CALL ADJUST
      CALL CALCT12
      GOTO 30

400    T12(IY,IT)=T12(IY,IT-1)
      T11(IY,IT)=T11(IY,IT-1)
      BR(IY,IT)=BR(IY,IT-1)

30    CONTINUE
20    CONTINUE

      CALL PLOTTHD
      STOP
      end

```

SUBROUTINE CALCT12

```

COMMON /ZCM/ T12(40,40),T11(40,40),BR(40,40),srm(40)
COMMON /STUFF/ TEM(40,40),IY,IT,AT,TI(9),AI(9)
common /label/ ht,zl,xt,C
DIMENSION AA(8)
cfte=1./6.895e3
COV=.31028
pn=.32
en=.25

```

```
sr=srm(iy)
```

```

ST=FLOAT(it-1)*XT/39.
IF( ST .NE. 0.) GOTO 23
DO 11 K=1,8
AA(K)=0.
11 CONTINUE
DT=0.
PAT=1.
GOTO 26
23 DT=XT/39.

```

```

26 TEMP2=0.
    TEMP=0.
    DO 300 Ik=1,8
BB=1./(TI(IK)*PAT)
CC=1./(TI(IK)*AT)
a=(ai(ik)*ti(ik)*ti(ik))
A1=A*TI(IK)
AA(IK)=AA(IK)+((BB+CC)/2.)*DT
b=exp(-AA(IK))
d=(1.+en*sr*ti(ik))**2
D1=(1.+EN*SR*TI(IK))**3
temp=temp+a*b/d
TEMP2=TEMP2+A1*B/D1

```

```

300 CONTINUE
    T12(iy,it) = CFTE*SR*TEMP
    T11(IY,IT) = CFTE*SR*SR*TEMP2*2.
    BR(IY,IT)=COV*SQRT(4.*T12(IY,IT)**2+T11(IY,IT)**2)

```

```

PAT=AT
return
END

```

SUBROUTINE ADJUST

```
common /stuff/ tem(40,40),iy,it,at,ti(9),ai(9)
```

```
dimension tinot(8),ainot(8)
```

```
data tg/100./
```

```
t=tem(iy,it)
```

```
atnot=9.131e-11
```

```
at=10**((-17.44*(t-tg))/(51.6+t-tg))
```

```
DATA TI/69.8,15.7,6.98,1.57,0.698,0.157,0.0698,0.0157,0./
```

```
DATA AI/86.,442.,1640.,16560.,58000.,564000.,1.94E6,1.86E7,0./
```

```
AT=AT/ATNOT
```

```
return
```

```
end
```

```

subroutine temp
common /stuff/ tem(40,40),iy,it,at,ti(9),ai(9)
common /label/ ht,zl,xt
external eqn,lbound,hbound,ui
dimension array(80,40), aux(2,220)
data naux/220/

call pdparc(eqn,lbound,hbound,ui,-HT,HT,0.,XT,200,100,array,
1 80,40,aux,naux)

do 30 i=1,40
  do 40 j=1,40
    tem(i,j)=array(i+39,j)
40  continue
30  continue

c   print*, tem

end

SUBROUTINE PDPARC(EQN, LBOUND, HBOUND, UI,
1 XL, XH, TI, TF, NDX, NDT,
2 ARRAY, NX, NT, AUX, NAUX)
C
C METHOD OF CRANK-NICHOLSON
C WITH SECOND-ORDER CORRECT BOUNDARY CONDITIONS(OFFSET MESH).
REAL XL, XH, TI, TF, ARRAY, AUX, UI
INTEGER NDX, NDT, NX, NT, NAUX
EXTERNAL EQN, LBOUND, HBOUND, UI
DIMENSION ARRAY(NX,NT), AUX(2, NAUX)
C
C THE ARRAY ROW AUX(1, I) MAY MEAN EITHER U(I) OR THE RATIO
C DIFC(I) / BETA(I). EITHER COMMENT CARDS OR CONTEXT INDICATES
C WHICH MEANING APPLIES. THE ROW AUX(2, I) HOLDS A PARAMETER
C GAMMA(I).
REAL A, AA, BETA, DDX, DIFA, DIFB, DIFC, DIFD, DT, DX, HDT, HDX,
1 P, Q, T, TEM1, TEM2, TT, UM1, X, XX
INTEGER I, IMAX, J, JJ, K, N, NFREQT, NFREQX
DIMENSION A(4), P(3), Q(3)
C
C COMPUTE SPACE AND TIME INTERVALS
DX = (XH - XL) / FLOAT(NDX)
HDX = 0.5 * DX
DDX = DX * DX
DT = (TF - TI) / FLOAT(NDT)
HDT = 0.5 * DT
C
C COMPUTE STORAGE FREQUENCIES FOR ARRAY
NFREQX = NDX / (NX - 1)
NFREQT = NDT / (NT - 1)
C
C INITIALIZE DEPENDENT VARIABLE ARRAY

```

```

      XX = XL - DX - HDX
      IMAX = MDX + 2
      DO 10 I = 1, IMAX
C
C   U(I) = UI(XX + FLOAT(I) * DX)
10   AUX(1, I) = UI(XX + FLOAT(I) * DX)
C
C   STORE ARRAY VALUES
      J = 1
20   N = 1
      DO 30 I = 1, NX
C
C   ARRAY(I, J) = (U(N) + U(N+1)) / 2.
      ARRAY(I, J) = 0.5 * (AUX(1, N) + AUX(1, N + 1))
30   N = N + NFREQX
C
C   RETURN WHEN ARRAY IS FILLED
      J = J + 1
      IF (J .GT. NT) RETURN
C
C   MAIN SUBROUTINE LOOP
      JJ = (J - 2) * NFREQT
      DO 80 K = 1, NFREQT
C
C   INCREMENT TIME
      T = TI + FLOAT(JJ + K) * DT
      TT = T - HDT
C
C   COMPUTE LEFT BOUNDARY COEFFICIENTS
      CALL LBOUND(T, P)
      UM1 = AUX(1,1)
C
C   TEM1 AND TEM2 ARE TEMPORARY STORAGE LOCATIONS FOR
C   INTERMEDIATE RESULTS
      TEM1 = 0.5 * P(2)
      TEM2 = P(1) / DX
      BETA = TEM1 - TEM2
C
C   AUX(1, 1) = DIFC(1) / BETA(1)
      AUX(1, 1) = (TEM1 + TEM2) / BETA
C
C   GAMMA(1) = P(3) / BETA(1)
      AUX(2, 1) = P(3) / BETA
C
C   COMPUTE DIFFERENCE EQUATION COEFFICIENTS DIFA, DIFB, DIFC, AND DIFD
      DO 60 I = 2, IMAX
      IF (I .GE. IMAX) GO TO 40
      X = XX + FLOAT(I) * DX
      CALL EQN(X, TT, A)
      AA = 0.5 * A(1)
      TEM1 = 0.25 * A(2) * DX
      DIFA = AA - TEM1
      DIFC = AA + TEM1
      TEM1 = -2. * AA + 0.5 * DDX * A(3)

```

```

      TEM2 = DDX / DT
      DIFB = TEM1 - TEM2
C
C   DIFD = - DDX * A(4) - DIFC(I) * U(I + 1) - (TEM1 + TEM2) * U(I)
C   - DIFA = U(I - 1)
      DIFD = -DDX * A(4) - DIFC * AUX(1, I + 1) - (TEM1 + TEM2)
      1 * AUX(1, I) - DIFA * UM1
C
C   UM1 = U(I)  --SAVE VALUE FOR NEXT ITERATION
      UM1 = AUX(1, I)
      GO TO 50
C
C   COMPUTE RIGHT BOUNDARY COEFFICIENTS
40   CALL HBOUND(T, Q)
      TEM1 = 0.5 * Q(2)
      TEM2 = Q(1) / DX
      DIFA = TEM1 - TEM2
      DIFB = TEM1 + TEM2
      DIFD = Q(3)
C
C   COMPUTE PARAMETERS OF THOMAS-CHOLESKI METHOD
C
C   BETA(I) = DIFB - DIFA * (DIFC(I - 1) / BETA(I - 1))
50   BETA = DIFB - DIFA * AUX(1, I - 1)
      AUX(1, I) = DIFC / BETA
C
C   GAMMA(I) = (DIFD - DIFA * GAMMA(I - 1)) / BETA(I)
      AUX(2, I) = (DIFD - DIFA * AUX(2, I - 1)) / BETA
60   CONTINUE
C
C   COMPUTE NEW VALUES OF DEPENDENT VARIABLE
C
C   U(IMAX) = GAMMA(IMAX)
      AUX(1, IMAX) = AUX(2, IMAX)
      I = IMAX - 1
C
C   U(I) = GAMMA(I) - (DIFC(I) / BETA(I)) * U(I + 1)
70   AUX(1, I) = AUX(2, I) - AUX(1, I) * AUX(1, I + 1)
      I = I - 1
      IF (I .GT. 0) GO TO 70
80   CONTINUE
C
C   GO TO STORE NEW VALUES
      GO TO 20
      END

```

```

      subroutine eqn(x,t,a)
      dimension a(4)
      a(1)=1.24e-4
      a(2)=0.
      a(3)=0.
      a(4)=0.
      end

```

```
subroutine lbound(t,p)
dimension p(3)
p(1)=0.
p(2)=1.
p(3)=170.*EXP(-.55)
end
```

```
subroutine hbound(t,q)
dimension q(3)
q(1)=0.
q(2)=1.
q(3)=170.*EXP(-.55)
end
```

```
function ui(x)
ui=170.
end
```

SUBROUTINE PLOTHD

EXTERNAL Z

CALL T4025

CALL SCL3(0.,1.,0.,1.,0.,1.,60.,30.,10.,0)

CALL LAB

CALL I3DFNZ(Z)

c CALL GRID3(0.,1.,0.,1.,40,40,1)

call grid3(0.,1.,0.,1.,40,39,1)

CALL ENDPLT

END

FUNCTION Z(X,Y,I,J)

COMMON /ZCM/ T12(40,40),T11(40,40),BR(40,40),srm(40)

common /label/ ht,zl,xt,c

Z=T11(I,J)/zl

RETURN

END

SUBROUTINE LAB

COMMON /LABEL/ HT,ZL

call letter(3.,.7,0.,0.)

call proj3(.5,1.3,0.,a,b,c)

call move(a,b)

call label('y(in)')

call proj3(1.3,.5,0.,a,b,c)

call move(a,b)

call label('t(sec)')

call proj3(1.5,-.5,1.,a,b,c)

call move(a,b)

call label(' T11-T22')

call proj3(1.5,0.,.7,a,b,c)

call move(a,b)

call label('(psi)')

call letter(1.,1.,0.,0.)

call twrite(7)

do 100 i=0,10


```
call proj3(1.075,(float(i)/10.),0,a,b,c)
call move(a,b)
write(7,50) 2*i

call proj3((float(i)/10.),1.05,0,a,b,c)
call move(a,b)
write(7,60) float(i)*ht/10.

c call proj3(1.1,-.1,(float(i)/10.-.045),a,b,c)
call proj3(1.1,-1.,(float(i)/10.+1),a,b,c)
call move(a,b)
write(7,70) FLOAT(i)*.1*(z1)
c write(7,80) float(i)*.4

50 format(i2)
60 format(f6.4)
70 format(F6.0)
c80 format(f4.2)

100 continue

return
end
```

Simulation Results for Nonisothermal Stress Relaxation

Nonisothermal relaxation of shear stress, primary normal stress difference, and birefringence for each molding condition from B to J in Table IV.2 are plotted in this Appendix.

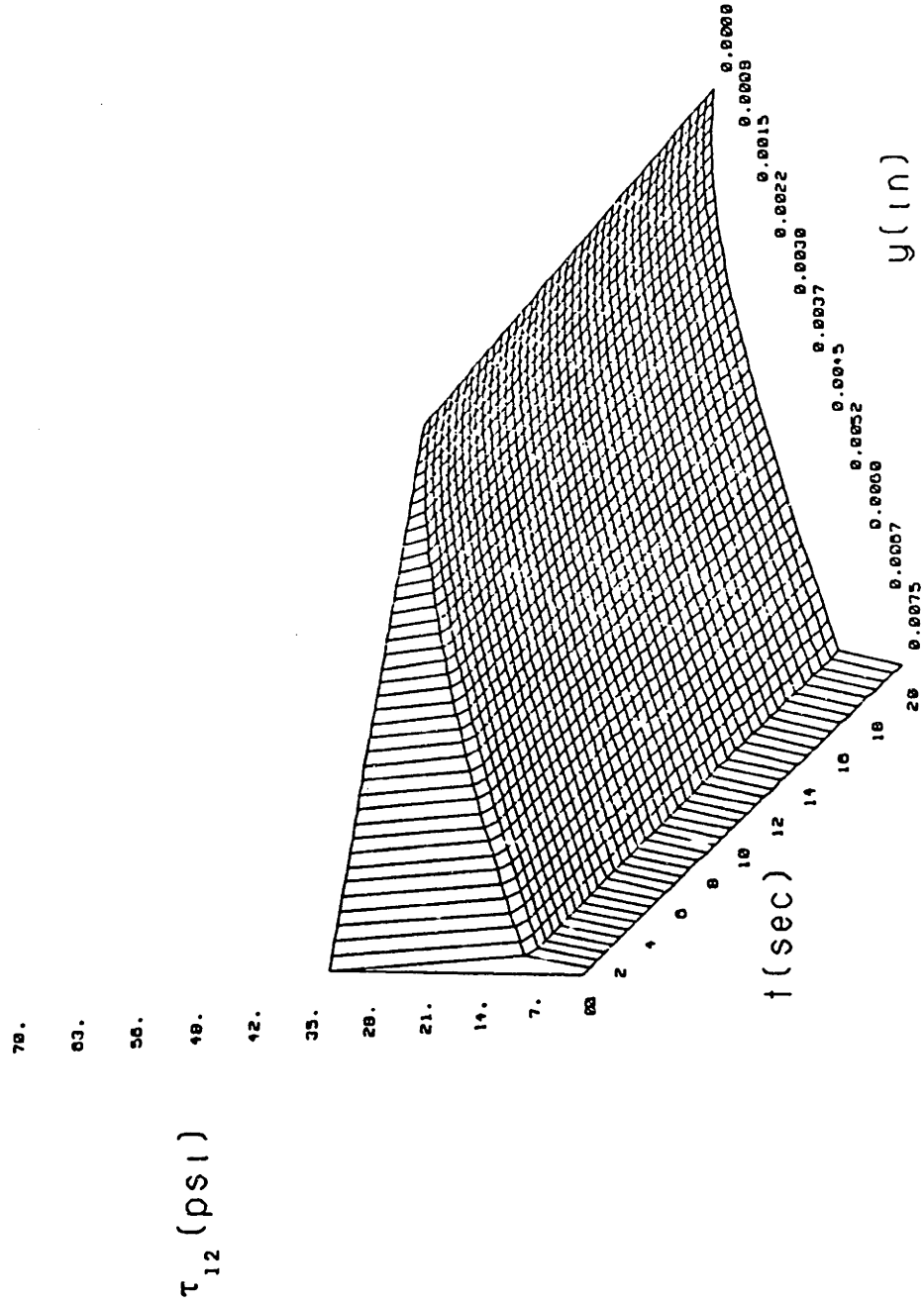


Figure E1 : Nonisothermal relaxation of the shear stress for $dP/dx = 4168$ psi/in. (condition B in Table IV.2).

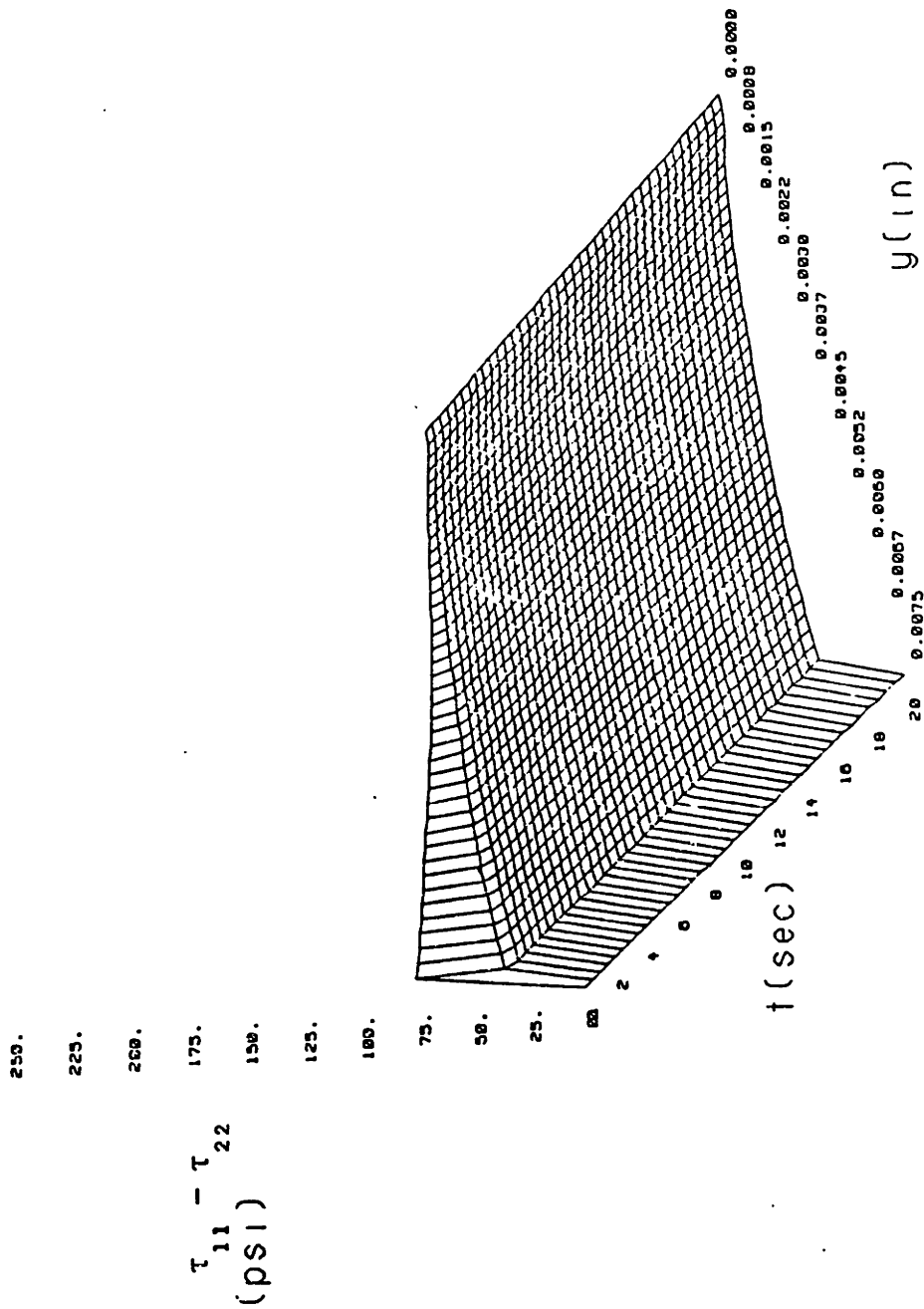


Figure E2 : Nonisothermal relaxation of the primary normal stress difference for $dp/dx = 4168 \text{ psi/in.}$ (condition B in Table IV.2).

100.
90.
80.
70.
60.
50.
40.

$\Delta n \cdot 10^4$

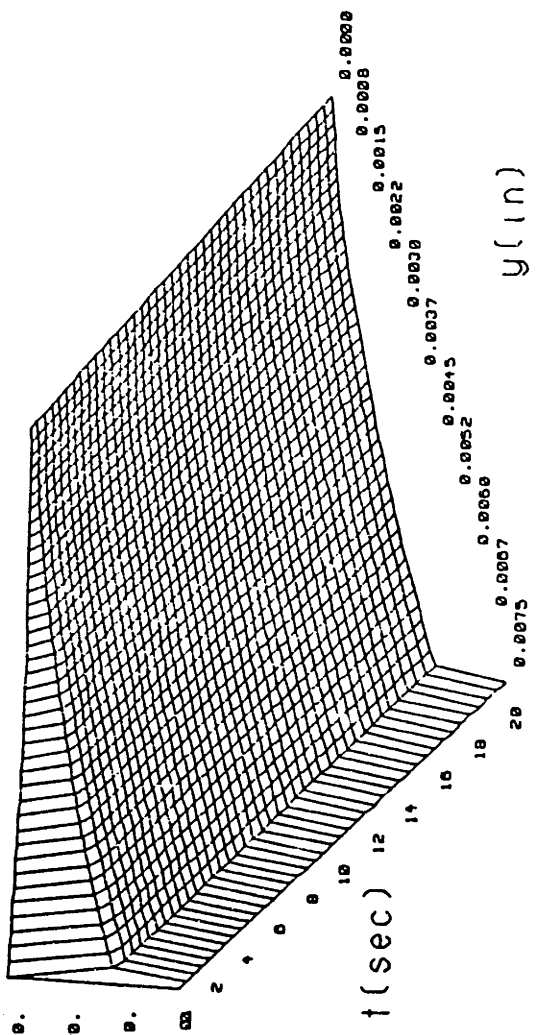


Figure E3 : Nonisothermal relaxation of the birefringence for $dP/dx = 4168 \text{ psi/in.}$ (condition B in Table IV.2).

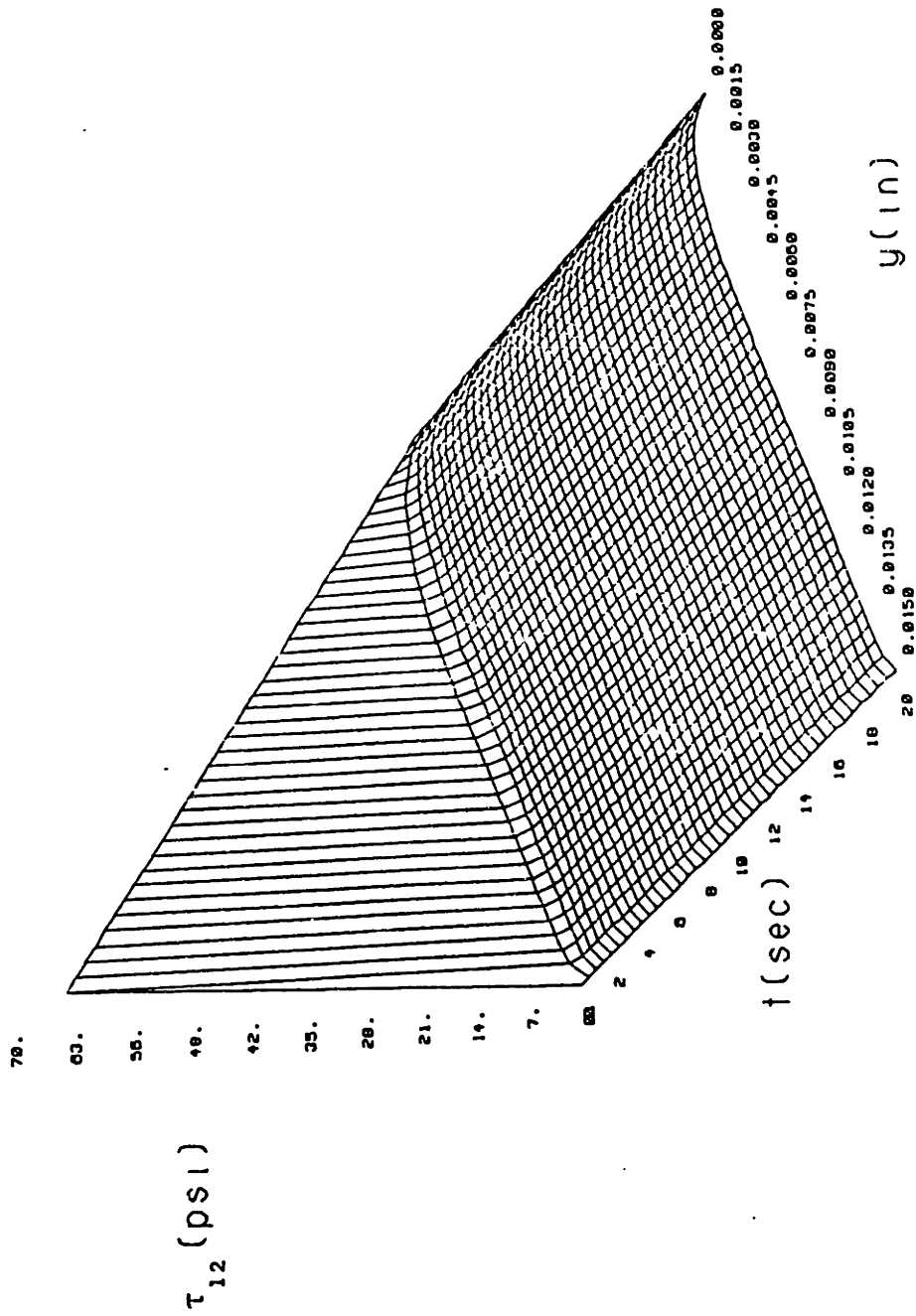


Figure E4 : Nonisothermal relaxation of the shear stress for $dP/dx = 4168$ psi/in. (condition C in Table IV.2).

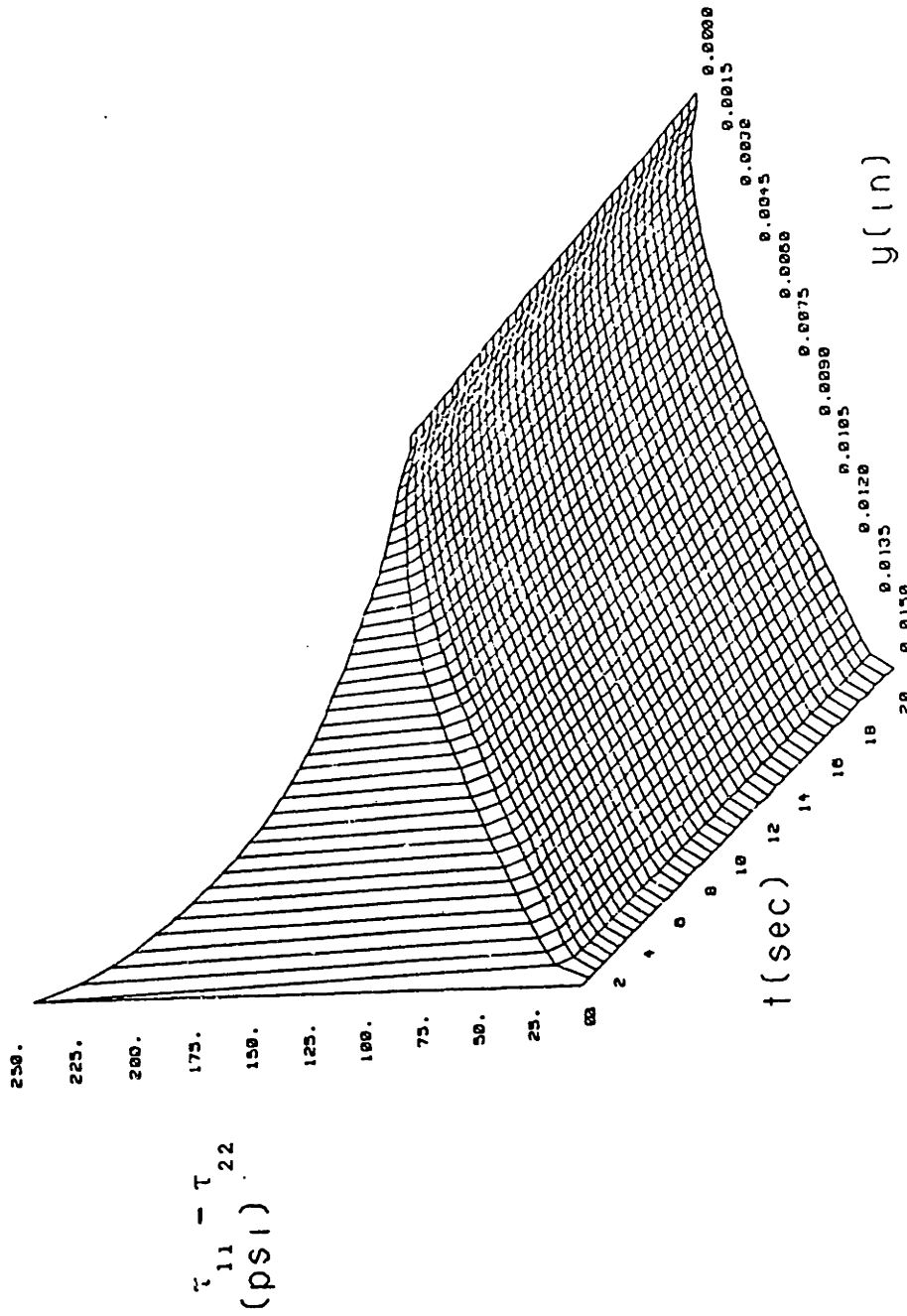


Figure E5 : Nonisothermal relaxation of the primary normal stress difference for $dp/dx = 4168$ psi/in. (condition C in Table IV.2).

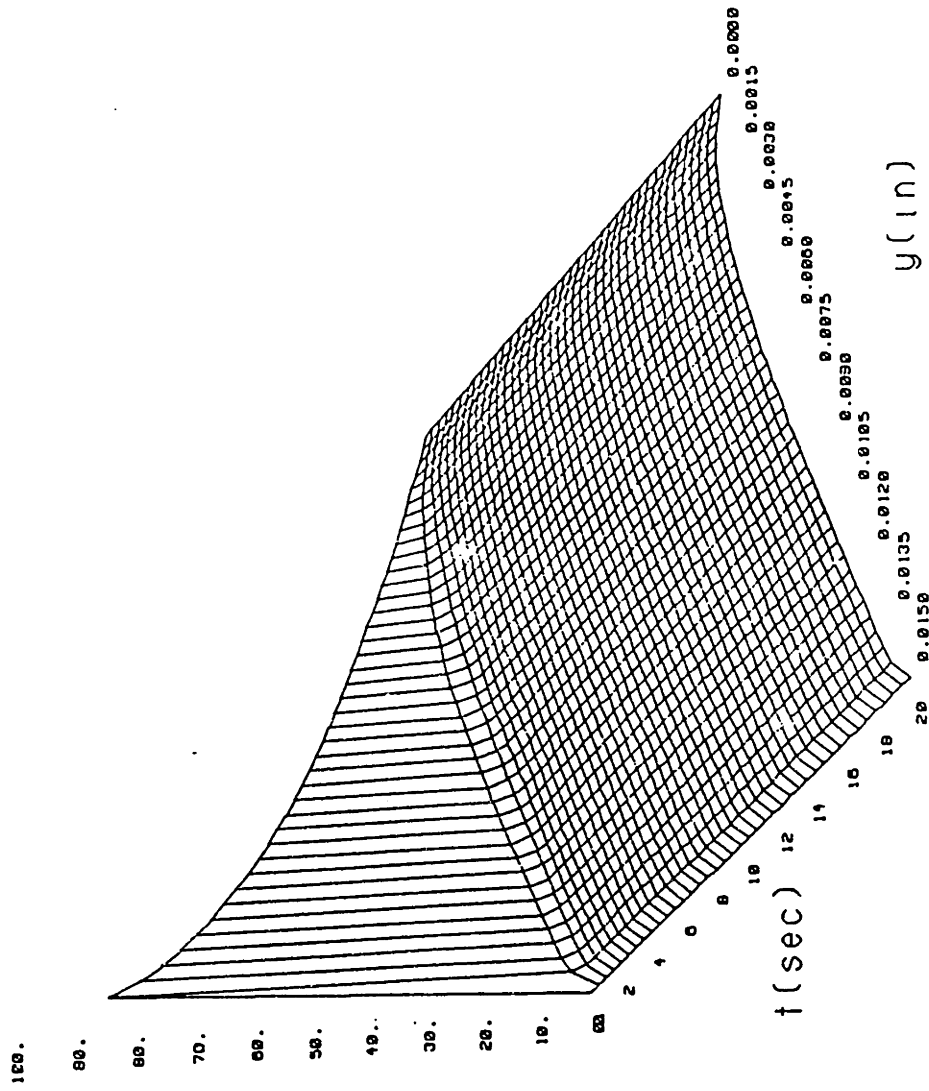


Figure E6 : Nonisothermal relaxation of the birefringence for $dP/dx = 4168 \text{ psi/in.}$ (condition C in Table IV.2).

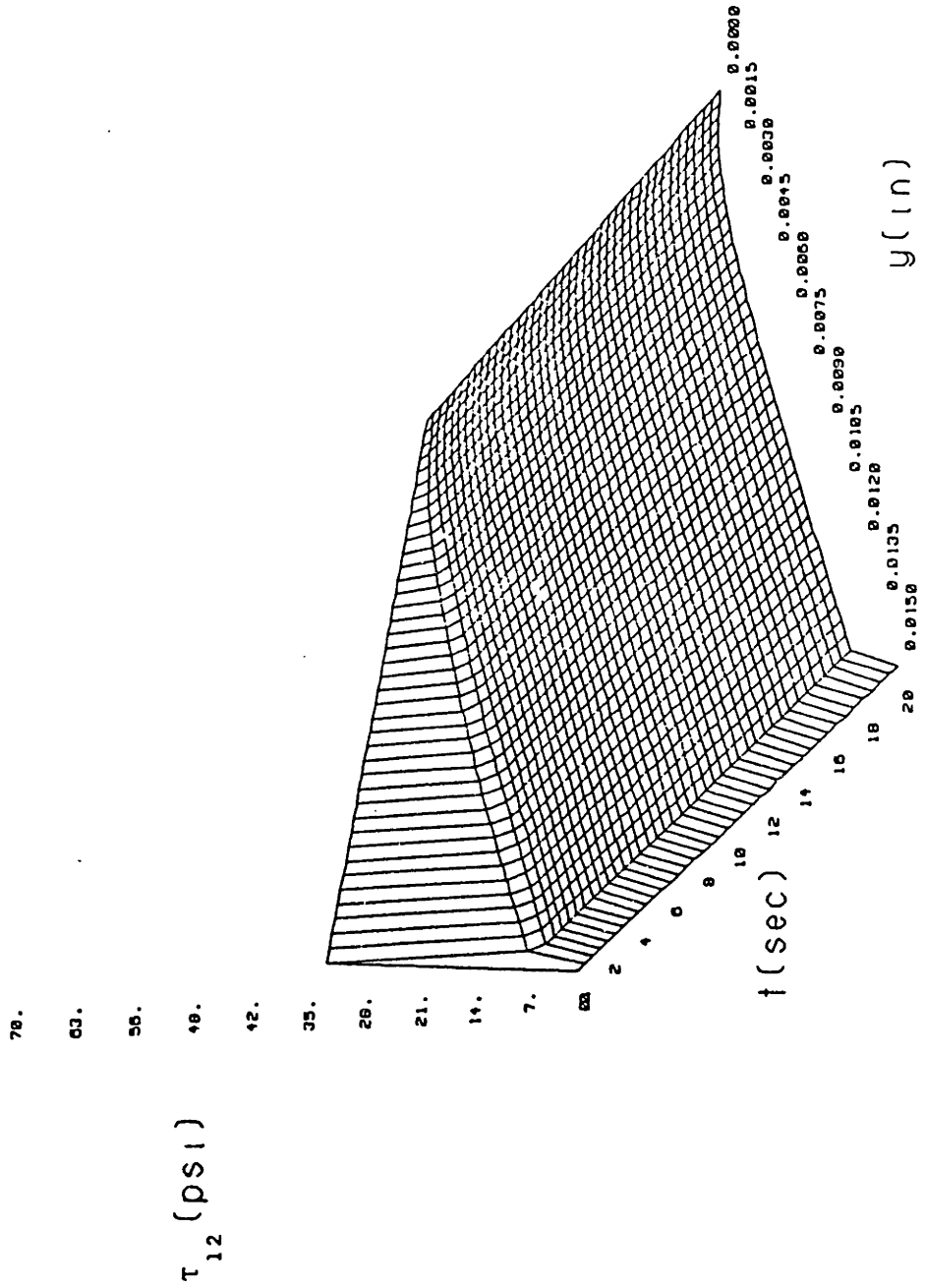


Figure E7 : Nonisothermal relaxation of the shear stress for $dP/dx = 2084$ psi/in. (condition D in Table IV.2).

$\tau_{11} - \tau_{22}$
 (psi)

250.
 225.
 200.
 175.
 150.
 125.
 100.

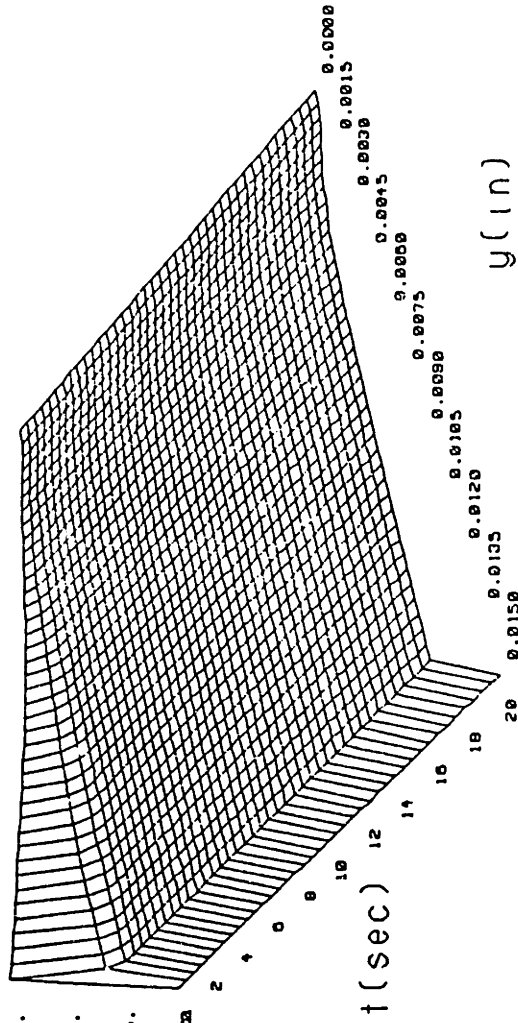


Figure E8 : Nonisothermal relaxation of the primary normal stress difference for $dp/dx = 2084$ psi/in. (condition D in Table IV.2).

100.
 80.
 60.
 40.

$\Delta n \cdot e4$

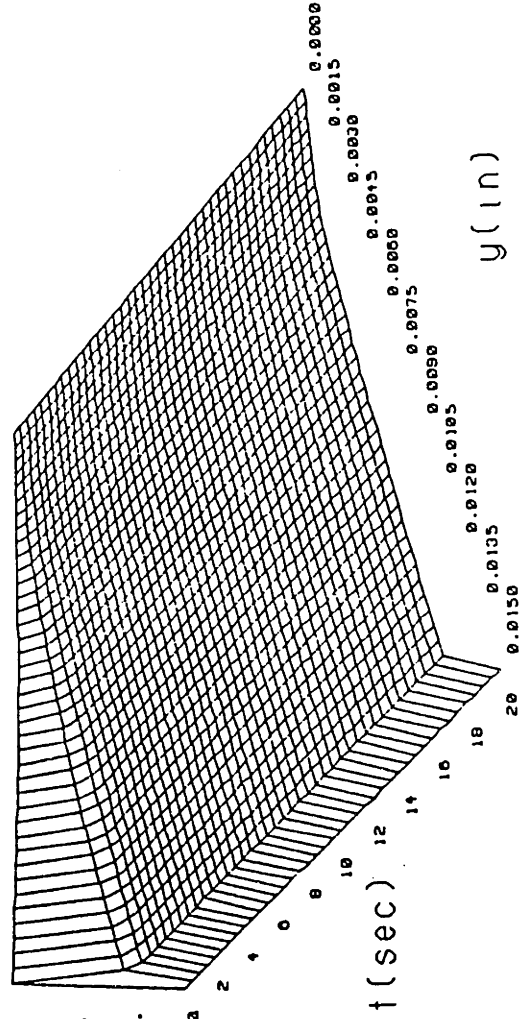


Figure E9 : Nonisothermal relaxation of the birefringence for $dP/dx = 2084 \text{ psi/in.}$ (condition D in Table IV.2).

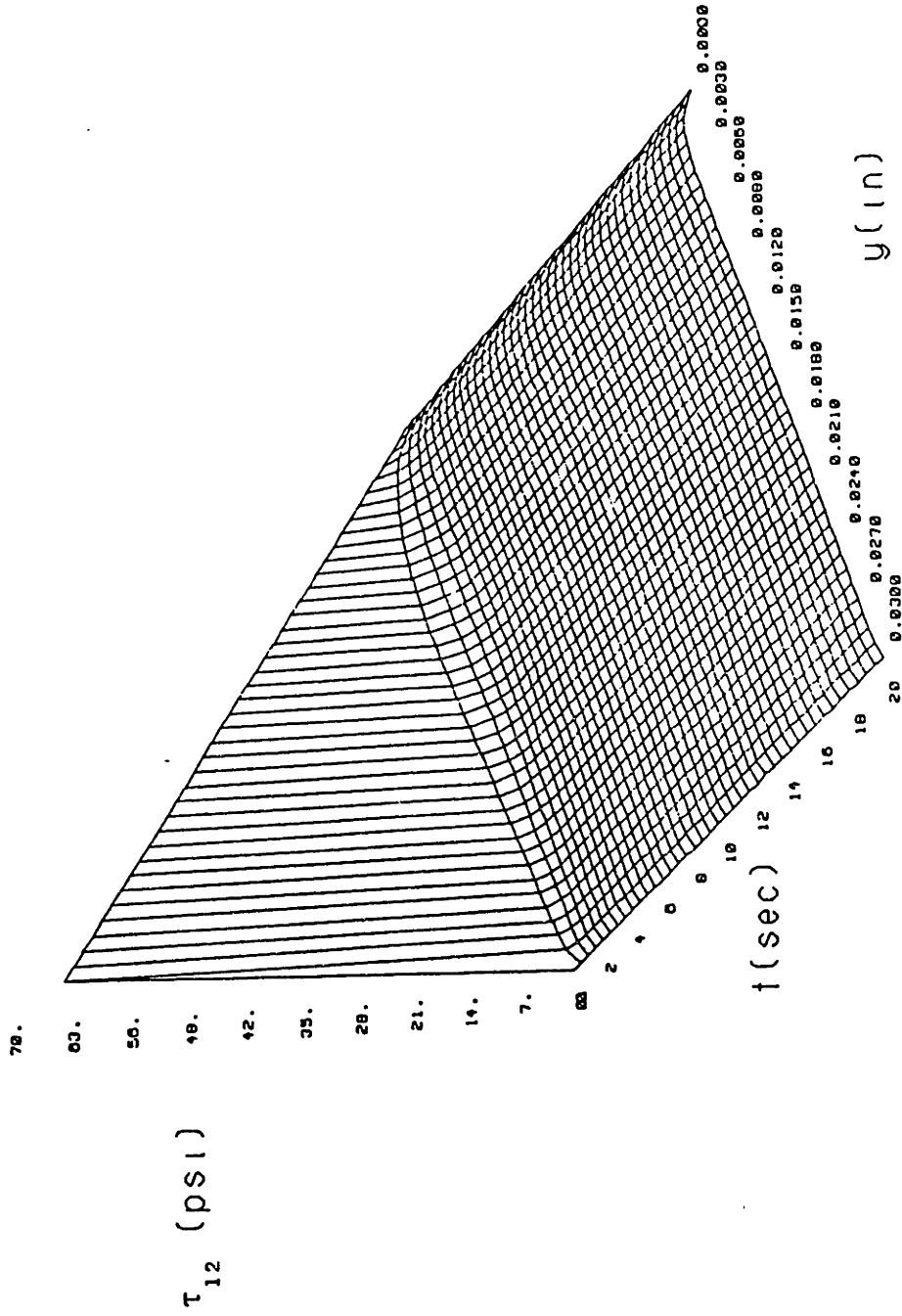


Figure E10 : Nonisothermal relaxation of the shear stress for $dP/dx = 2084$ psi/in. (condition E in Table IV.2).

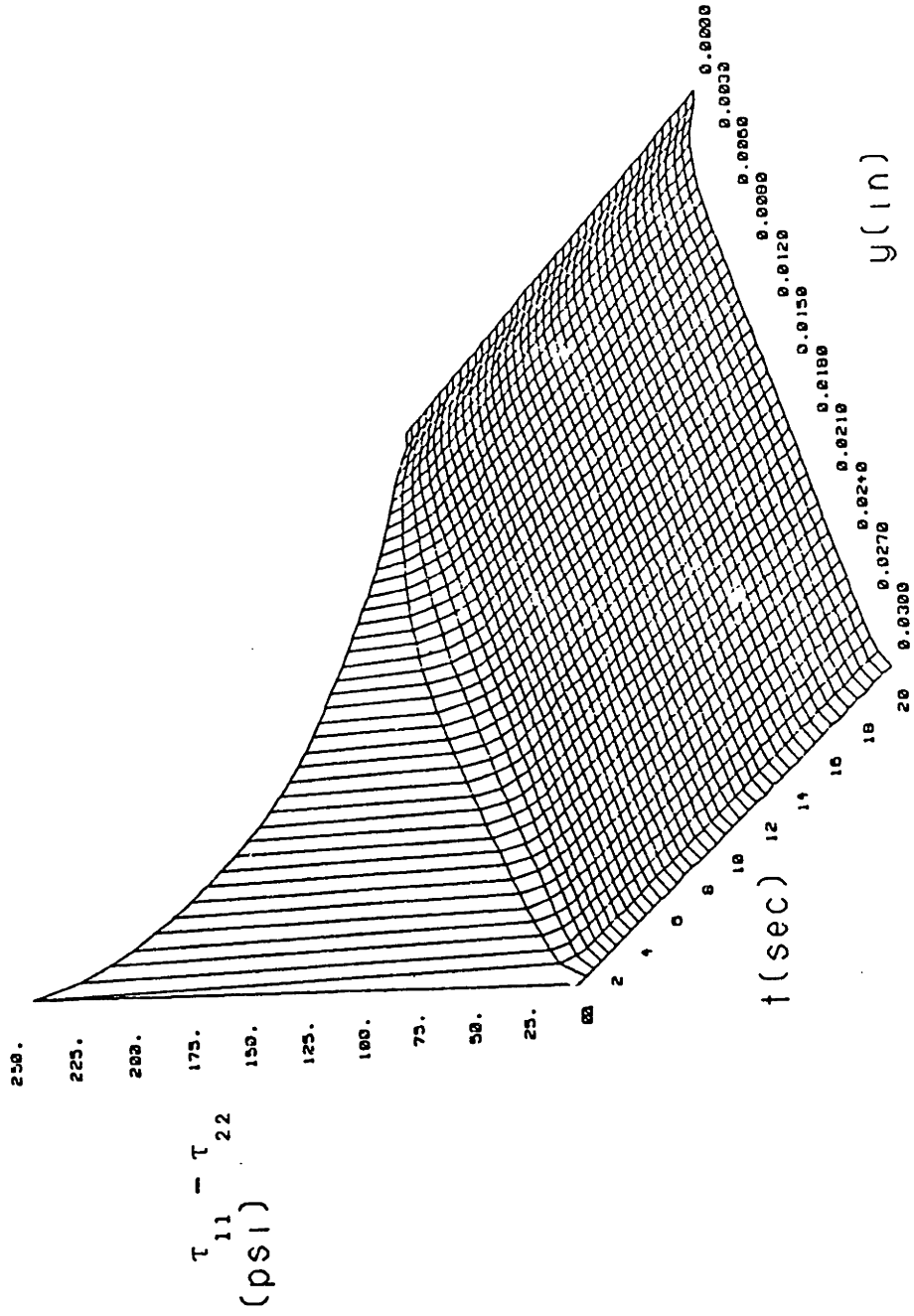


Figure E11 : Nonisothermal relaxation of the primary normal stress difference for $dp/dx = 2084$ psi/in. (condition E in Table IV.2).

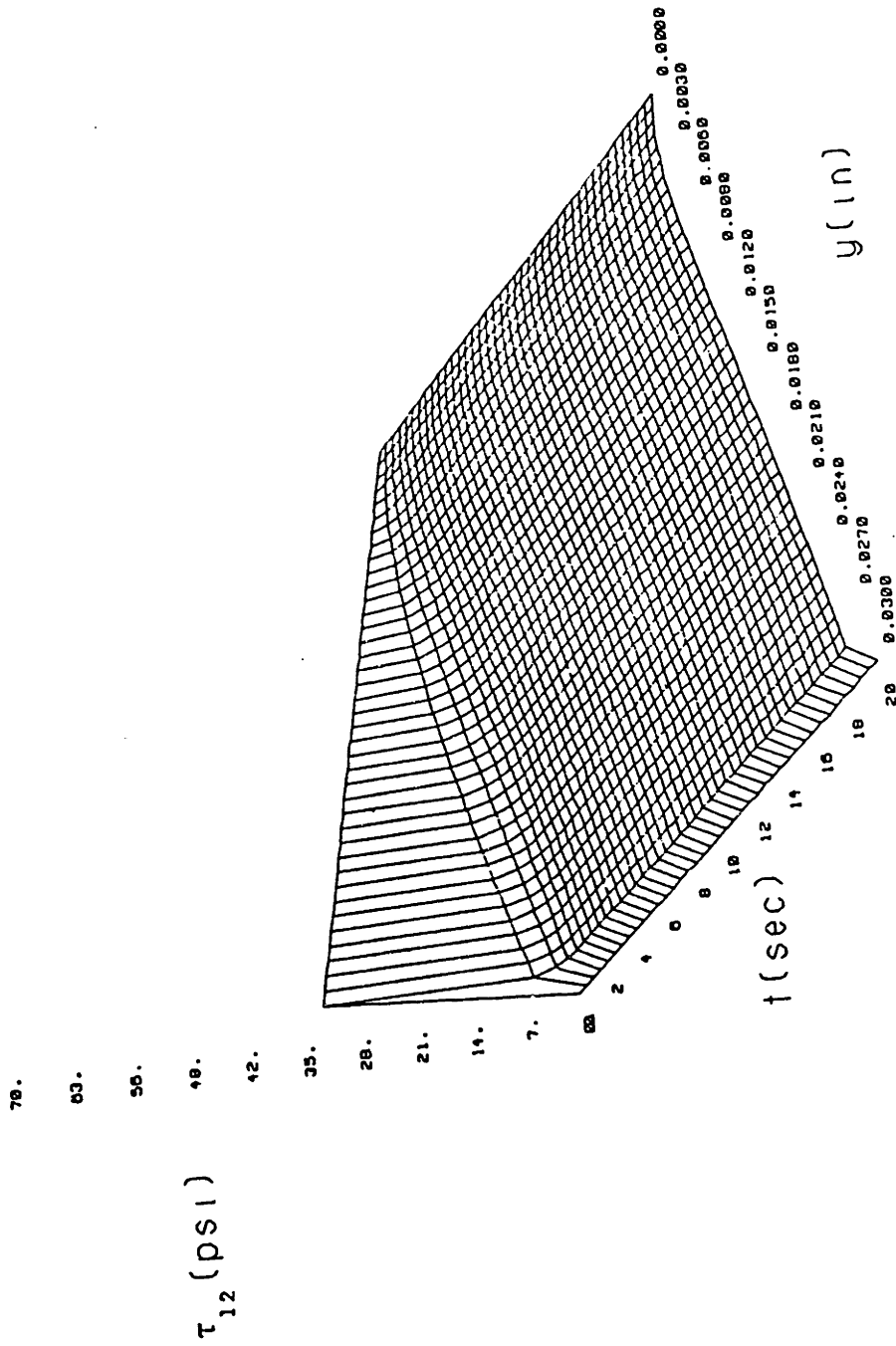


Figure E13 : Nonisothermal relaxation of the shear stress for $dP/dx = 1042$ psi/in. (condition F in Table IV.2).

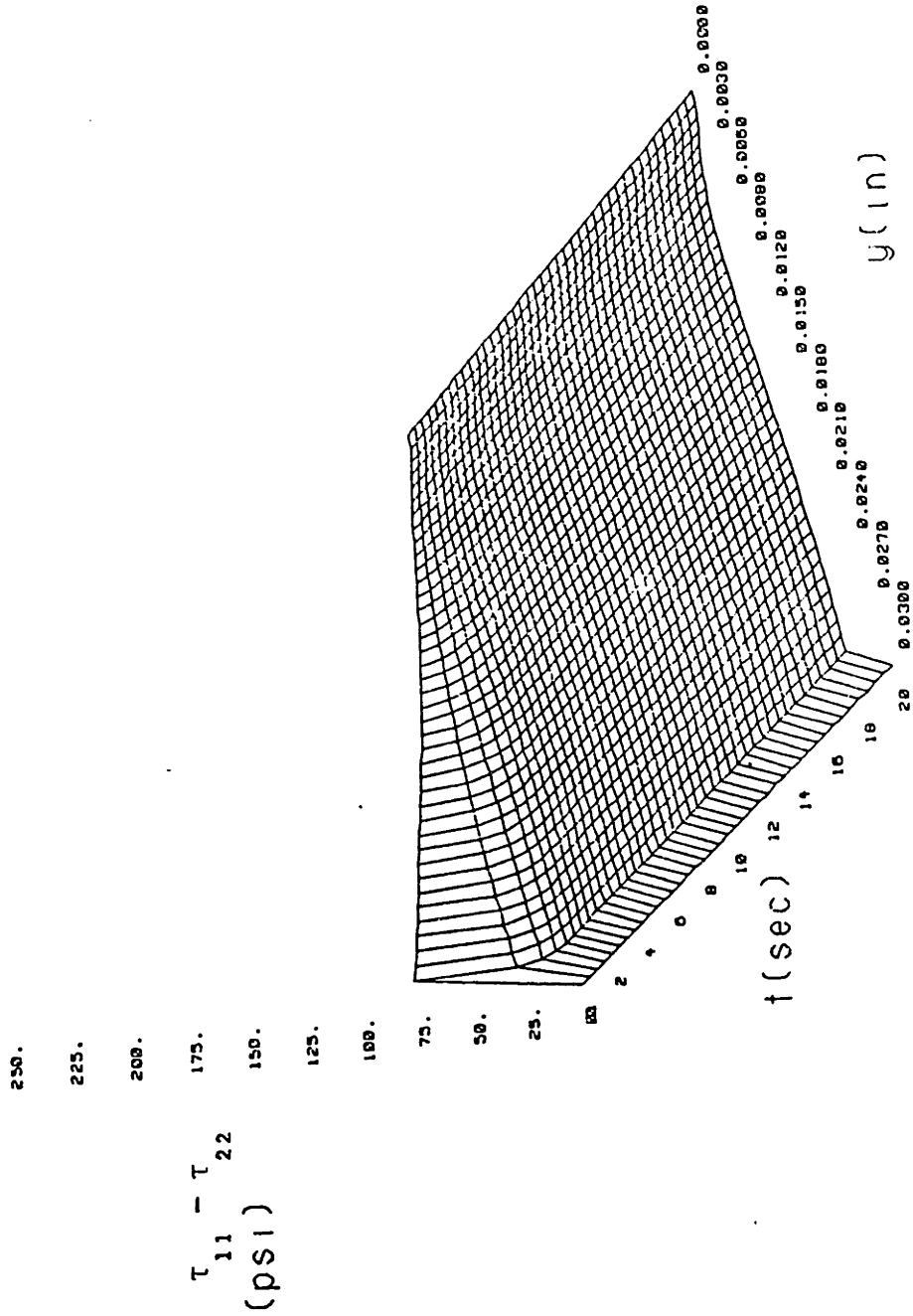


Figure E14 : Nonisothermal relaxation of the primary normal stress difference for $dP/dx = 1042$ psi/in. (condition F in Table IV.2).

100.
90.
80.
70.
60.
50.
40.

$\Delta n \cdot e4$

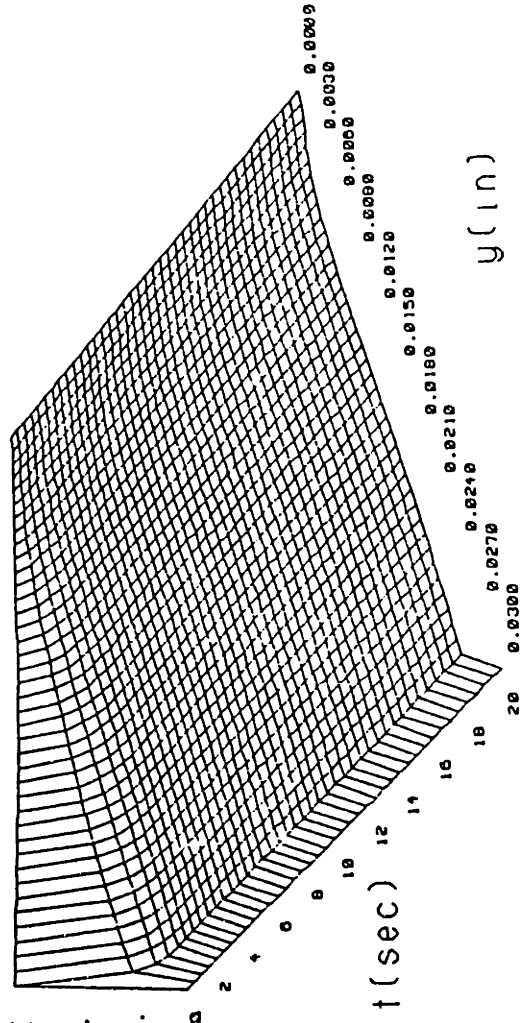


Figure E15 : Nonisothermal relaxation of the birefringence for $dP/dx = 1042$ psi/in. (condition F in Table IV.2).

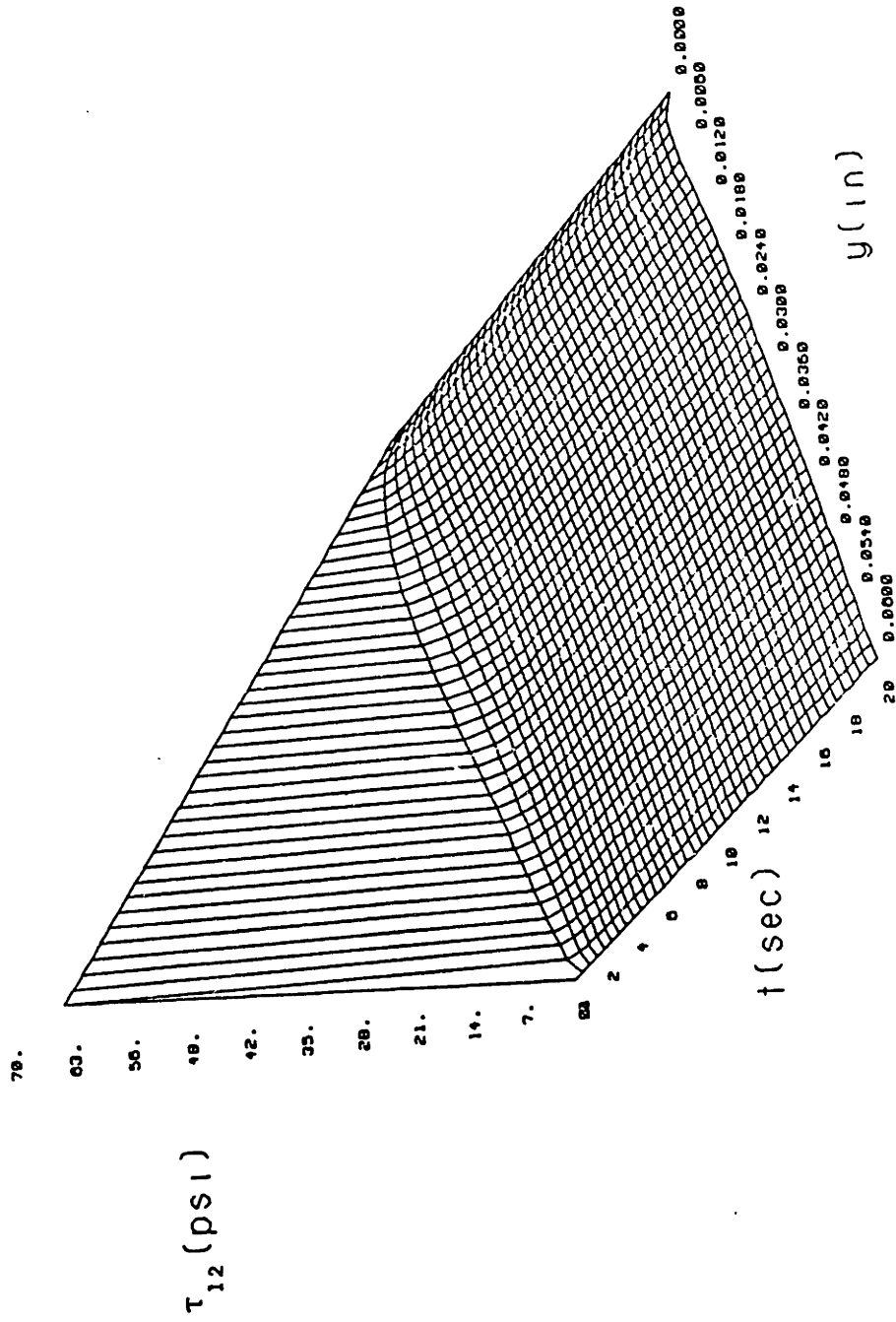


Figure E16 : Nonisothermal relaxation of the shear stress for $dP/dx = 1042 \text{ psi/in.}$ (condition G in Table IV.2).

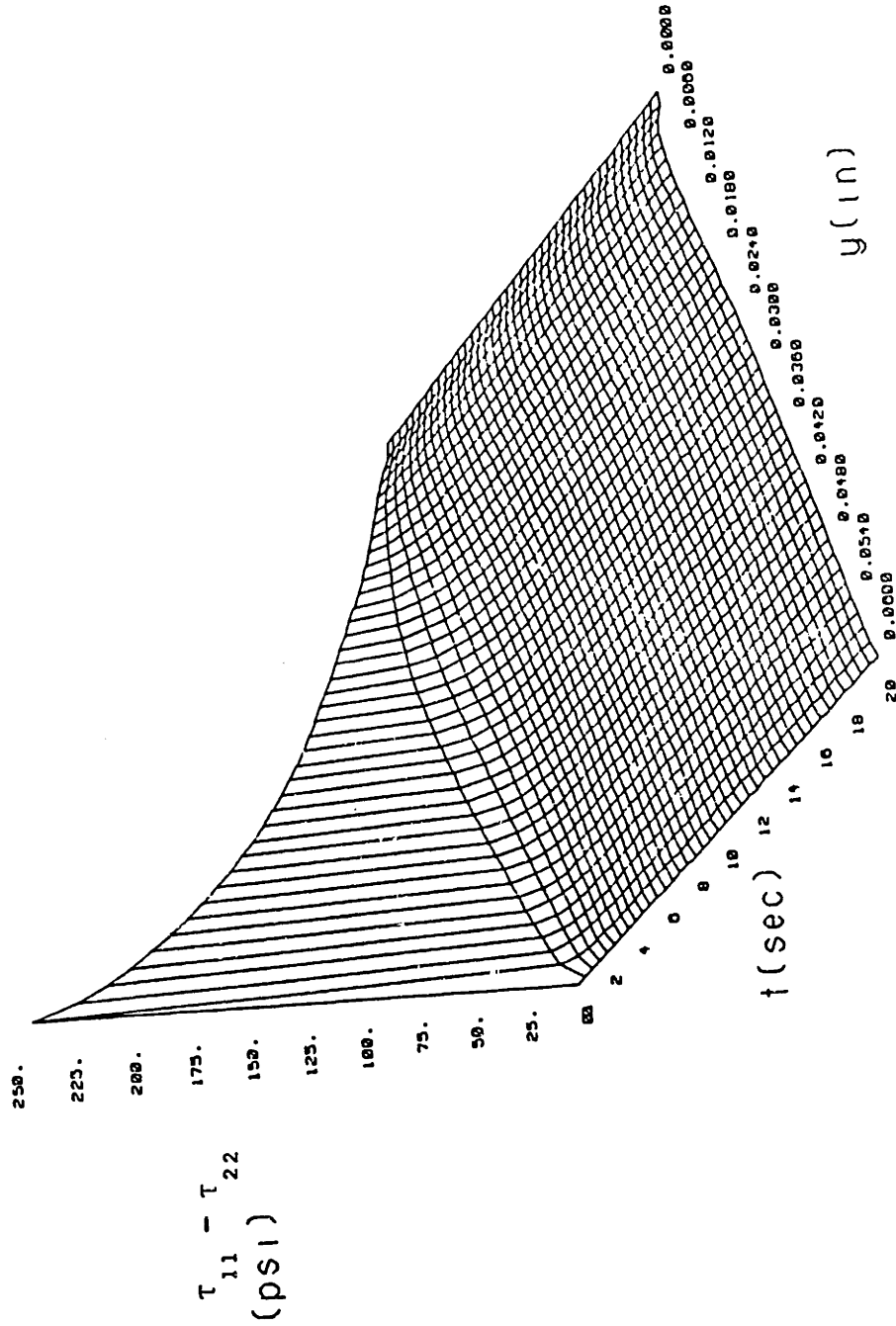


Figure E17 : Nonisothermal relaxation of the primary normal stress difference for $dP/dx = 1042$ psi/in. (condition G in Table IV.2).

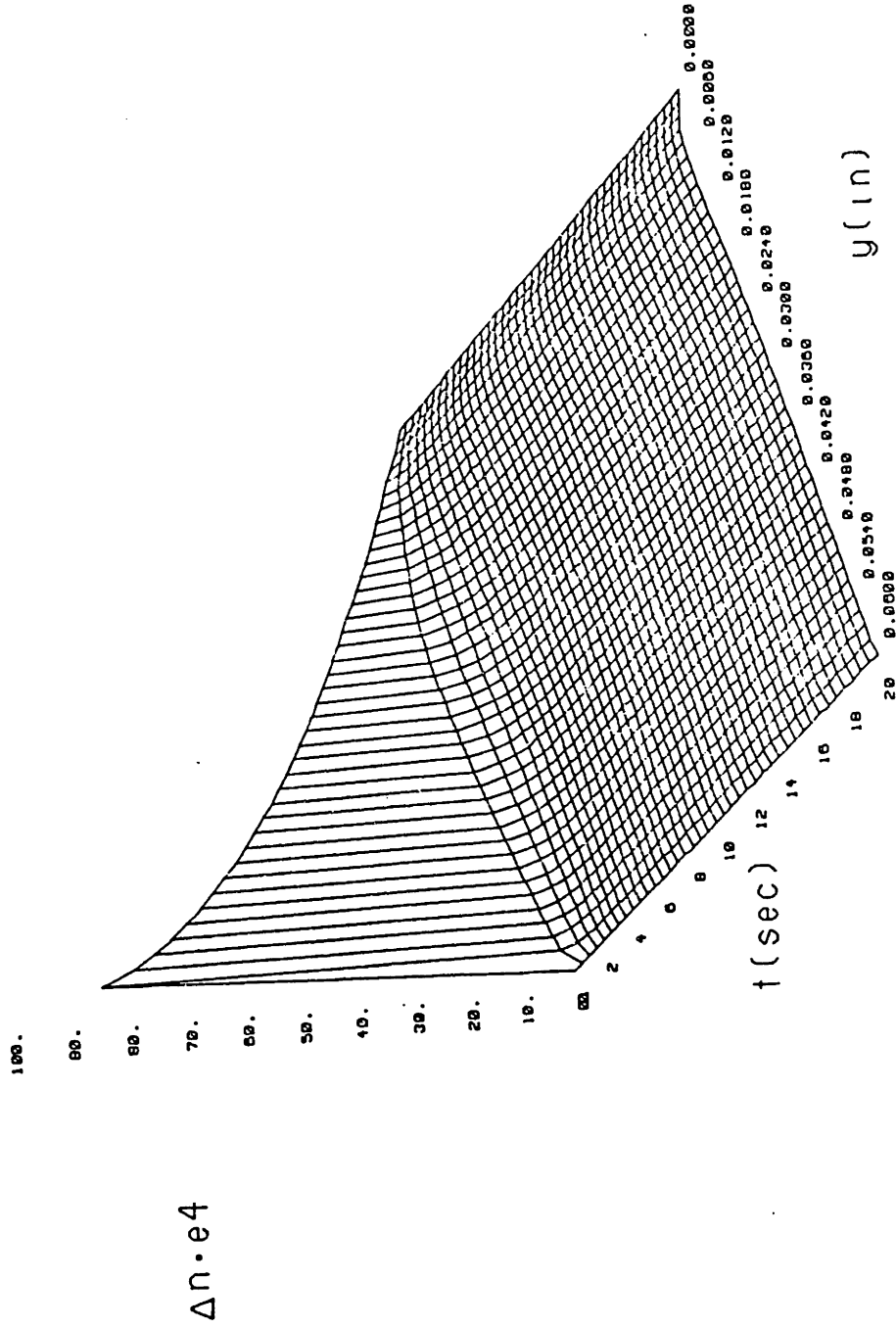


Figure E18 : Nonisothermal relaxation of the birefringence for $dP/dx = 1042 \text{ psi/in.}$ (condition G in Table IV.2).

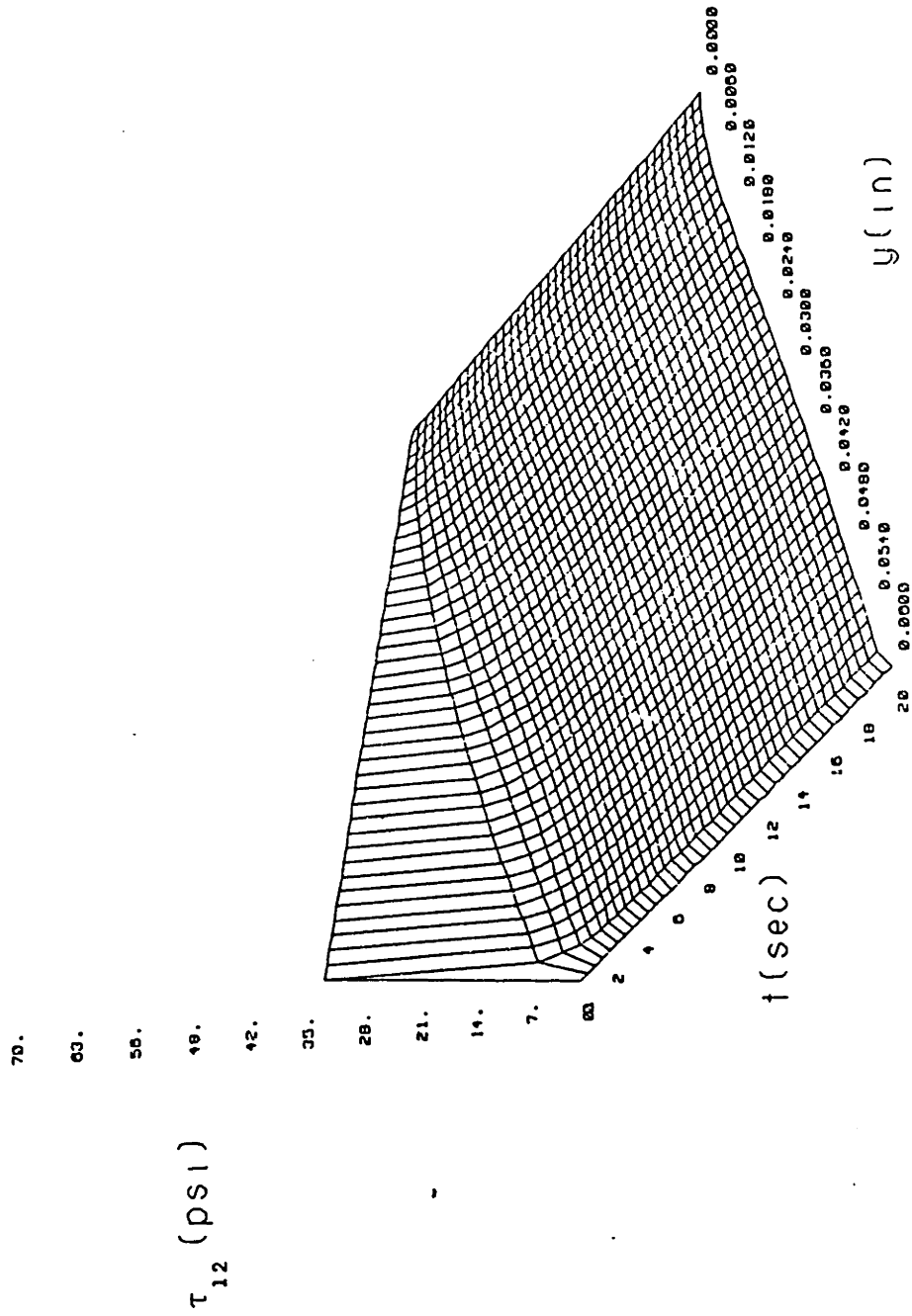


Figure E19 : Nonisothermal relaxation of the shear stress for $dP/dx = 521$ psi/in. (condition H in Table IV.2).

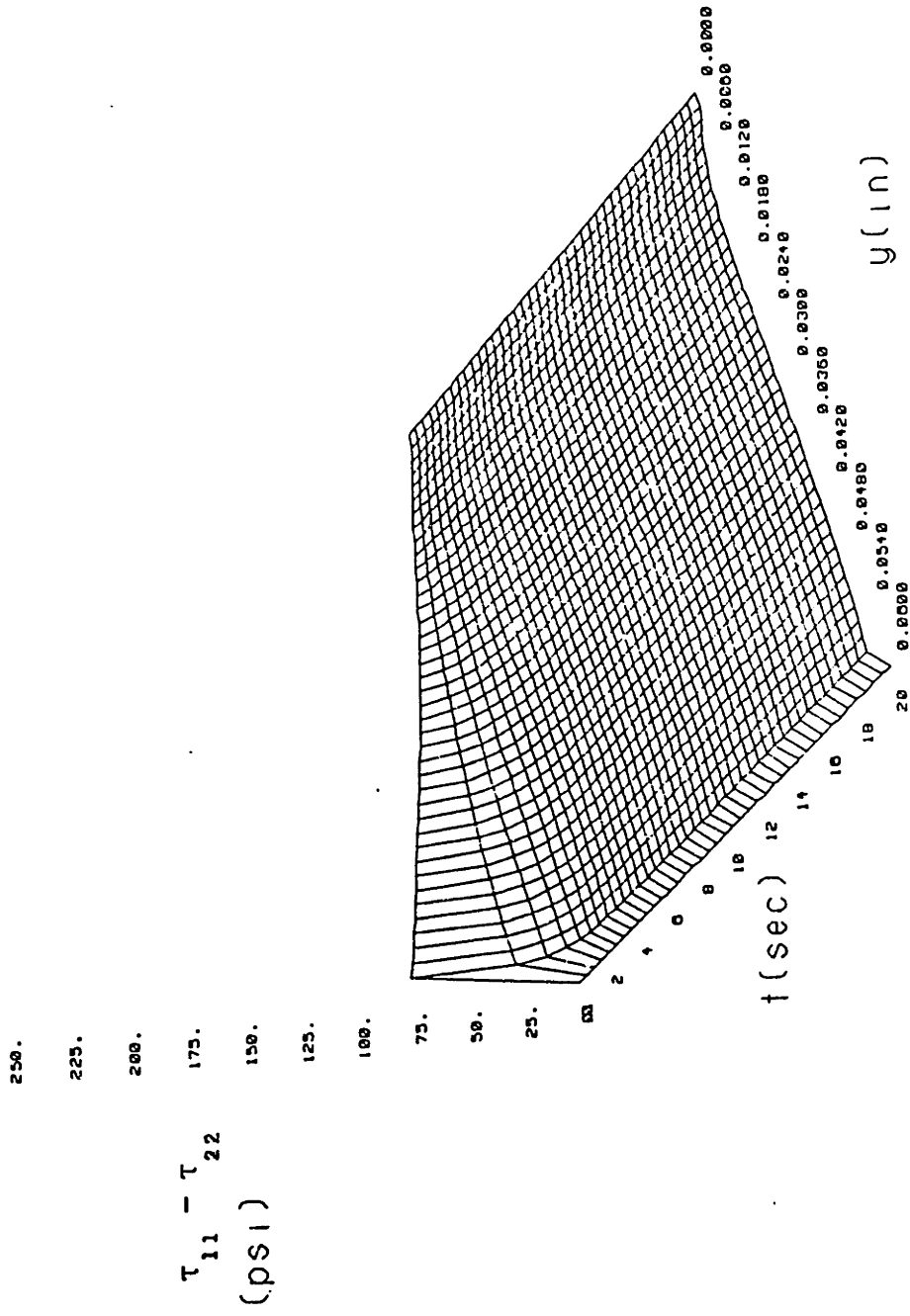


Figure E20 : Nonisothermal relaxation of the shear stress for $dP/dx = 521$ psi/in. (condition H in Table IV.2).

100.
90.
80.
70.
60.
50.
40.

$\Delta n \cdot e4$

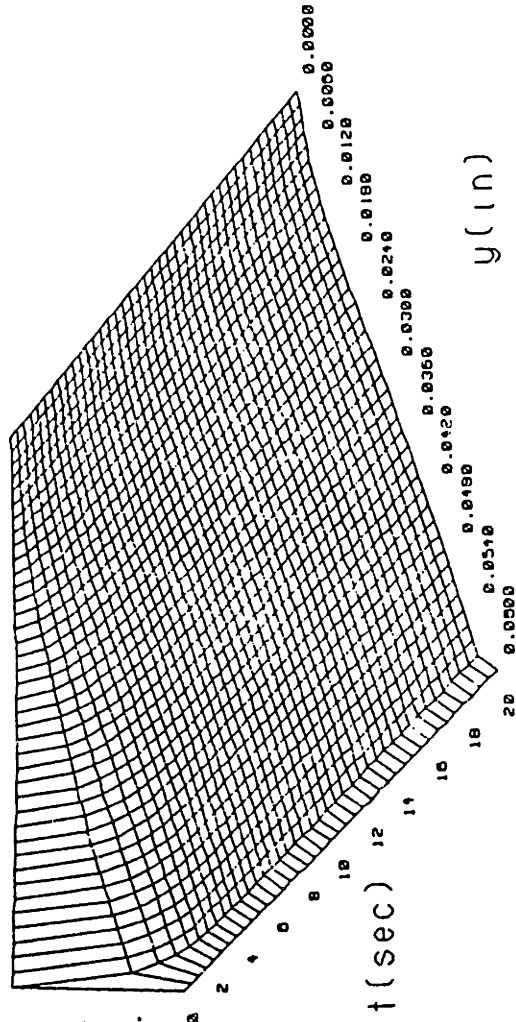


Figure E21 : Nonisothermal relaxation of the primary normal stress difference for $dp/dx = 521 \text{ psi/in.}$ (condition H in Table IV.2).

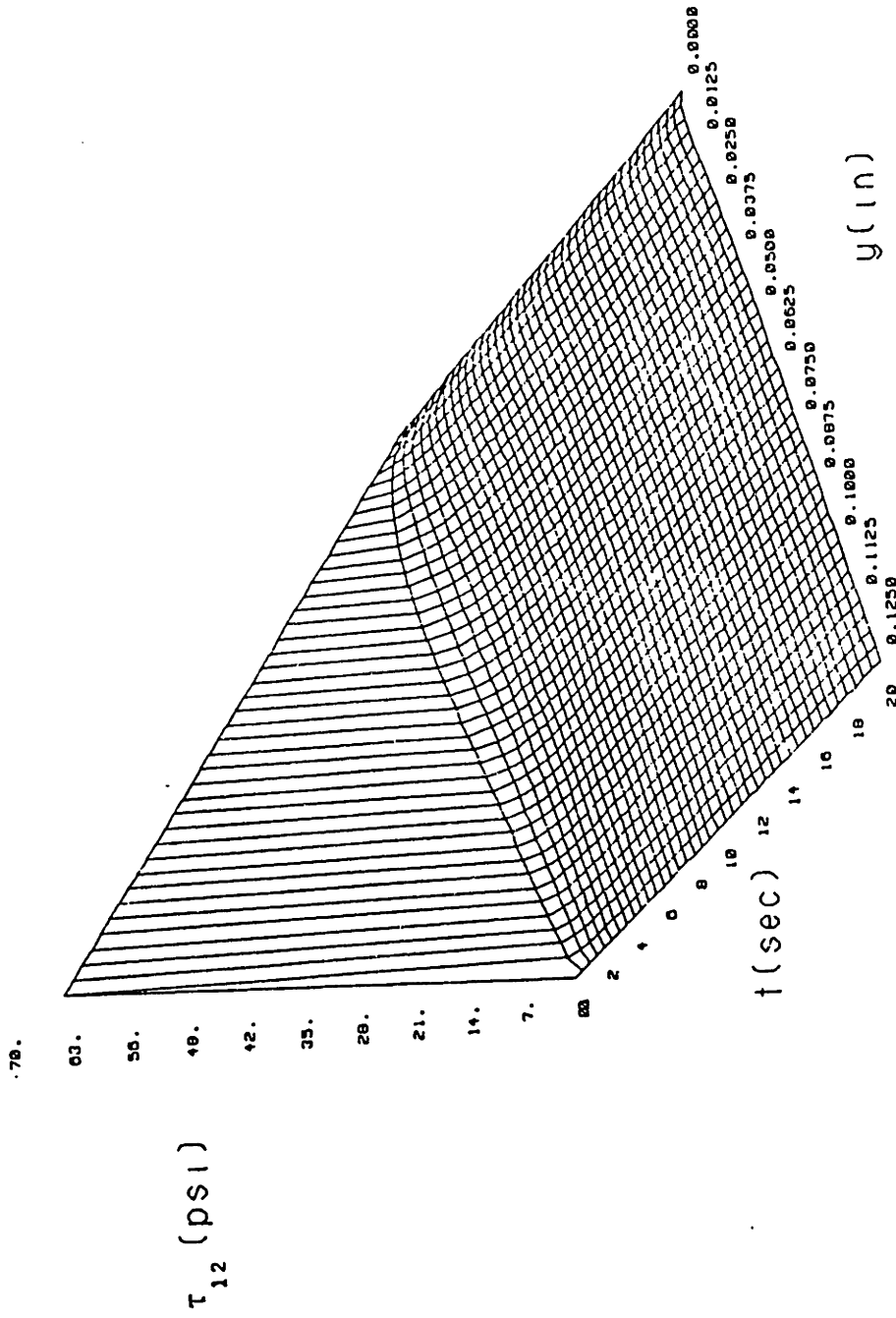


Figure E22 : Nonisothermal relaxation of the shear stress for $dP/dx = 500 \text{ psi/in.}$ (condition I in Table IV.2).

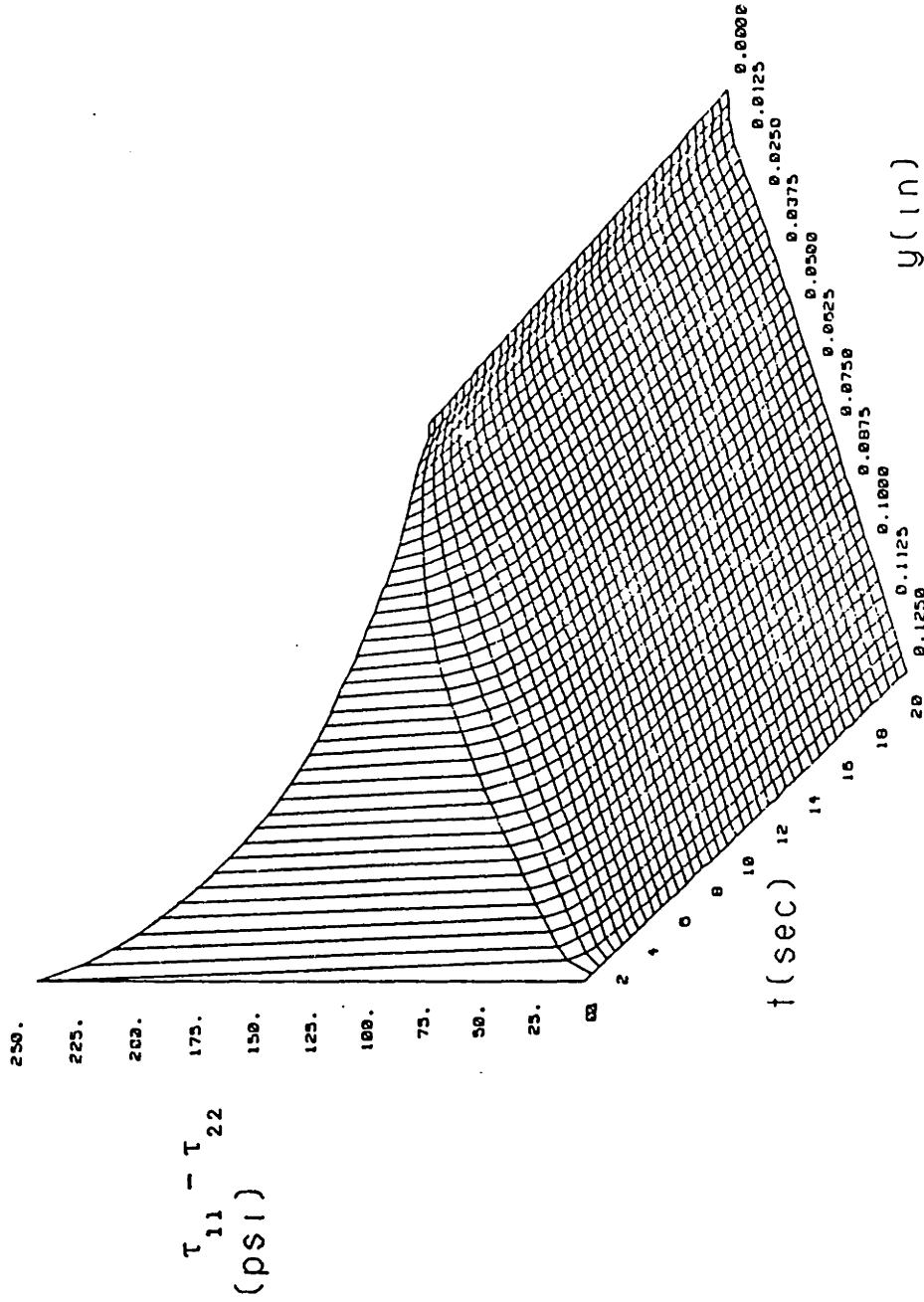


Figure E23 : Nonisothermal relaxation of the primary normal stress difference for $dP/dx = 500$ psi/in. (condition I in Table IV.2).

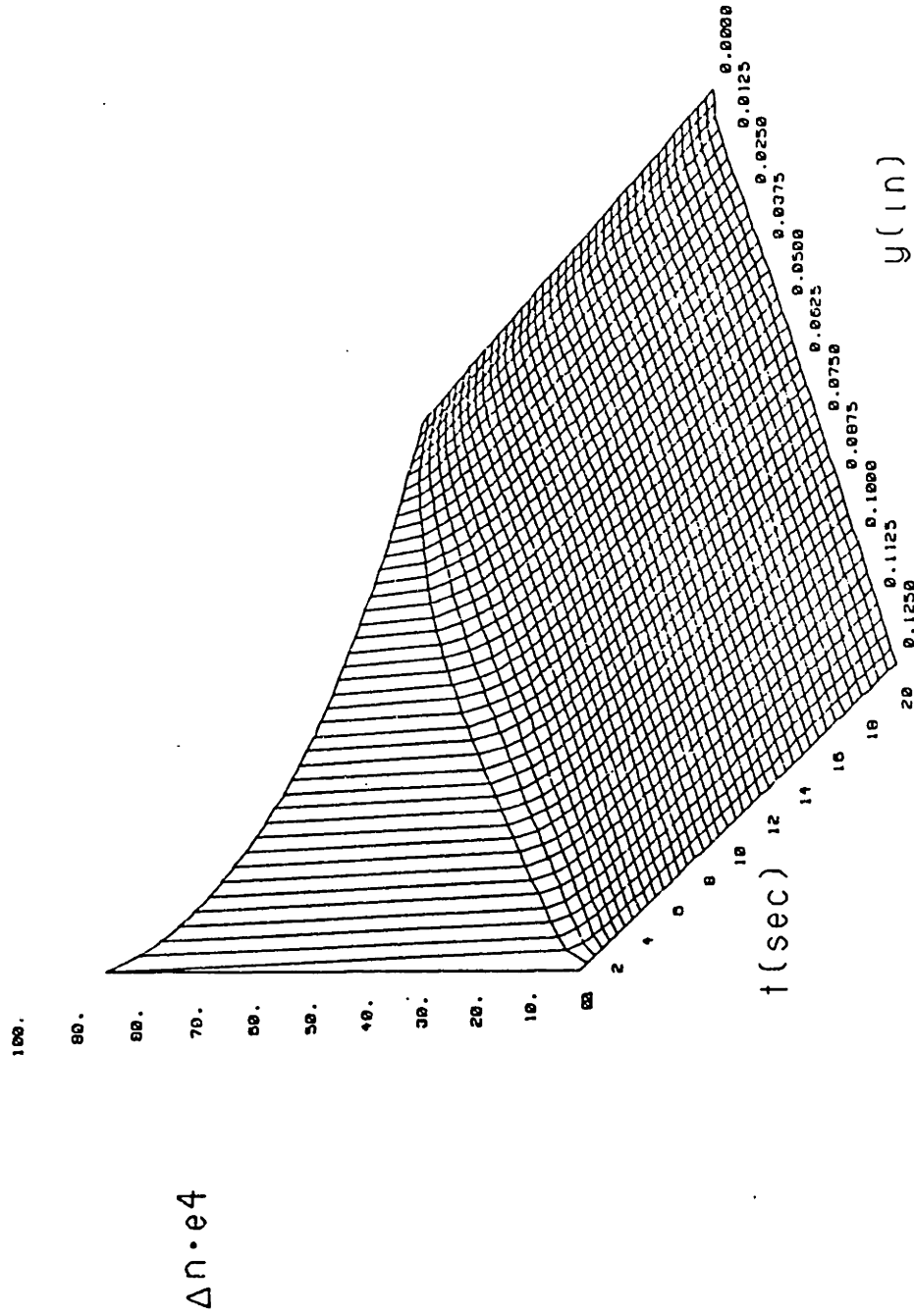


Figure E24 : Nonisothermal relaxation of the birefringence for $dP/dx = 500 \text{ psi/in.}$ (condition I in Table IV.2).

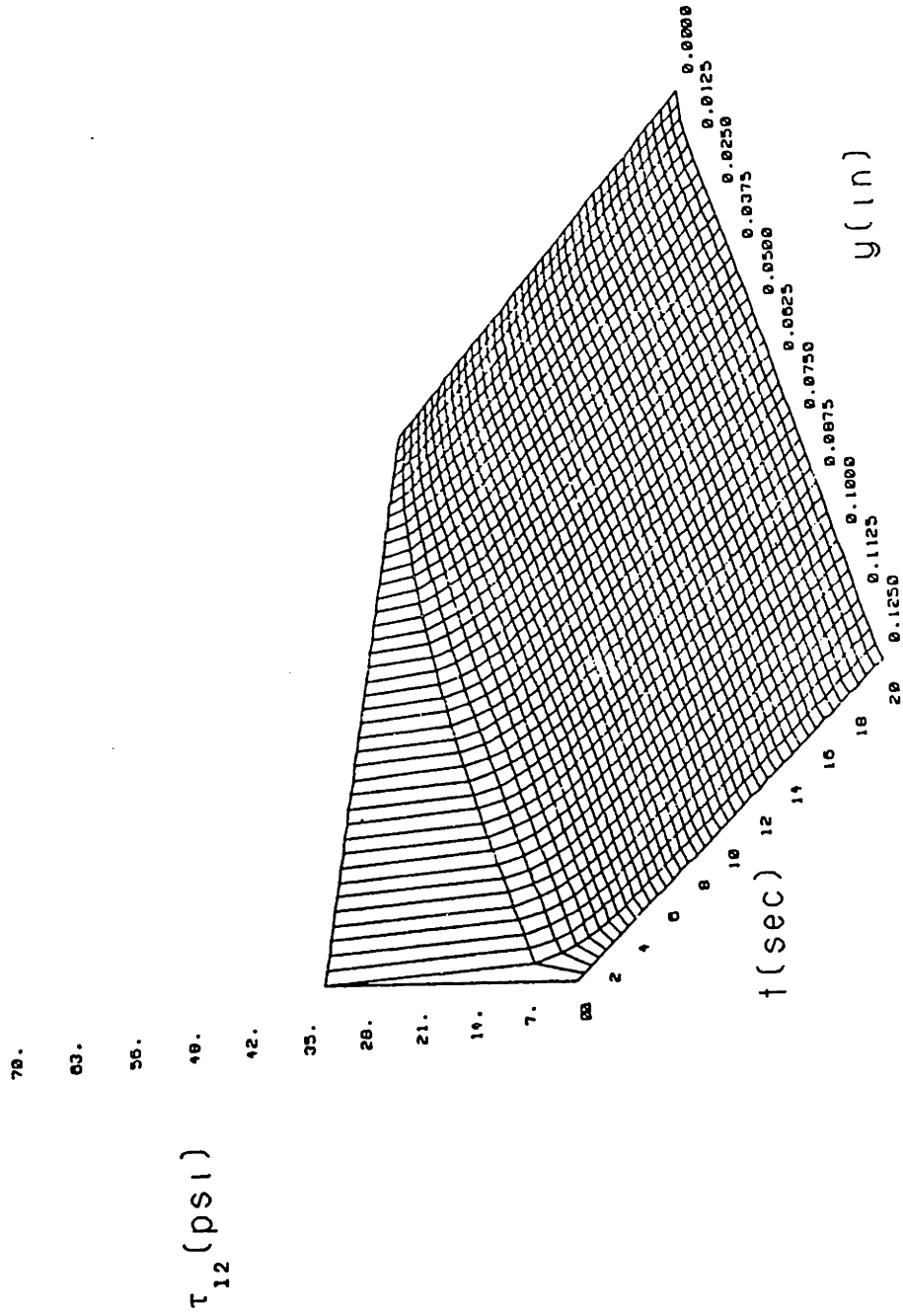


Figure E25 : Nonisothermal relaxation of the shear stress for $dP/dx = 250$ psi/in. (condition J in Table IV.2).

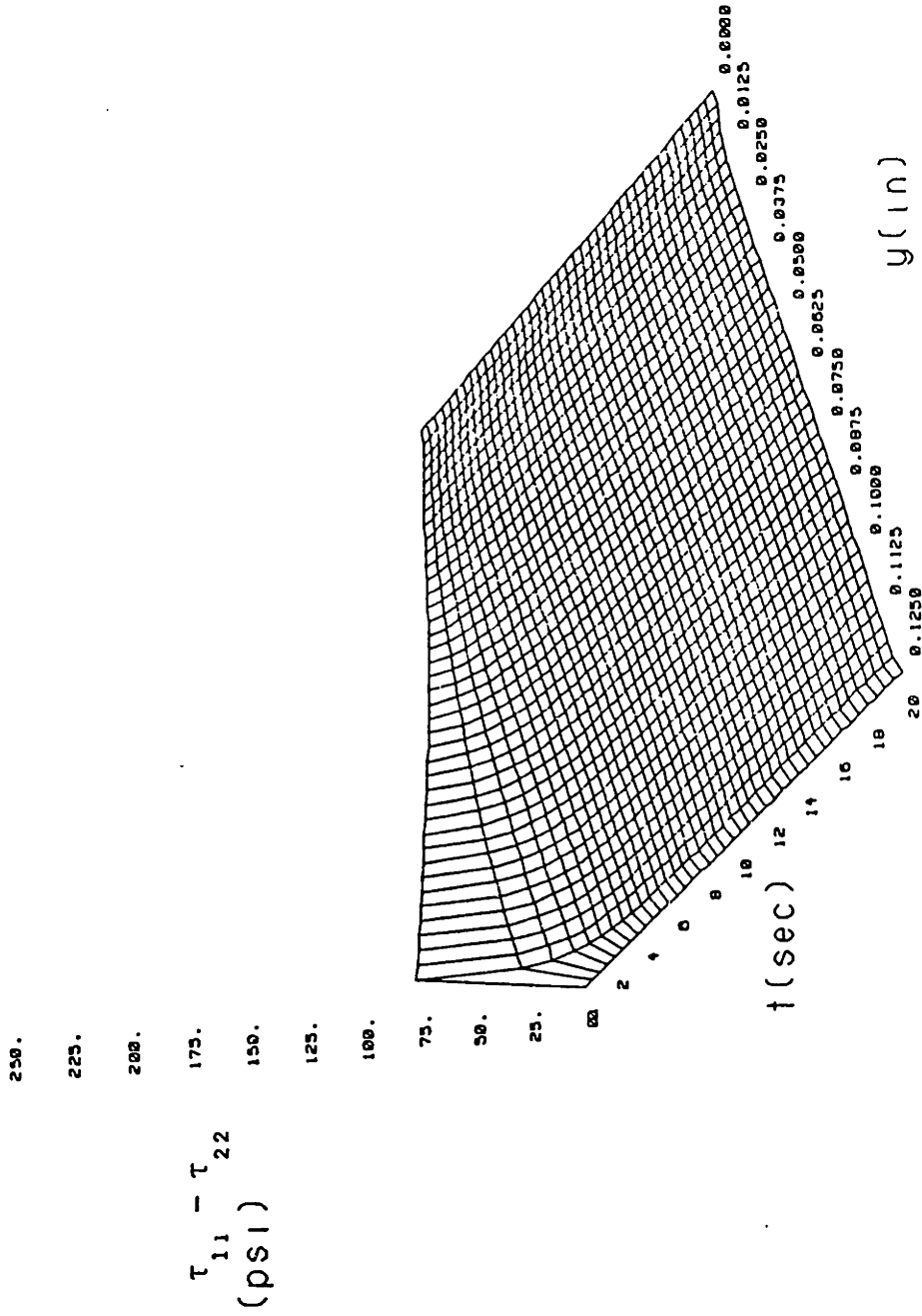


Figure E26 : Nonisothermal relaxation of the primary normal stress difference for $dp/dx = 250$ psi/in. (condition J in Table IV.2).

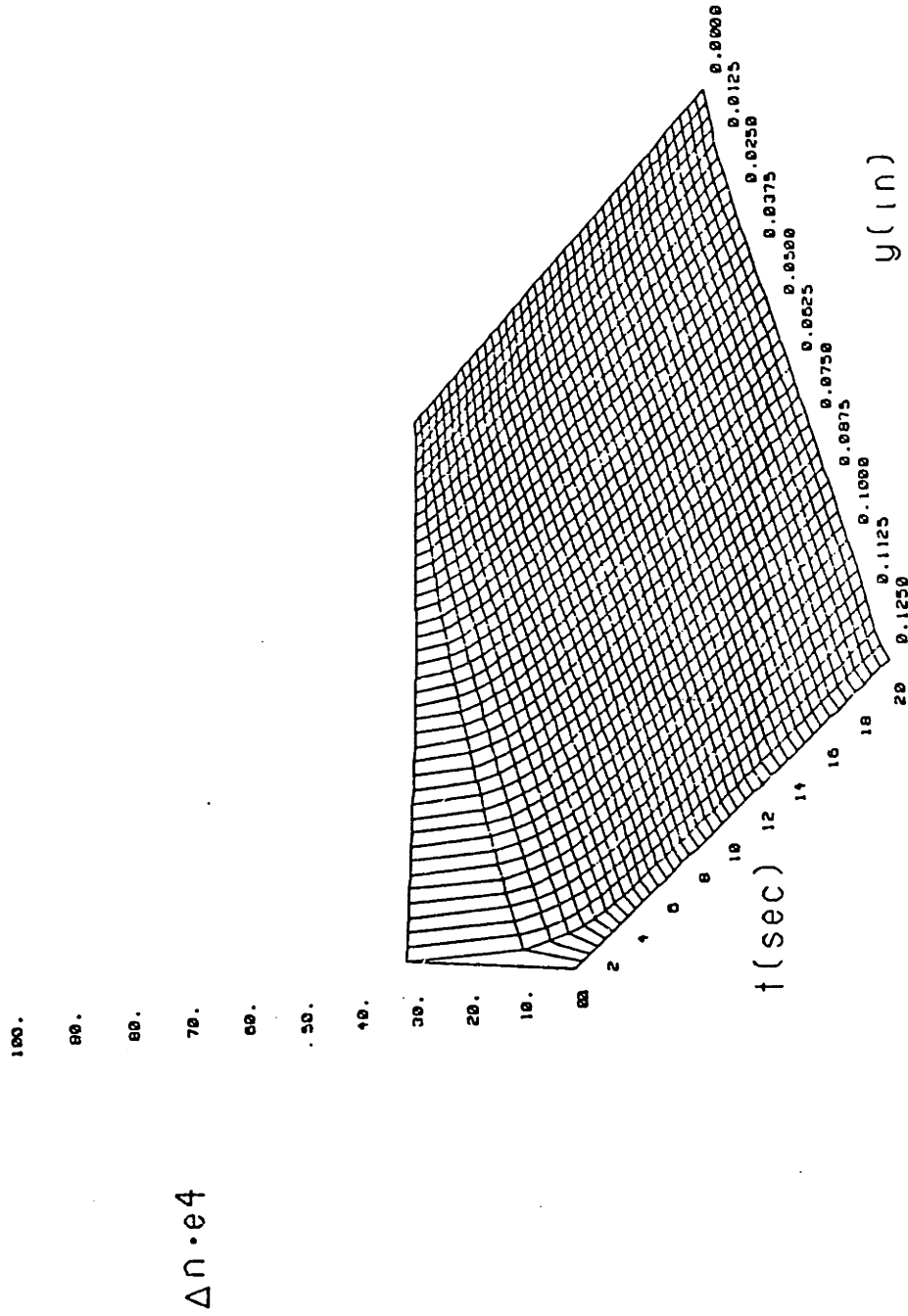
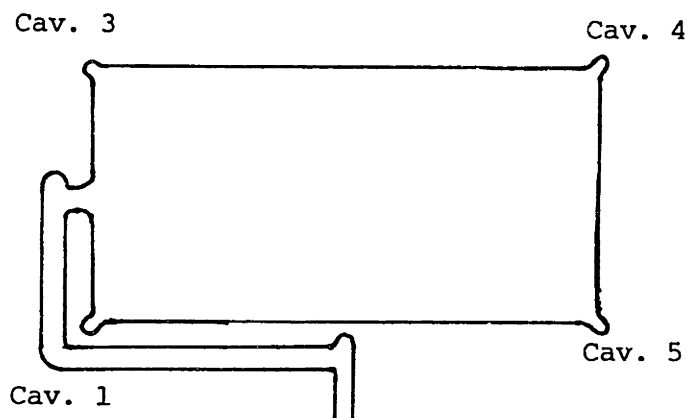


Figure E27 : Nonisothermal relaxation of the birefringence for $dP/dx = 250 \text{ psi/in.}$ (condition J in Table IV.2).

APPENDIX F

Data for the Conventional Molding

Cavity Location Code;



Part Code;

<u>Machine Control</u>	<u>Melt Temp. (°F)</u>	<u>Mold Temp. (°F)</u>
OL open loop	L 470	L 70
CL closed loop	M 520	M 120
	H 570	H 170

(example) CLLL : closed loop machine control
 melt temperature of 470°F
 mold temperature of 70°F

POLYSTYRENE (Dow 685D) Thickness : 0.015 inch

Part Code	Cavity Pressures										RAM Velocity	Remarks
	Cav. 1 (psi)		Cav. 3 (psi)		Cav. 4 (psi)		Cav. 5 (psi)					
	Min.	Max.	Min.	Max.	Min.	Max.	Min.	Max.	Min.	Max.		
CLLL	2120	2660	0	2639	---	---	---	---	---	0	max.	Part Not Full
CLLH	2544	3315	1319	3216	---	---	---	---	---	0	max.	
CLMM	3161	4009	2969	3916	---	---	---	---	---	0	max.	
CLHL	3161	3855	3133	3917	---	---	---	---	---	0	max.	
CLFH	4009	4241	3793	4370	---	---	---	---	---	0	max.	

POLYSTYRENE (Dow 685D) Thickness : 0.030 inch

Part Code	Cavity Pressures										RAM Velocity
	Cav. 1 (psi)		Cav. 3 (psi)		Cav. 4 (psi)		Cav. 5 (psi)				
	Min.	Max.	Min.	Max.	Min.	Max.	Min.	Max.	Min.	Max.	
C1LL		7324		7421	---	0	---	0	---	0	3"/sec.
C1LL		7131		7215	1619	1868	1755	1984	1755	1984	4"/sec.
C1LL		6650		6802	0	1661	840	1908	840	1908	5"/sec.
C1HH	732	5686	2062	6185	4733	5813	4578	5684	4578	5684	2"/sec.
C1HH		6554		6597	2034	2284	2060	2327	2060	2327	3"/sec.
C1HH		5975		5978	1287	2325	1335	2251	1335	2251	4"/sec.
C1HH		5493		5566	1080	1744	1259	1755	1259	1755	5"/sec.

POLYSTYRENE (Monsanto 3350) Thickness : 0.015 inch

Part Code	Cav. 1 (psi)		Cav. 3 (psi)		Cav. 4 (psi)		Cav. 5 (psi)		RAM Velocity	Remarks
	Min.	Max.	Min.	Max.	Min.	Max.	Min.	Max.		
OLLL	2891	3084	495	2226	---	0	---	0	max.	Part Not Full
OLLM	2467	2699	536	2226	---	0	---	0	max.	
OLML	2544	2968	1732	2433	---	0	---	0	max.	
OLMM	2274	2968	165	2268	---	0	---	0	max.	
OLMH	2776	3315	2144	2886	---	0	---	0	max.	
OLHL	1928	2506	124	2062	---	0	---	0	max.	
OLHM	2313	2699	990	2268	---	0	---	0	max.	
OLHH	2313	2621	247	2226	---	0	---	0	max.	

POLYSTYRENE (Monsanto 3350) Thickness : 0.015 inch

Part Code	Cav. 1 (psi)		Cav. 3 (psi)		Cav. 4 (psi)		Cav. 5 (psi)		RAM Velocity	Remarks
	Min.	Max.	Min.	Max.	Min.	Max.	Min.	Max.		
CLLL	2621	3045	0	3051	---	0	---	0	max.	Part Not Full
CLLH	2467	3084	0	3051	---	0	---	0	max.	
CLMM	2621	3007	2144	2969	---	0	---	0	max.	
CLHL	3007	3470	2969	3298	---	0	---	0	max.	
CLHH	3778	4086	3710	4123	---	0	---	0	max.	

POLYSTYRENE (Monsanto 3350) Thickness : 0.030 inch

Part Code	Cavity Pressures										RAM Velocity
	Cav. 1 (psi)		Cav. 3 (psi)		Cav. 4 (psi)		Cav. 5 (psi)				
	Min.	Max.	Min.	Max.	Min.	Max.	Min.	Max.	Min.	Max.	
CLLL		7710		7009	---	0	---	0	---	0	3"/sec.
CLLL		9252		8865	---	0	---	0	---	0	4"/sec.
CLLL		7710		7628	249	1453	1068	1602			5"/sec.
CLLL		7710		7628	0	830	534	1221			6"/sec.
CLLH		7710		7215	---	0	---	0	---	0	3"/sec.
CLLH	12722	12914	9482	11338	0	1495	0	1526			4"/sec.
CLLH		8288		8040	2989	3239	2672	3052			5"/sec.
CLHL		6554		6802	1536	1993	1602	1907			3"/sec.
CLHL		5879		5875	0	1246	0	1297			4"/sec.
CLHL		5686		5978	1080	1868	1145	1831			5"/sec.
CLHH		6746		6802	996	1993	1145	1984			3"/sec.
CLHH		6264		6494	996	2408	1030	2365			4"/sec.
CLHH		5783		5772	0	839	458	1068			5"/sec.

BIOGRAPHICAL NOTE

Byung H. Kim was born in Taegu, Korea on November 12, 1956. His family immigrated to San Jose, California, in 1971. After graduating from Silver Creek High School in 1975, he earned a Bachelor of Science Degree in Mechanical Engineering from the University of California, Berkeley, in 1978. He entered graduate school at M.I.T. in the fall of 1978. He was a research assistant and wrote a thesis on "Determination of Moisture Level in Polymers." He was awarded the Master of Science Degree in 1980. Based on his master's thesis, he obtained U.S. Patent #4352059. His LTIM method discovered during the doctoral work is patent pending. Both his Master's and Ph.D. work resulted in the establishment of Axiomatics Corp., of Sudbury, Mass., and Intelitec Corp. of Billerica, Mass., respectively. Upon completion of his doctoral thesis he will join the faculty of the University of Massachusetts, Amherst, as an Assistant Professor of Mechanical Engineering.